TABLE OF CONTENTS

CHAPTER		PAGE	
I.	INTRODUCTION.	1	1/A13
II.	FLIGHT PATH STUDIES--BASIC CONCEPTS	5	1/B3
III.	GENERATION OF THUNDERSTORM AND TURBULENCE MODELS.	9	1/B7
IV.	RESULTS AND DISCUSSION.	17	1/C1
V.	CONCLUSION.	64	2/A9
REFERENCE LIST		66	2/A11
APPENDICES		70	2/B1
A.	EQUATIONS OF MOTION.	71	2/B2
B.	COMPUTER PROGRAM DOCUMENTATION	80	2/B11

NAS1-26: 3052

NASA Contractor Report 3052

COMPLETED
ORIGINAL

Investigations of Simulated Aircraft Flight Through Thunderstorm Outflows

Walter Frost and Bill Crosby

CONTRACT NAS8-32217
SEPTEMBER 1978

NASA

NASA Contractor Report 3052

Investigations of Simulated Aircraft Flight Through Thunderstorm Outflows

Walter Frost and Bill Crosby
FWG Associates, Inc.
Tullahoma, Tennessee

Prepared for
George C. Marshall Space Flight Center
under Contract NAS8-32217

National Aeronautics
and Space Administration

Scientific and Technical
Information Office

1978

FOREWORD

The work reported herein was supported by the National Aeronautics and Space Administration, Marshall Space Flight Center, Space Sciences Laboratory, Atmospheric Sciences Division, under contract number NAS8-32217.

The authors are indebted to Mr. Jack Enders of the Aviation Safety Technology Branch, Office of Advanced Research and Technology (OAST), NASA Headquarters, Washington, D. C., for his support of this research. Special thanks also to to Dr. G. H. Fichtl and Mr. Dennis W. Camp of the Marshall Space Flight Center who were the scientific monitors of the program.

LIST OF ILLUSTRATIONS

FIGURE PAGE

1. Automatic Landing Geometry Using ILS [6] 7
2. The Two Main Potentially Hazardous Shear Situations [8]. . . . 10
3. Lift and Drag Acting on an Airplane [10] 12
4. Variation of Lift and Drag with Change in Vertical Wind Component [10]. 12
5. Diagram of Forces Acting on an Airplane. 14
6. Transient Condition from Decreasing Head Wind (or Increasing Tail Wind) [11] 16
7. Flight Paths of DC-8 Landing with Fixed Controls from 1,000-Ft (305 m) Level, Glide Slope -2.7°. 20
8. Flight Paths of DC-8 Landing with Fixed Controls from 300-Ft (91 m) Level, Glide Slope -2.7° 21
9. Flight Paths of DHC-6 Landing with Fixed Controls from 1,000-Ft (305 m) Level, Glide Slope -2.7°. 22
10. Flight Paths of DHC-6 Landing with Fixed Controls from 1,000-Ft (305 m) Level, Glide Slope -7.0°. 23
11. Flight Paths of DHC-6 Landing with Fixed Controls from 300-Ft (91 m) Level, Glide Slope -7.0° 24
12. Flight Paths of B-747 Landing with Fixed Controls from 1,000-Ft (305 m) Level, Glide Slope -2.7°. 25
13. Flight Paths of B-747 Landing with Fixed Controls from 1,000-Ft (305 m) Level, Glide Slope -6.0°. 26

FIGURE PAGE

14. Flight Paths of Augmentor-Wing STOL Landing with Fixed Controls from 1,000-Ft (305 m) Level, Glide Slope -7.0° . . . 27

15. Flight Paths of Augmentor-Wing STOL Landing with Fixed Controls from 300-Ft (91 m) Level, Glide Slope -7.0° 28

16. Winds "Seen" by DC-8 Landing with Fixed Controls in Thunderstorm Cases 9 and 11. 30

17. Comparison of Aircraft Landing with Fixed Controls in Thunderstorm Cases 9 and 11 from 1,000-Ft (305 m) Level, Glide Slope -2.7°. 31

18. Comparison of DC-8 Landing with Fixed Controls in Thunderstorm Case 9 Considering Individual Wind Components and Both Wind Components. 36

19. DC-8 Type Aircraft Landing with Fixed Controls in Wind Field Associated with JFK Eastern 66 Accident and Winds Encountered along Flight Path A 38

20. Comparison of Flight Path Angle of DC-8 and B-747 Landing with Fixed Controls in Thunderstorm Cases 9 and 11 40

21. Comparison of Indicated Airspeed of DC-8 and B-747 Landing with Fixed Controls in Thunderstorm Case 9 41

22. Comparison of Indicated Airspeed of DC-8 and B-747 Landing with Fixed Controls in Thunderstorm Case 11. 42

23. Example of the Role of Ground Effect Terms 44

24. Flight Path Comparison of Aircraft Landing with Fixed Controls from 1,000-Ft (305 m) Level with Increased Approach Angle in Thunderstorm Cases 9 and 11. 47

FIGURE PAGE

25. Flight Path Comparison of STOL and DHC-6 Landing with Fixed Controls from 300-Ft (91 m) Level, Glide Slope -7.0°, 50

26. Flight Path Comparison of DC-8 Landing with (1) Fixed Controls, (2) Automatic Controls, and (3) Automatic Controls with Turbulence Included, in Several Different Thunderstorm Cases 53

27. Typical Wind Profiles Along a -2.7° Glide Slope as "Seen" by DC-8 Landing with Automatic Controls in Thunderstorm Case 9. 55

28. Typical Wind Profiles Along a -2.7° Glide Slope as "Seen" by DC-8 Landing with Automatic Controls in Thunderstorm Case 11 56

29. Rate of Change of Thrust Required of DC-8 Landing with Automatic Control System in Thunderstorm Cases 9 and 11. . . 57

30. Comparison of Flight Paths for DC-8 Type Aircraft With and Without Thrust Rate Limiter 59

31. Rate of Change of Elevator Angle Required of DC-8 Landing with Automatic Control System in Thunderstorm Case 9 60

32. Rate of Change of Elevator Angle Required of DC-8 Landing with Automatic Control System in Thunderstorm Case 11. . . . 61

33. Comparison of Flight Paths with Idealized and More Conventional Control Systems for DHC-6 Type Aircraft 63

34. Relationship Between the Various Forces Acting on an Aircraft [20]. 72

FIGURE PAGE

35. Main Calling Program Flow Diagram for Aircraft with Fixed Controls. 81

36. Main Calling Program Flow Diagram for Aircraft with Automatic Controls. 32

37. Main Calling Program Flow Diagram for Aircraft with Automatic Controls, Including Turbulence Generation Subroutines 83

LIST OF TABLES

TABLE		PAGE
1.	Flight Simulations.	19
2.	Phugoid Period and Horizontal Wavelength.	33
3.	Deviation from Touchdown Point for Condition 1.	34
4.	Comparison in Touchdown Point Deviations from the 1,000-Ft (305 m) Level Using Different Glide Slope Angles.	49
5.	Comparison in Horizontal Deviation from Touchdown Points from Different Altitudes with Different Glide Slope Angles.	52

ABBREVIATIONS AND NOMENCLATURE

AGL	Above ground level
$\bar{c}$	Wing mean aerodynamic chord
c.g.	Center of gravity
C_D	Coefficient of drag
C_L	Coefficient of lift
C_m	Pitching-moment coefficient
$\vec{D}$	Drag
$\vec{F}_T$	Thrust of engines
FRL	Fuselage reference line
g	Magnitude of the acceleration due to gravity
h_a	Reference altitude
I_{yy}	Moment of inertia about symmetry plane of the aircraft
IAS	Indicated airspeed
ILS	Instrument landing system
$\vec{L}$	Lift
L_T	Effective moment arm of the thrust vector
m	Aircraft mass
$m\vec{g}$	Gravitational force
M	Pitching moment
NSSL	National Severe Storms Laboratory
NTSB	National Transportation Safety Board
$\dot{q}$	Time derivative of the pitching rate
s	Wing area
STOL	Short take-off and landing

t, T	Time
T	Phugoid period
V	
$\bar{V}$	
V_a	
$\bar{V}_a$	
$\bar{W}$	Wind vector
W_x	Horizontal wind speed
W_z	Vertical wind speed
x	Horizontal distance
z	Vertical distance

Greek Symbols

α	Angle between $\bar{V}$ and the FRL
α'	Angle between $\bar{V}_a$ and the FRL (angle of attack)
δ	Angle between $\bar{V}_a$ and $\bar{V}$
δ_E	Elevator deflection angle
δ_T	Angle between the thrust vector and the FRL
γ	Angle between $\bar{V}$ and x-axis (flight path angle)
γ'	Angle between $\bar{V}_a$ and x-axis
λ	Phugoid wavelength
θ	Path angle

Other Notations

$( )_{GE}$	Ground effect term
$( )_o$	Initial condition
$( )_w$	Value in "wind" frame of reference
$( )_{WR}$	Wing body term

$( )_\infty$ Free stream value

$(\dot{})$ Time derivative

$(\vec{})$ Vector

CHAPTER I

INTRODUCTION

In the analysis of aircraft motion, wind effects are a key parameter, and thus deserve careful consideration. Past studies of this type have taken only constant winds into account. However, the analysis conducted in association with this contract utilizes a numerical tabulation of eleven thunderstorm outflows (converted to horizontal spatial coordinates with Taylor's hypothesis) measured with the 1,500-ft (500 m) instrumented, meteorological tower at the National Severe Storms Laboratory in Norman, Oklahoma [1].[1] These tabulated data, when combined with two-dimensional equations of aircraft motion, allow for the computation of the aircraft behavior at any position in (x,z) plane within the flow regime.

The necessity for a study of this nature precipitates from the alarming rate of increase in fatal and near-fatal accidents which have been attributed to wind shear. Presented below are several prime examples of wind shear related accidents:

1. Eastern Airlines B-727 crashed on approach to John F. Kennedy International Airport Runway 22L on June 24, 1975, resulting in 113 fatalities. Probable cause: adverse winds associated with a very strong thunderstorm along the ILS (Instrument Landing System) glide path [2].

---

[1] Numbers in brackets correspond to similarly numbered references in the Bibliography.

2. Continental Airlines B-727 crashed after takeoff on August 7, 1975, on Runway 35L at Denver-Stapleton International Airport, seriously injuring 15 persons. Probable cause: aircraft encounter with severe wind shear (generated by outflow from a thunderstorm over the departure path) at an altitude and airspeed which precluded recovery to level flight [3].

3. Iberian Airlines DC-10-30 crashed on December 19, 1973, 500 ft (152 m) short of Runway 33L at Boston-Logan International Airport, injuring 13 passengers. Probable cause: increased rate of descent induced by an encounter with a low-altitude wind shear and the captain's inability to compensate for it [4].

4. Delta Airlines DC-9 impacted a flood-control dike 785 ft (240 m) from the Runway 20 threshold at Chattanooga Municipal Airport on November 27, 1973, injuring 42 persons. Probable cause: excessive rate of descent initiated by a wind shear condition which existed in the lower levels of the approach path [5].

In numerous NTSB (National Transportation Safety Board) aircraft accident reports related to weather, the low-level wind shear hazard theme, particularly during takeoff and landing maneuvers below 1,500 ft (500 m), recurs. In all likelihood, many more aircraft accidents attributable to wind shear have not been recorded as such, due to the relatively new awareness of this phenomenon.

Realistic mathematical models of wind shear conditions are needed for use in flight simulators for the training of flight crews in aircraft handling techniques when encountering this type of situation. Fast time computer analysis to relate the potential hazards of wind shear to different types of aircraft and control systems is another

desired achievement for safety-design considerations. To do this, a computer code for investigating flight through thunderstorms has been developed which solves two-dimensional, non-linear equations of aircraft motion, incorporating with it the influence of wind shear. The equations of motion with wind shear are developed in Appendix A. Full documentation of the computer code is given in Appendix B. A further refinement of the main code adds randomly-generated turbulence effects to the existing variable wind profiles. Using this approach, a realistic simulation of aircraft motion while passing through thunderstorm outflows is determined, as the study will show.

In obtaining the results presented, a careful study of aircraft flight paths through eleven modeled thunderstorm outflows was conducted. As a consequence of this analysis it was found that the effect of shear can be considered in terms of the aircraft's deviation from the glide path and touchdown point, and from the trajectory it follows. The trajectory, particularly with fixed controls, often traced the form of a phugoidal oscillation of varying amplitude, period, and frequency. The phugoidal oscillations are discussed further in Chapter IV.

In all, 125 flights were simulated using the aerodynamic coefficients and physical data characteristic of the following aircraft: B-747, DC-8, augmentor-wing STOL, and DHC-6 Twin Otter. The first three being heavy, transport-type aircraft, and the fourth, a light, STOL utility transport. A complete discussion of the aircraft equations of motion is included in Appendix A--Equations of Motion and expressions for the aerodynamic coefficients are found in

Appendix B--Computer Program Documentation. Landing simulations with either fixed controls or automatic feedback controls are carried out for each aircraft.

CHAPTER II

FLIGHT PATH STUDIES--BASIC CONCEPTS

The flight path simulation studies with fixed controls uses two basic non-dimensionalized initial altitudes: $z = 3.33$ (1,000 ft or 305 m) and $z = 1.0$ (300 ft or 91 m). The aircraft is trimmed at these altitudes for a fixed glide slope angle. The corresponding throttle and elevator angle settings are then held constant for the remainder of the landing. Different phases of the investigations used different glide slope angles in the following manner:

1. 2.7° for DC-8, B-747: normal ILS glide path.
2. 6.0° for B-747: steep angle approach.
3. 7.0° for STOL, DHC-6: normal ILS glide path.
4. 2.7° for DHC-6: shallow angle approach.

The introduction of wind shear (gradient of vertical and horizontal mean wind components) causes deviation from the glide slope, as well as from the expected touchdown points. These deviations were then compared to the no-wind condition. From this comparison, the magnitude of the deviation was found to be directly related to the associated wind shear (negative values for head wind and updraft, positive values for tail wind and downdraft). However, some of the values tend toward unrealistic effects. These were a direct consequence of the inability of the aircraft to negotiate the imposed wind field with the controls fixed. Overcoming the unrealistic effects of fixed controls led to the development of an automatic control system for the same two-dimensional system of equations [6].

The first consideration in the creation of an automatic control system is to regard every phase of the flight as the accomplishment of a set task (i.e., flight along a specified trajectory). Thus, the desired path, in this case an ILS beam of 2.7°, is known and the departures from it, designated as errors, can be calculated. These errors are a result of the imposed wind shear. The control system then consists of numerical correction of the errors through thrust, elevator angle, and pitch angle commands to maintain a specific trajectory. This type of system was tested, in this investigation, only for a DC-8 model.

The control system consists of four phases: hold, capture, track, and flare. In this simulation, the DC-8 is initially trimmed at 1,000 ft (305 m) for straight and level flight. The first phase holds the aircraft's altitude until it intersects the ILS beam. It then switches to the glide slope capture mode, consequently activating the thrust and elevator controls to capture the beam. As soon as the specified glide path is established, the third phase, a glide slope tracking mode, becomes effective. The command signals actuate the governing control systems such that the DC-8 remains on the glide path. This is maintained until switching to the flare mode's initiation altitude of 60 ft (18 m) AGL (above ground level). The aircraft remains in the flare mode for the duration of the flight (see Figure 1).

For this investigation the scope of the automatic landing problem was restricted in two ways:

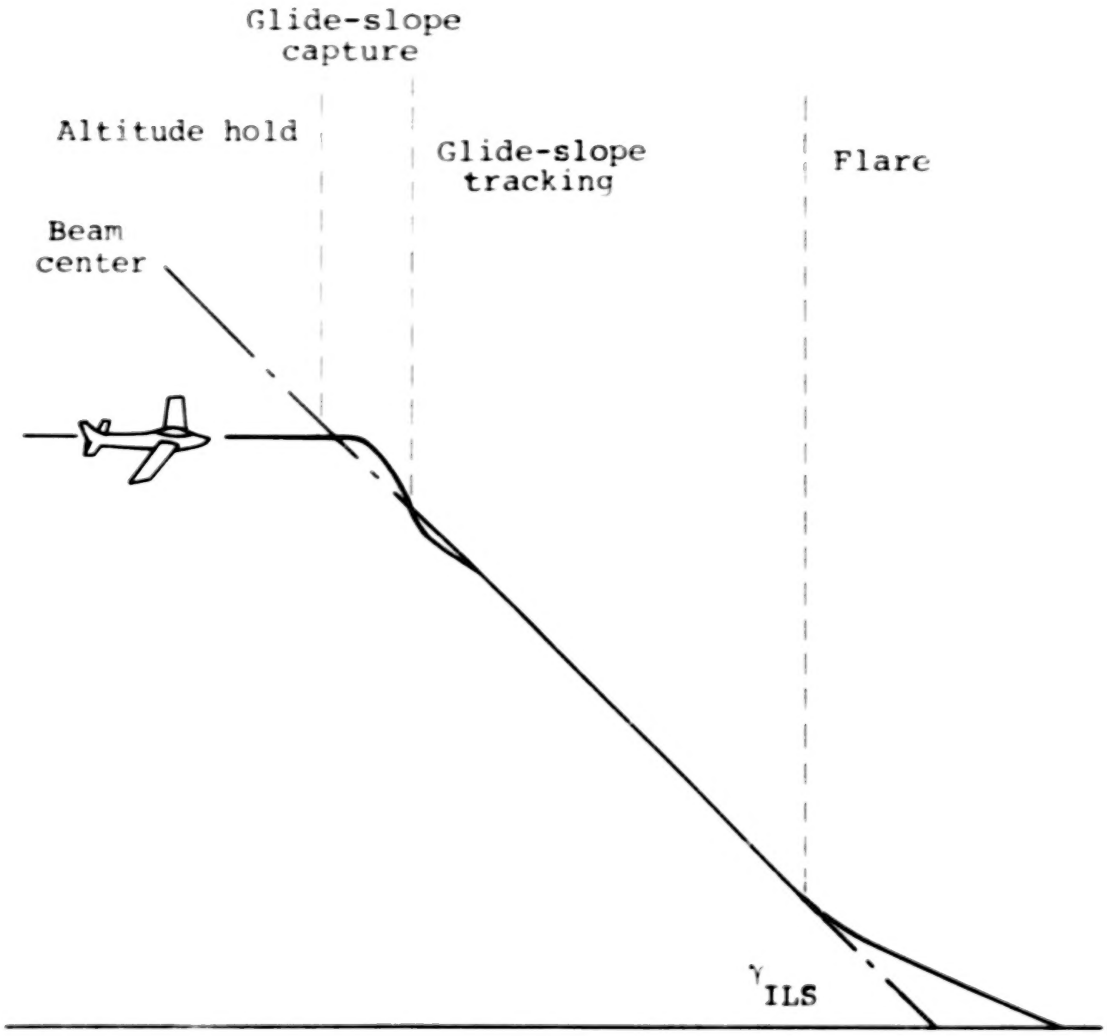

Figure 1. Automatic landing geometry using ILS [6].

1. Aircraft simulation equations are restricted to three degrees of freedom by considering the longitudinal axis only, as noted in Appendix A--Equations of Motion.

2. System guidance information is assumed to come from error-free sensors and an error-free ILS beam.

These are reasonable restrictions and may be justified by the following.

1. Wind-shear related accidents from NTSB aircraft accident reports indicated a hazard primarily from aircraft being forced below minimum safe altitudes, landing short or long, rather than lateral variation from the glide slope [6].

2. It is beneficial to maintain simplicity of the automatic control routines, since the objective of this study is the effects of wind shear and not a study of ILS system errors.

CHAPTER III

GENERATION OF THUNDERSTORM AND TURBULENCE MODELS

The eleven wind fields used in this study are a direct measurement of storms passing the WKY-TV/NSSL (National Severe Storms Laboratory) 1,500-ft (500 m) meterological tower in Norman, Oklahoma, during the months of May to July from 1971 to 1973. The thunderstorm wind shear data were recorded in the form of time histories of the longitudinal, lateral, and vertical wind vector components measured by aerovanes and anemometers [1]. Time histories of these data were then converted to horizontal spatial coordinates with Taylor's hypothesis (i.e., $x = Wt$), thus forming a two-dimensional wind field in a vertical plane. The data were then numerically tabulated in an 11x41 array. The tabulated wind speed values are coupled with a computer look-up routine developed to provide the wind speed values and gradients at any position (x,z) called for in the main program. A complete discussion of the wind field model is given in [7].

Reference [8] notes two potentially dangerous shear situations during descent which are inherent to all eleven thunderstorm cases studied. The first of these is a tail wind shearing out to a calm or head wind component. This results in an increase in the relative airspeed and the associated lift causes the aircraft to rise above the glide slope (see Figure 2a). To combat this, thrust and/or pitch attitude must be continuously reduced. However, an aircraft with fixed controls tends to overshoot the touchdown point.

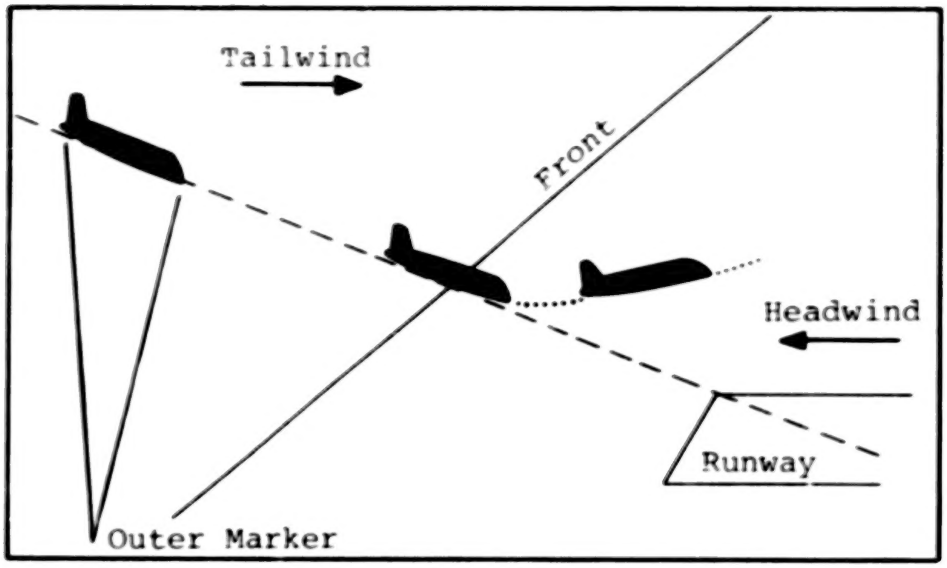

(a) Approach in tailwind with shear

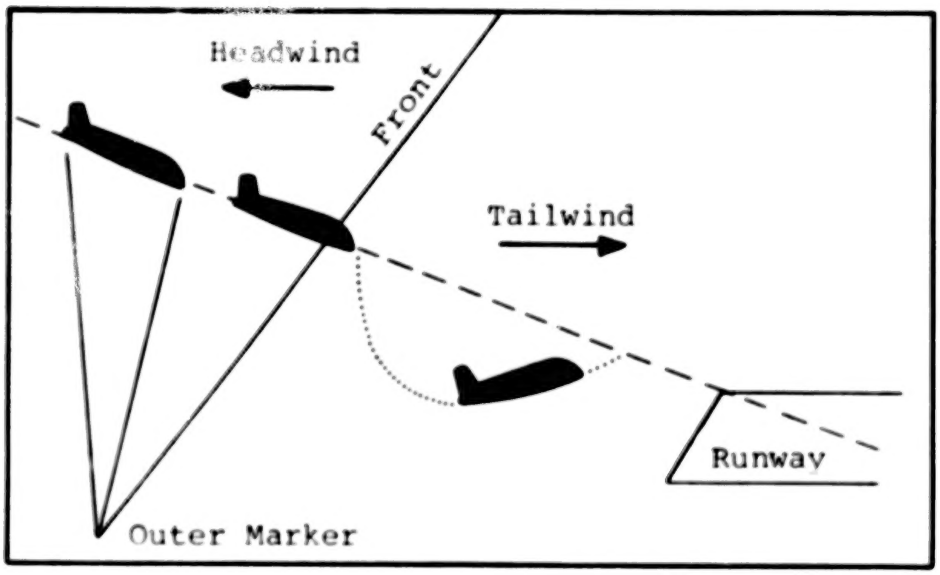

(b) Approach in headwind with shear

Figure 2. The two main potentially hazardous shear situations [8].

The second hazard situation arises from a head wind shearing out to a calm or tail wind component. In this instance, the airspeed decreases causing the aircraft to pitch down with an associated loss of altitude, and with fixed controls, to land short (see Figure 2b).

With all thunderstorm gust fronts, strong vertical and horizontal shears occur [9]. Vertical shear is a variation in the wind speed components with height z, whereas horizontal shear refers to variation with horizontal distance x. In the case of two-dimensional wind field vertical updrafts and downdrafts tend to compound the effects cited previously. This is explained by the following discussion.

Since the total steady aerodynamic force on an aircraft is conventionally decomposed into lift and drag components, the forces acting on the aircraft may be resolved, as shown in Figure 3.

Noting the lift and drag forces always act normal and parallel to the relative wind, respectively, the lift and drag in a perturbed wind condition is shown in Figure 4. The quantities L_o and D_o represent the lift and drag forces acting on the airplane during steady flight condition, and are normal and parallel to the relative wind--taken parallel to the x-axis in this case. Thus, when the aircraft encounters an up or down draft, as well as a change in wind speed, the relative wind shifts to a new position in a direction opposite to the vector sum of V_a and w_z, as shown in Figure 4. This perturbed position of the relative wind causes an increase in the angle of attack α_p. The vector quantities L and D then represent the aerodynamic forces acting on the aircraft during the disturbed wind condition [10].

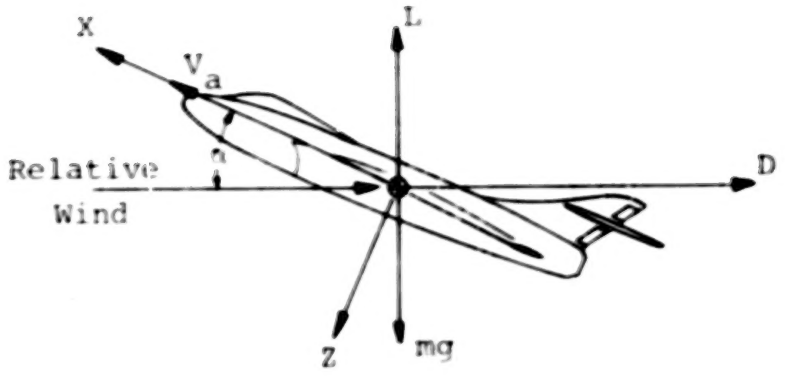

Figure 3. Lift and drag acting on an airplane [10].

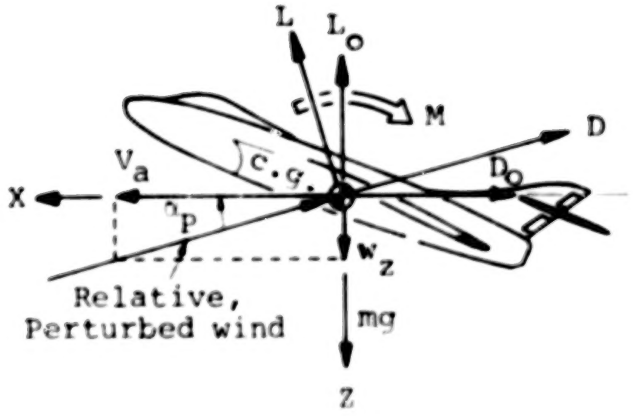

Figure 4. Variation of lift and drag with change in vertical wind component [10].

To further illustrate this, consider the simple example of an airplane in level flight. The relative airspeed is given by $\vec{V}_a = \vec{W} - \vec{V}^E$, and the lift, $\vec{L}$, and drag, $\vec{D}$, are normal and parallel to $\vec{V}_a$, respectively. Assume $|\vec{V}^E| = 100$ mph (45 m s^{-1}) and that $C_L/C_D = 2.0$, for simplicity. Also assume a 16-mph (7 m s^{-1}) tail wind shearing to a 4.5-mph (2 m s^{-1}) head wind, which corresponds to Case 1 described in the foregoing. Figure 5a shows the vector relationship for the initial condition with the forces balanced, and Figure 5b shows the latter condition with the resultant force $\vec{F}$ acting upward and backward (forces--subscripted 1). This causes the airplane to go high on the glide slope and to increase airspeed.

If the shear is accompanied by an updraft of 7 mph (3 m s^{-1}) or a downdraft of 7 mph (3 m s^{-1}) the former case will act approximately 4° to left (subscripted 2), and in the latter case, 4° to the right (subscripted 3), as illustrated in the diagram. The accompanying updraft creates forces which cause the airplane to be higher on the glide slope, whereas the downdraft creates forces which cause greater loss of airspeed.

Recently, McCarthy and Blick [11] performed an analysis for a B-727 class airplane with fixed controls encountering a half-sine wave tail wind of 23 mph (10 m s^{-1}) amplitude at the phugoid frequency along a -3° glide slope which experienced an initial decrease in altitude from the flight path; this relates to the second type of hazard discussed earlier. They found that for any decrease in airspeed V_a (from an increasing tail wind or decreasing head wind) the lift and drag are reduced since there is little change in thrust and essentially no change in weight, an unbalanced force forward and down

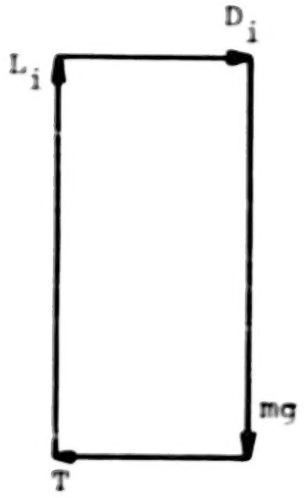

(a) Initial Condition

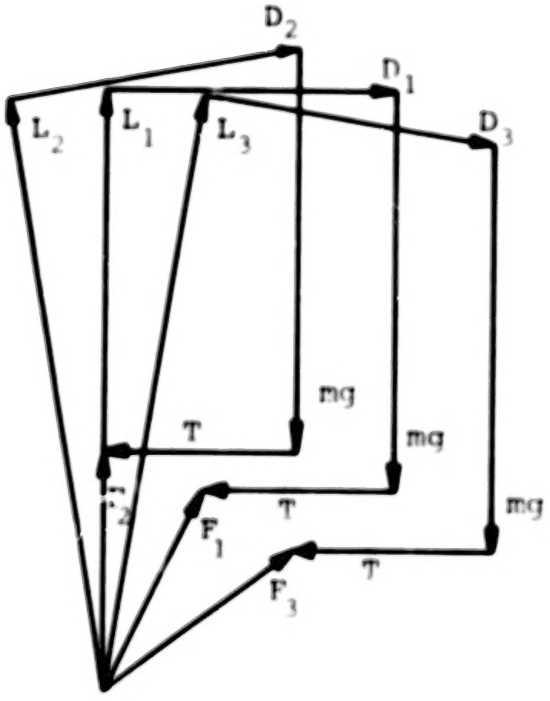

(b) Final Condition

Figure 5. Diagram of forces acting on an airplane.

is experienced, causing the airplane to accelerate in this direction (see Figure 6). Due to the inertia of the aircraft, the forward component of the unbalanced force is not large enough to cause the aircraft's speed to increase. This is due to the increased tail wind of their study being larger than the inertial airspeed perturbation during the first few seconds. However, the inertial airspeed eventually overcomes the reduction in the indicated airspeed caused by the horizontal gust (tail wind in this case), and the aircraft indicated airspeed starts to increase.

The variations in wind speeds for the thunderstorm model are 10-sec averaged values (see [7]). The wind field is thus a quasi-steady wind field, and to impose gusts of higher frequencies, a model of turbulence simulation was used with the random signals being superimposed on the flow field. The random turbulence signal provided by the turbulence modeling scheme has a Dryden energy spectrum and incorporates the non-Gaussian characteristics of the turbulence [12]. Reference [7] provides a complete discussion of the turbulence simulation technique used in this study. One flight simulation using automatic controls employing this turbulence simulation scheme was completed for a DC-8 type aircraft.

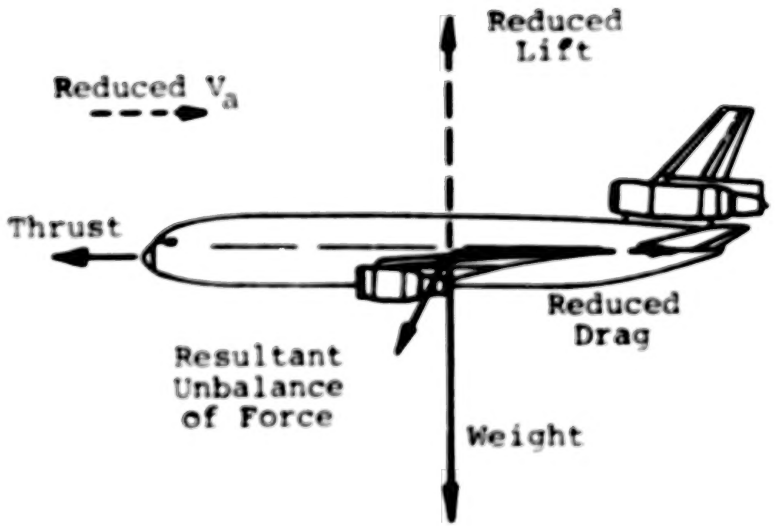

Figure 6. Transient condition from decreasing head wind (or increasing tail wind) [11].

CHAPTER IV

RESULTS AND DISCUSSION

For the figures appearing in this chapter, numerous computed aircraft parameters are plotted as they vary spatially along the flight path. However, for some parameters, such as automatic control inputs, temporal variations are important, and thus, are shown as such. Of principal interest in the fixed control mode is vertical position z, horizontal position x, and pitch angle γ. Also considered is the indicated airspeed (IAS) V_a. The spatial variations, z and x, are non-dimensionalized with the reference height h_a = 300 ft (91 m). Angle of pitch γ is expressed in radians, and V is non-dimensionalized with the initial value of the relative velocity V_a (i.e., the value assigned at trimmed conditions).

For cases utilizing the automatic control subroutines, the magnitudes of the control inputs--thrust F_T and elevator angle δ_E--thrust is non-dimensionalized with the thrust at trimmed conditions F_{T_D}, which is on the order of 2.87×10^4 lbs (1.3×10^4 kg) for a DC-8. Elevator angle is given in degrees, whereas the pitch angle is expressed in radians. Vertical and horizontal position of the aircraft with automatic controls is given, but only to establish that the aircraft maintains the specified trajectory. The control inputs which arise from corrections necessary to maintain a given glide slope are the variables of interest with an automatic control system, rather than deviations from the flight path, as is the case with fixed controls.

Table 1 lists the many various flights which have been simulated using the computer code documented in Appendix B.

Fixed Controls

The nine illustrations--Figures 7 through 15--following Table 1 constitute the complete set of resulting flight paths for the 120 simulations with fixed controls. One can see a large variety among the particular flight paths traced by the different aircraft, but on the large scale a definite recognizable pattern is observed and may be used to categorize the flight paths into two overlapping groups. These are (1) an oscillatory phugoidal motion (e.g., Figure 7, DC-8 Cases 1 through 10; Figure 9, DHC-6 Cases 2, 4, 6, 8, and 9; Figure 12, B-747 Cases 1 through 10; and Figure 14, augmentor-wing STOL Cases 1, 2, 3, 5, 6, 9, 10, and 11), and (2) a non-oscillatory motion (e.g., Figure 7, DC-8 Case 11; Figure 11, DHC-6 Cases 1 through 11; Figure 13, B-747 Cases 5, 7, 8, and 11; and Figure 15, augmentor-wing STOL Cases 1 through 11). As one would expect, there are exceptions to the two specified categories. First, in Figure 9, flight through thunderstorm Case 10 displays a divergent characteristic different from any other flight path. No explanation is offered except that this divergent flight path probably is a consequence of the longitudinal dynamics of the DHC-6 and the combined head wind and strong updraft conditions experienced in the wind field. The second exception can be found in Figure 14 with checking the flight paths traced through Cases 7 and 8 by the augmentor-wing STOL aircraft. Here the aircraft executes a loop while operating with fixed controls, possibly due to the airplane's inability to regain stable flight after an out-of-phase wind

Table 1. Flight Simulations

Aircraft Type	Initial Conditions: Altitude (ft [m])	Initial Conditions: Glide Slope Angle (deg)	Special Conditions: Ground Effect	Special Conditions: Automatic Controls	Special Conditions: Turbulence	Thunderstorm Cases
DC-8	1,000[305]	2.7				1 through 11
	300 [91]	2.7				1 through 11
	1,000[305]	2.7	X			1,2,9,11
	1,000[305]	2.7				1,9,11...W_z=0
	1,000[305]	2.7				1,9,11...W_x=0
	1,000[305]	0.0		X		1,2,9,11
	1,000[305]	0.0		X	X	1
DHC-6	1,000[305]	2.7				1 through 11
	1,000[305]	7.0				1 through 11
	300 [91]	7.0				1 through 11
B-747	1,000[305]	2.7				1 through 11
	1,000[305]	2.7	X			1 through 11
	1,000[305]	6.0	X			1 through 11
Augmentor-wing STOL	1,000[305]	7.0	X			1 through 11
	300 [91]	7.0	X			1 through 11

X: Indicates special conditions were employed during those runs.

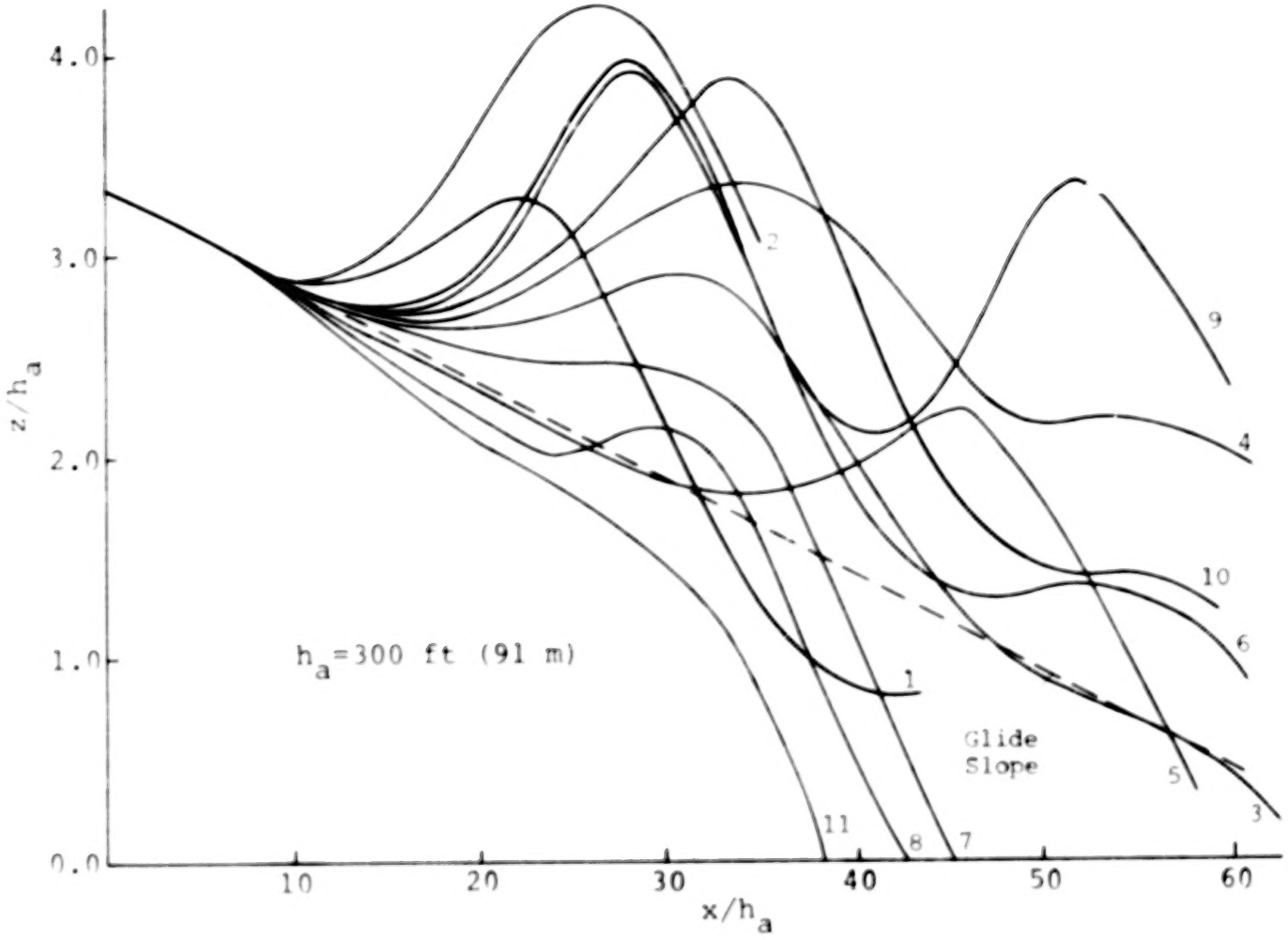

Figure 7. Flight paths of DC-8 landing with fixed controls from 1,000-ft (305 m) level, glide slope -2.7°.

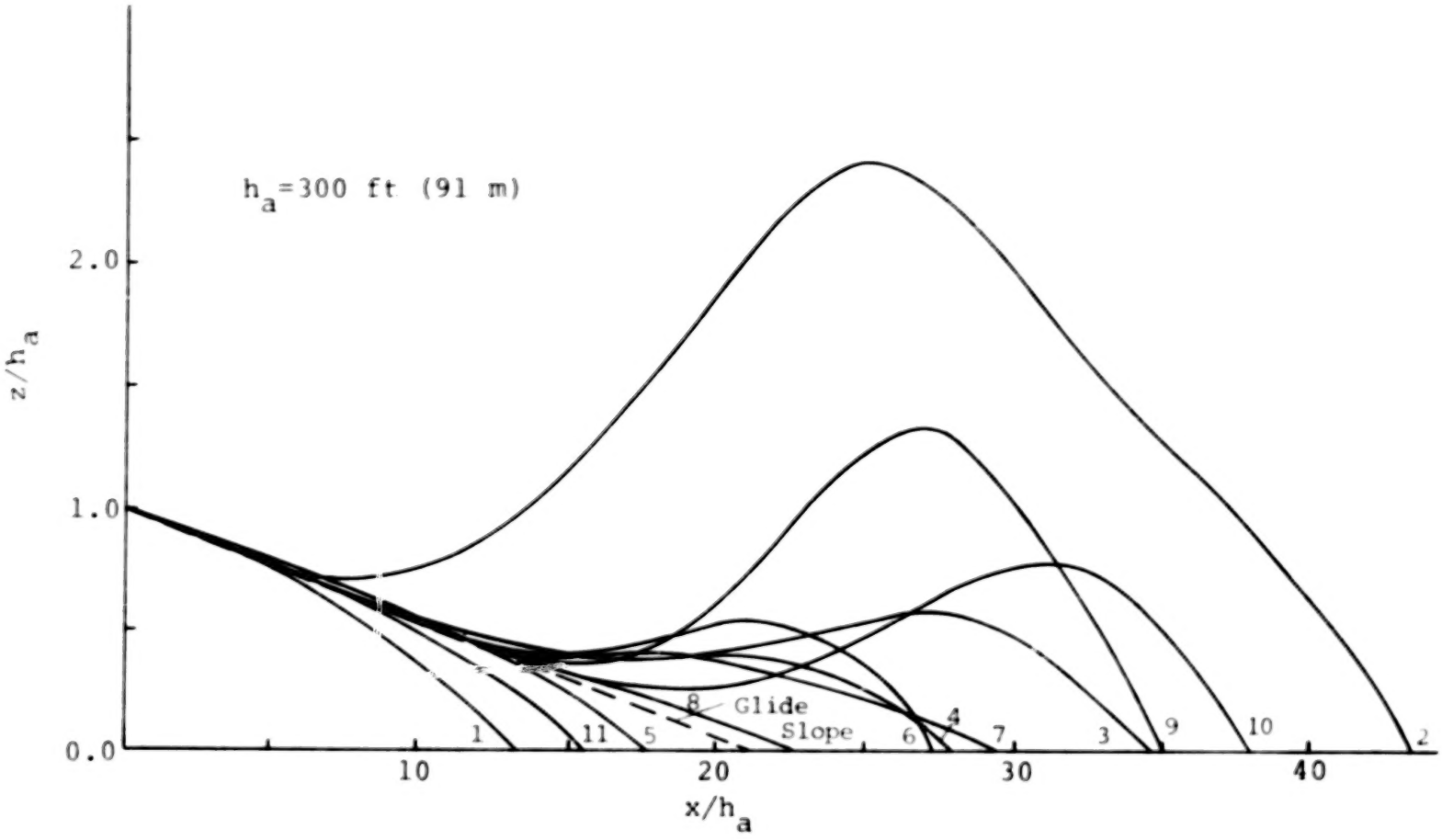

Figure 8. Flight paths of DC-8 landing with fixed controls from 300-ft (91 m) level, glide slope -2.7°.

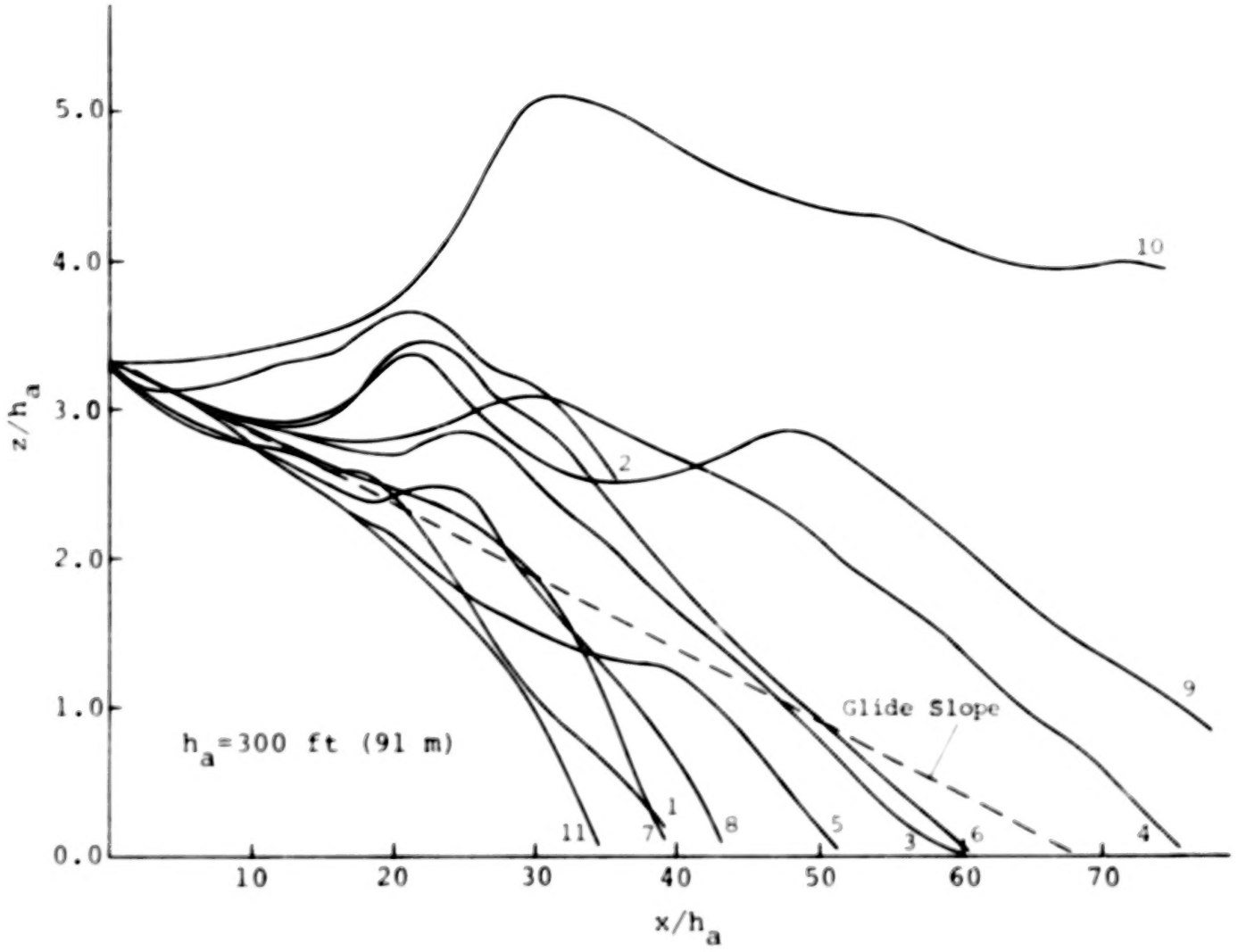

Figure 9. Flight paths of DHC-6 landing with fixed controls from 1,000-ft (305 m) level, glide slope -2.7°.

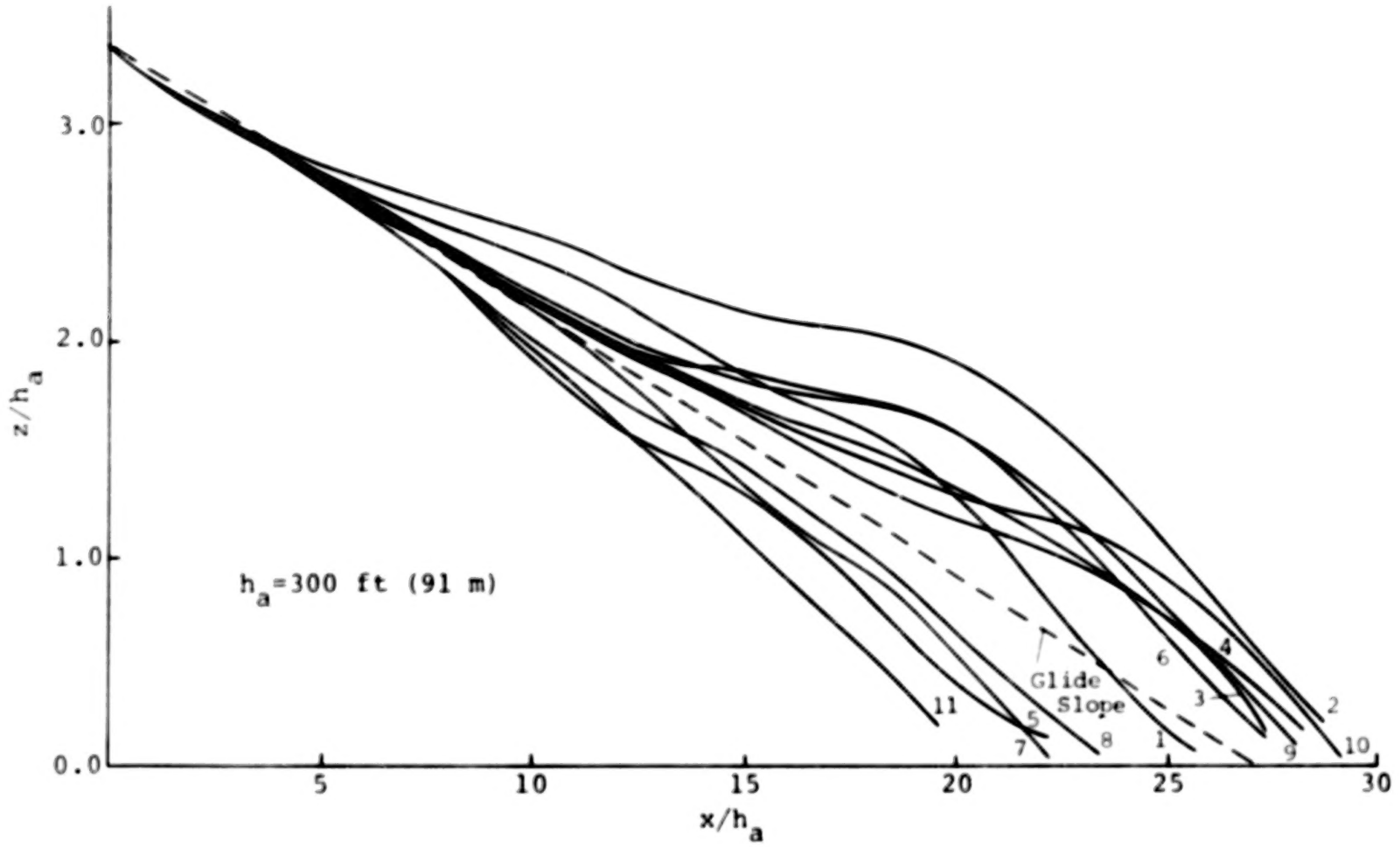

Figure 10. Flight paths of DHC-6 landing with fixed controls from 1,000-ft (305 m) level, glide slope -7.0°.

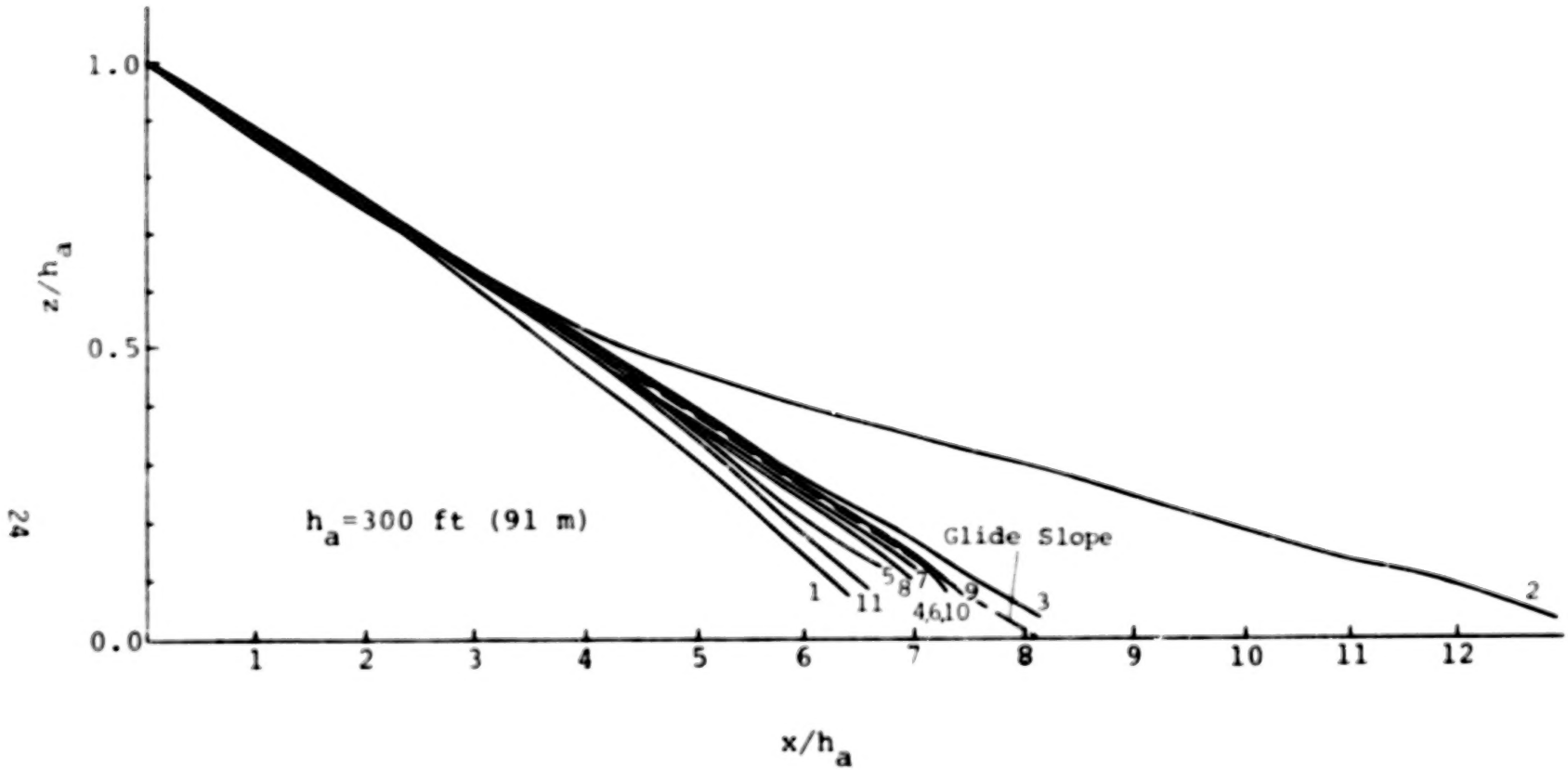

Figure 11. Flight paths of DHC-6 landing with fixed controls from 300-ft (91 m) level, glide slope -7.0°.

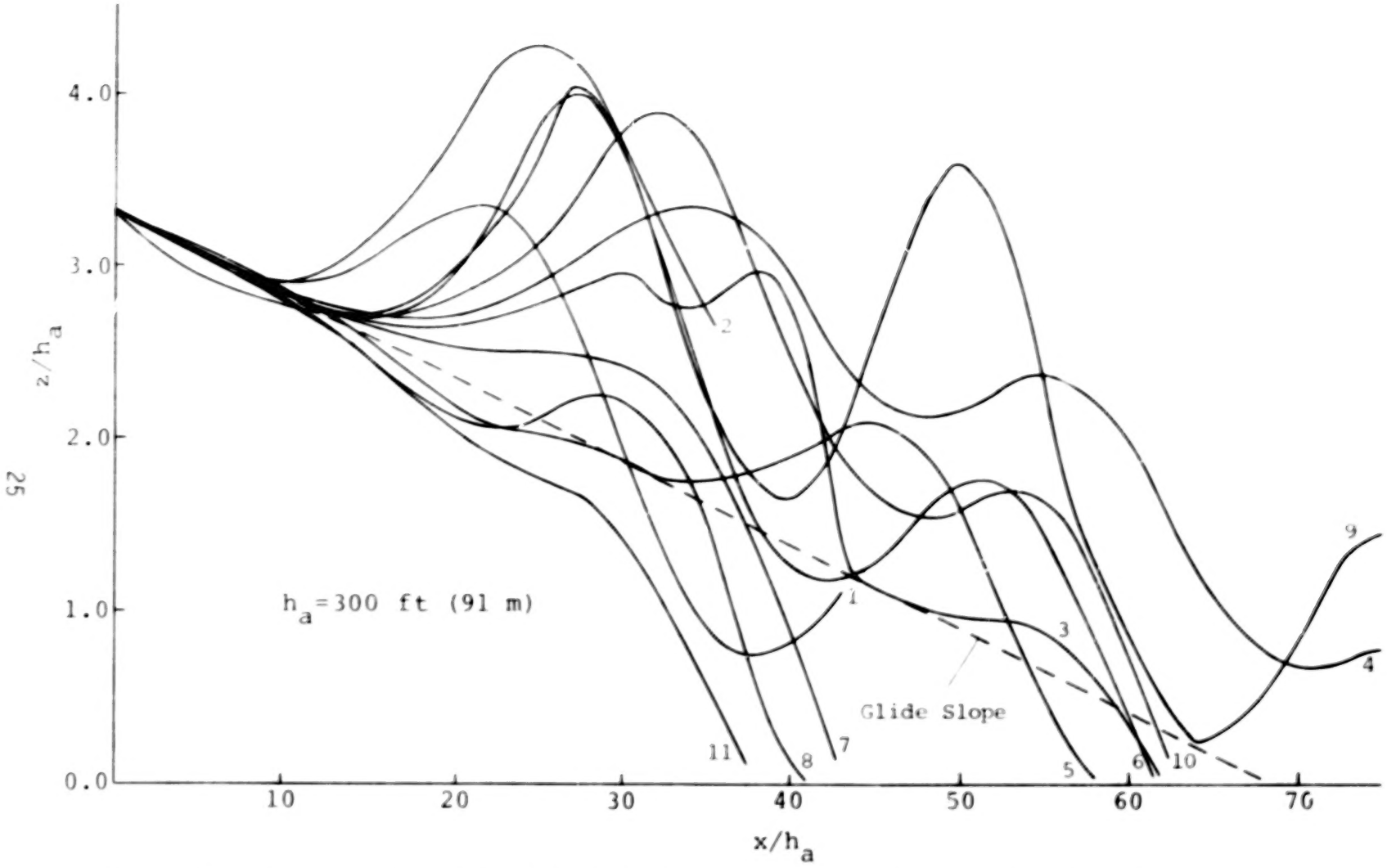

Figure 12. Flight paths of B-747 landing with fixed controls from 1,000-ft (305 m) level, glide slope -2.7°.

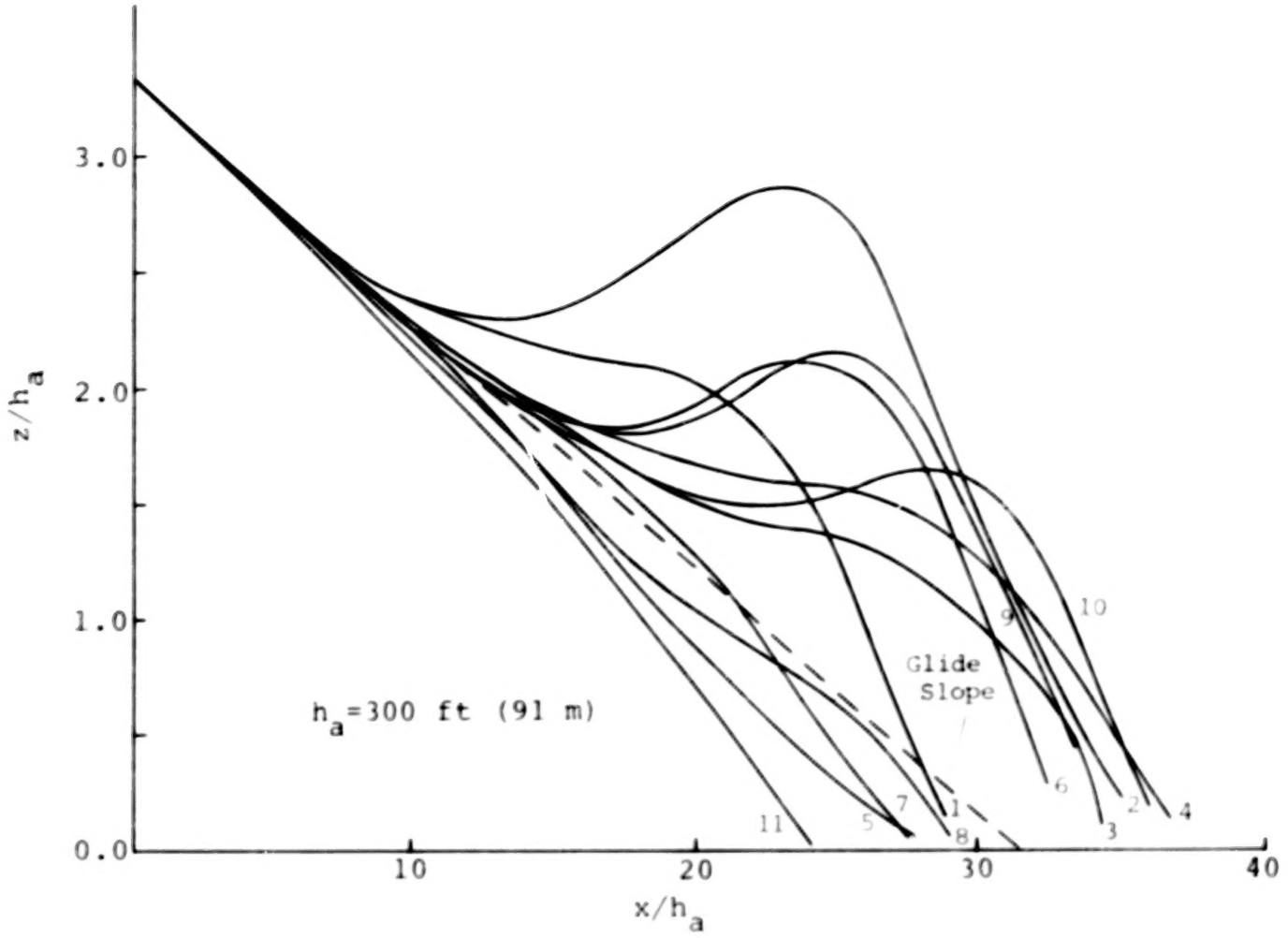

Figure 13. Flight paths of B-747 landing with fixed controls from 1,000-ft (305 m) level, glide slope -6.0°.

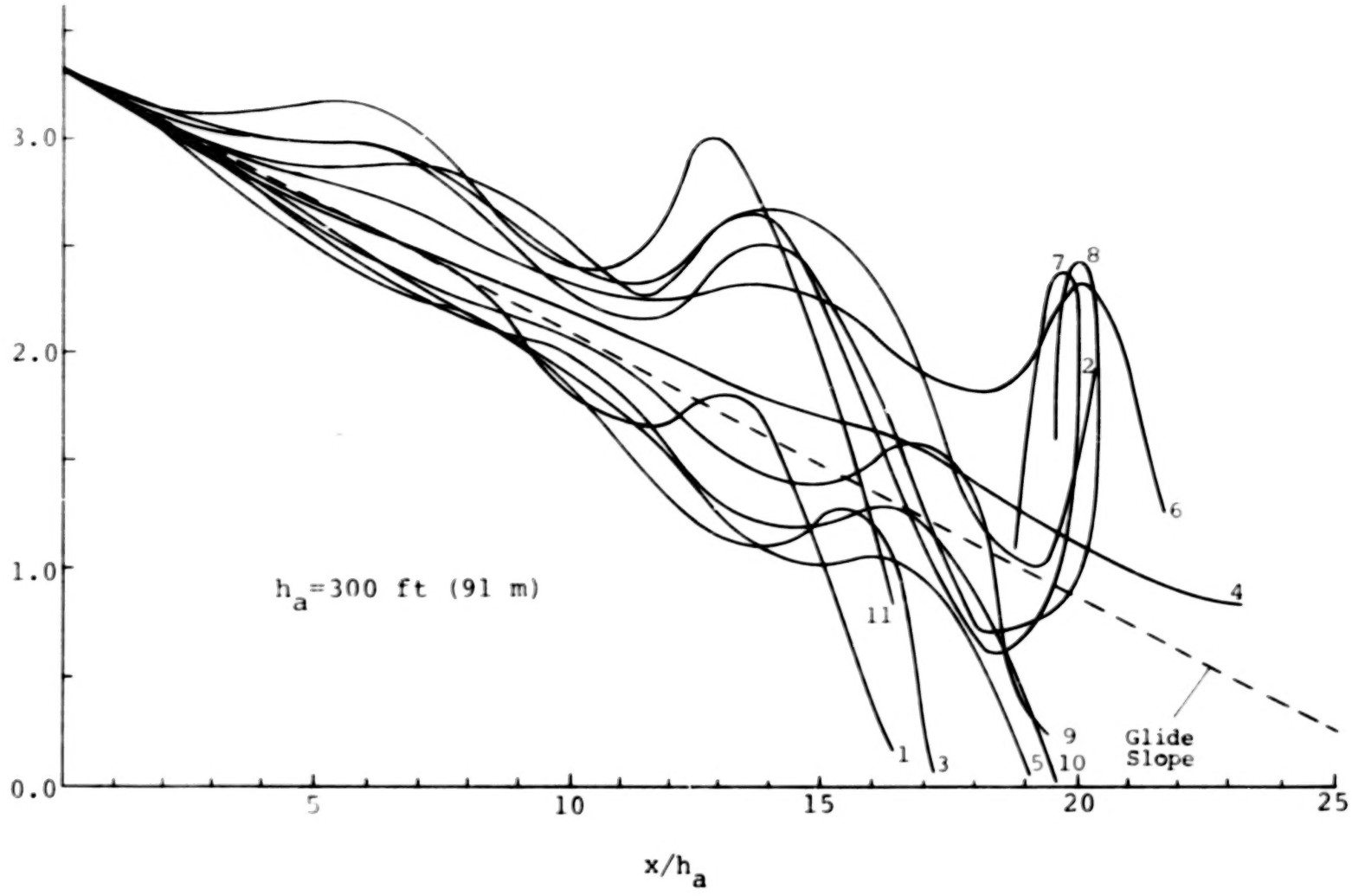

Figure 14. Flight paths of augmentor-wing STOL landing with fixed controls from 1,000-ft (305 m) level, glide slope -7.0°.

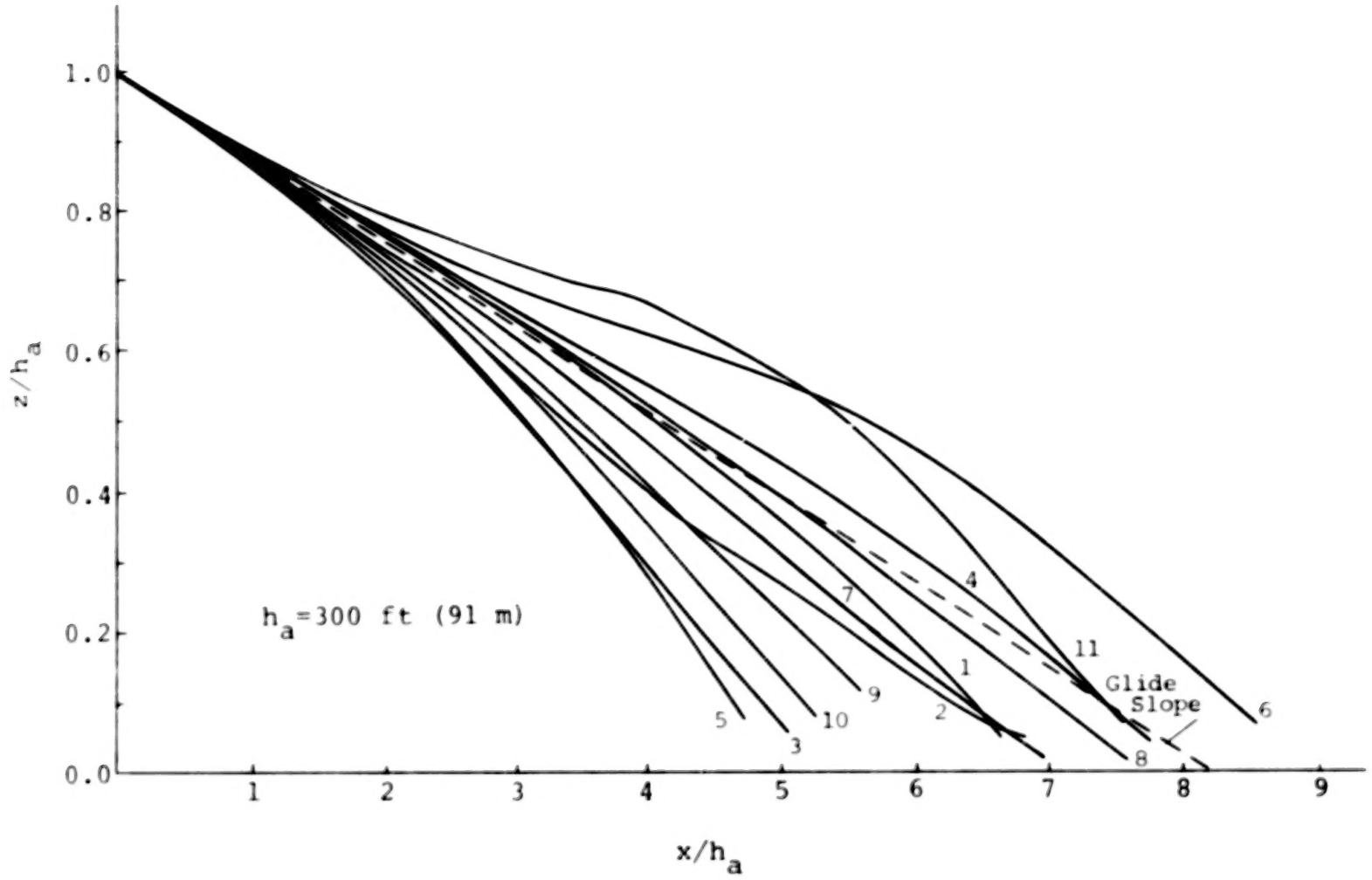

Figure 15. Flight paths of augmentor-wing STOL landing with fixed controls from 300-ft (91 m) level, glide slope -7.0°.

shear. This flight path is, of course, unacceptable and demonstrates the STOL aircraft cannot negotiate a thunderstorm with the controls fixed. Those flight paths which terminate before landing are a result of the aircraft flying outside of the experimental wind field data.

Since there are two easily distinguishable classes of flight paths that have been established, redundancy arising from discussion of each individual flight path may be avoided by investigating representative cases of the flight paths. For this study, flight simulation data related to thunderstorm Cases 9 and 11 were chosen for detailed discussion. However, in some instances for reasons of comparison, results from additional cases are supplied. Cases 9 and 11 are inherently different in the sense that the aircraft reacts in the manner described , the two main hazards in [8] (but not necessarily describing the nd conditions causing these effects); therefore, their selection for providing representative flight paths.

Figure 16 illustrates the wind profiles "seen" by a DC-8 while landing with fixed controls through thunderstorm Cases 9 and 11. The wind speeds, W_x and W_z, are non-dimensionalized with the initial airspeed V_a. A negative value indicates a head wind or updraft, whereas a positive value is a tail wind or downdraft for the longitudinal and vertical winds, respectively. Of course, the wind profiles shown in the figure would be different depending on the point within the flow field that the aircraft's flight began. Beginning at different points in the wind field also causes a change in the initial trim conditions of the aircraft.

Figure 17 is a comparison of fixed control Cases 9 and 11 with the aircraft initially trimmed to follow a 2.7° glide slope. The

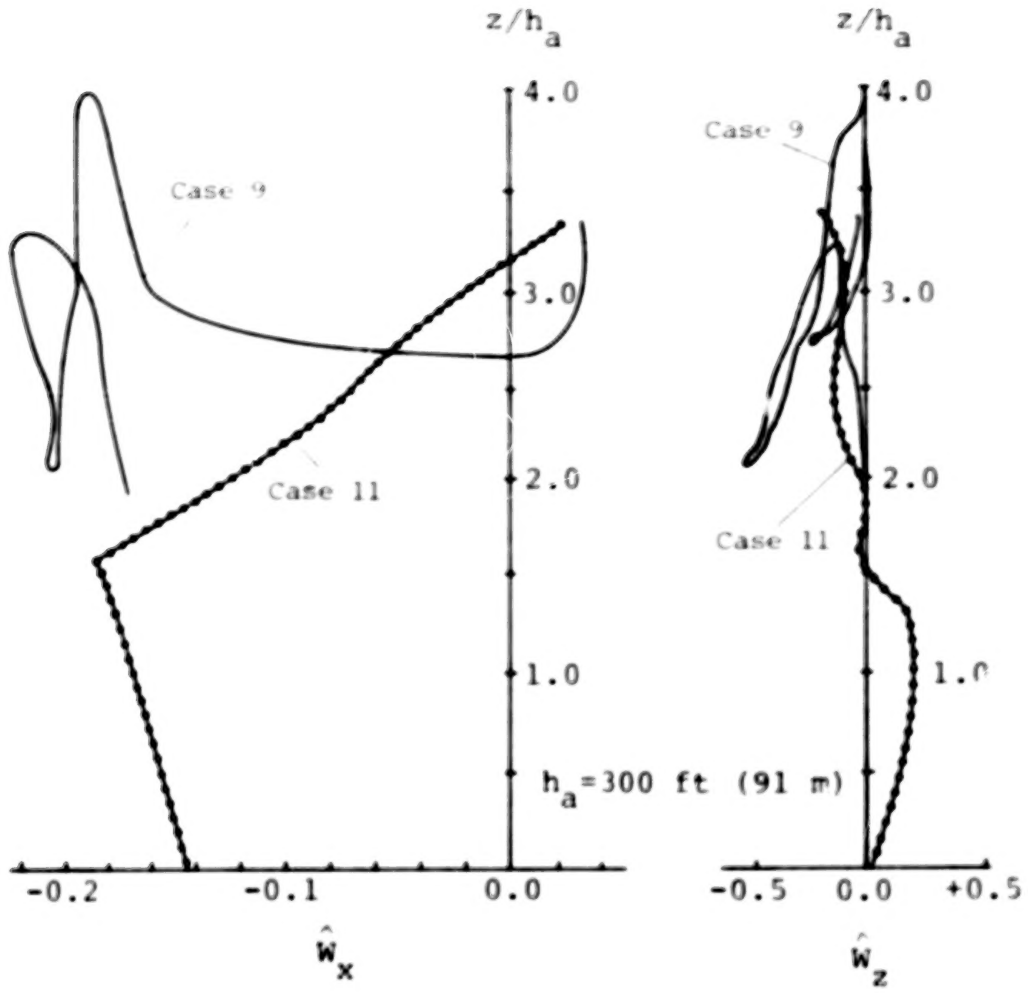

Figure 16. Winds "seen" by DC-8 landing with fixed controls in thunderstorm cases 9 and 11.

30

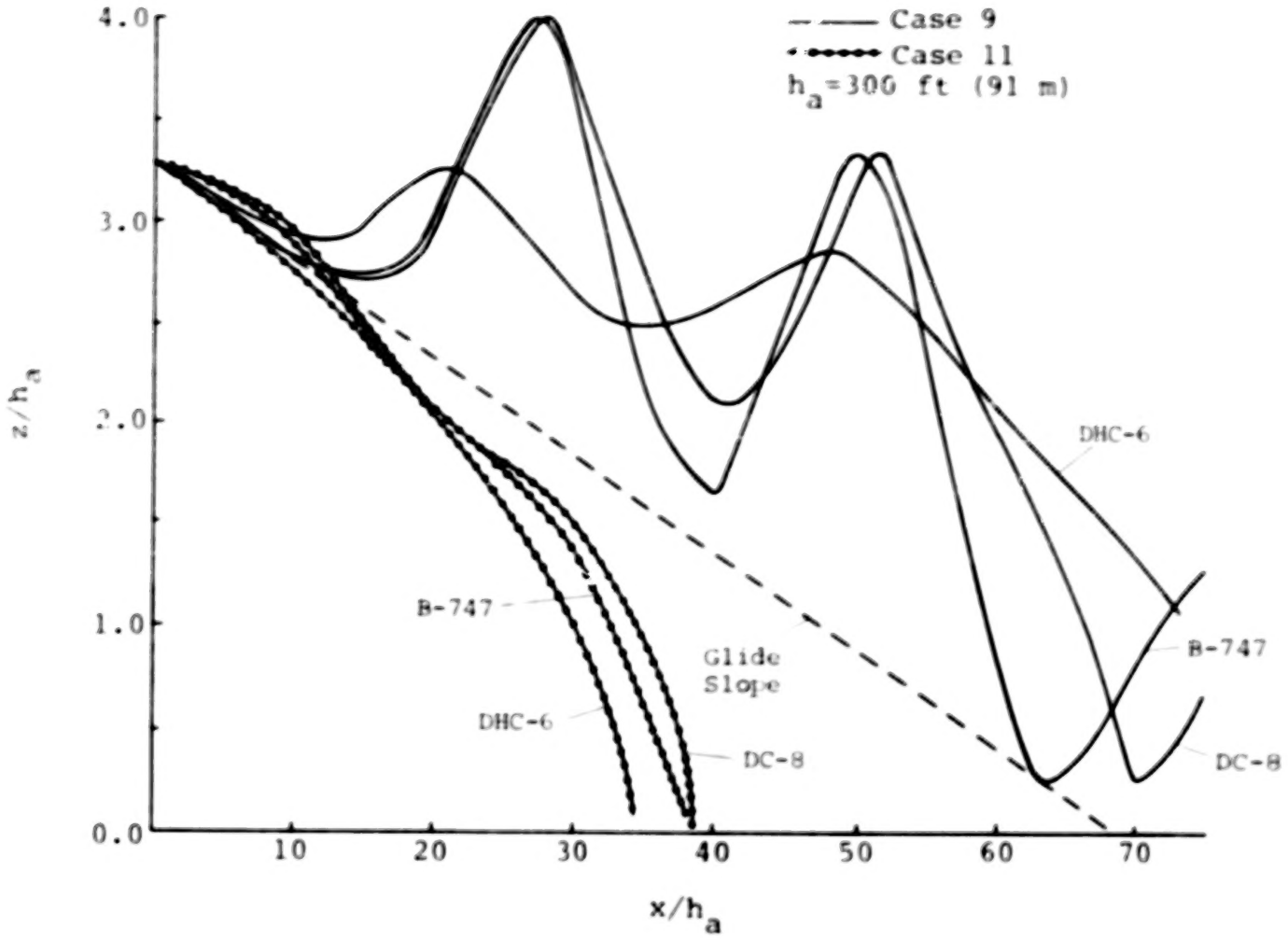

Figure 17. Comparison of aircraft landing with fixed controls in thunderstorm cases 9 and 11 from 1,000-ft (305 m) level, glide slope -2.7°.

aircraft involved are DC-8, B-747, and DHC-6. As to be expected in a non-equilibrium condition, none of the flights follow the established glide angle. In fact, the deviations shown are quite extreme and tend toward intolerable values. For Case 9 the aircrafts' phugoid oscillation is wildly excited. The frequency of oscillation for the aerodynamically similar DC-8 and B-747 is approximately the same, except for a slight phase shift. The oscillation of the slower, lighter DHC-6 is less pronounced, but still very much present. The non-linear, computer-simulated values and the linear-predicted values of the phugoid period and characteristic wavelength are presented in Table 2. The predicted values for the phugoid period are given by Etkin [13] as $T = \sqrt{2}\,\pi\, V_a/g$. The phugoid wavelength λ is then found from $\lambda = VT$, and non-dimensionalized as $\hat{\lambda} = \lambda/h_a$, where h_a = 300 ft (91 m). Notice that the simulated values from Figure 17 for a DC-8 and B-747 correspond closely with the linear-predicted values, but this relation does not hold true for the DHC-6. Table 2 also shows the phase shift between the DC-8 and B-747, which is dependent on the landing speed of the aircraft.

Tabulated values of the deviation from the expected touchdown point presented in Table 3 provide an indication of the severity of the wind shear effects due to the proportionality between the wind and deviation from the touchdown point, as mentioned previously. Many of the flights are forced to land short, a tragic event by any margin, as proved by examining wind shear related NTSB aircraft accident reports (see [2] through [5]). Overshooting of the touchdown point is not as alarming since a go-around can almost always be executed. The variability in the range of touchdown points is also indicated by Table 3.

Table 2. Phugoid Period and Horizontal Wavelength

Aircraft	V_a (ft s^{-1} [m s^{-1}])	T(sec)			λ(ft [m])			λ		
		Computed	Predicted	ε	Computed	Predicted	ε	Computed	Predicted	ε
DC-8	230 [70]	29.9	31.7	1.8	7,152 [2,180]	7,228 [2,203]	76 [23]	23.84	24.09	0.25
B-747	217 [66]	28.8	30.0	1.2	6,780 [2,067]	6,840 [2,085]	60 [18]	22.6	22.8	0.2
UHC-6	150 [46]	27.1	20.7	6.4	7,890 [2,405]	3,333 [1,016]	4,556 [1,390]	26.3	11.11	15.19

ε: |computed value - linear-predicted value|.

Table 3. Deviation from Touchdown Point for Condition 1
(Aircraft Trimmed at 1,000-Ft (305 m) Level for 2.7° Glide Slope)

Aircraft	Thunderstorm Case Number										
	1	2	3	4	5	6	7	8	9	10	11
DC-8	OD	OD	-1,875 (-572)	OS	-3,225 (-983)	OD	-7,425 (-2,263)	-8,025 (-2,446)	OS	OD	-9,150 (-2,788)
B-747	OD	OD	-2,100 (-640)	OS	-3,225 (-983)	-2,250 (-686)	-7,725 (-2,355)	-8,475 (-2,583)	OS	-1,800 (-550)	-9,450 (-2,880)
DHC-6	-8,550 (-2,606)	OD	-2,850 (-864)	+1,875 (+572)	-5,250 (-1,600)	-2,550 (-777)	-8,700 (-2,652)	-7,725 (-2,355)	OS	OS	-10,350 (-3,155)

±n: Distance from touchdown point in feet (meters).

OS: Severe overshoot--actual value not computed before exhausting data.

OD: Out of data range.

To assess the influence of shear in the longitudinal wind relative to that in the vertical wind, Figure 18 for Case 9 was employed. In this figure, landing with both wind components is compared to landings with only the individual wind components. Consider the line marked "glide slope" as the no-wind condition. This is the path the aircraft is initially trimmed to follow. However, after introducing a vertical wind component, W_z, only, one observes from Figure 18 that a slight departure from the glide slope occurs. A hint of phugoidal excitation is present also. With only a longitudinal wind component, W_x, the departure from the glide slope essentially coincides with the flight path for the total wind field. This suggests that shear in the longitudinal wind is the most significant contributor to the excitation of the phugoid mode. This lends support to the conclusion of McCarthy and Blick [14] that the longitudinal wind speed wavelength of thunderstorms causes instability in the phugoid mode.

They have shown that a horizontal gust produces a large peak in the aircraft velocity perturbation and a lesser peak in altitude perturbation at the aircraft phugoid frequency. This means that if a steady sinusoidal horizontal gust input on the order of 4 knots (2.06 m s^{-1}) were encountered, the aircraft, depending on its aerodynamic characteristics, would respond with a sinusoidal velocity perturbation of approximately 40 knots (20.6 m s^{-1}). At one point in its cycle the aircraft would approach a stall speed or go below it during each sine wave cycle. These authors found that vertical sinusoidal gusts do not affect the aircraft velocity as much as horizontal gusts. They noted that three minutes before Eastern flight 66 (Boeing 727) crashed at New York's Kennedy Airport on June 24, 1975, a light aircraft

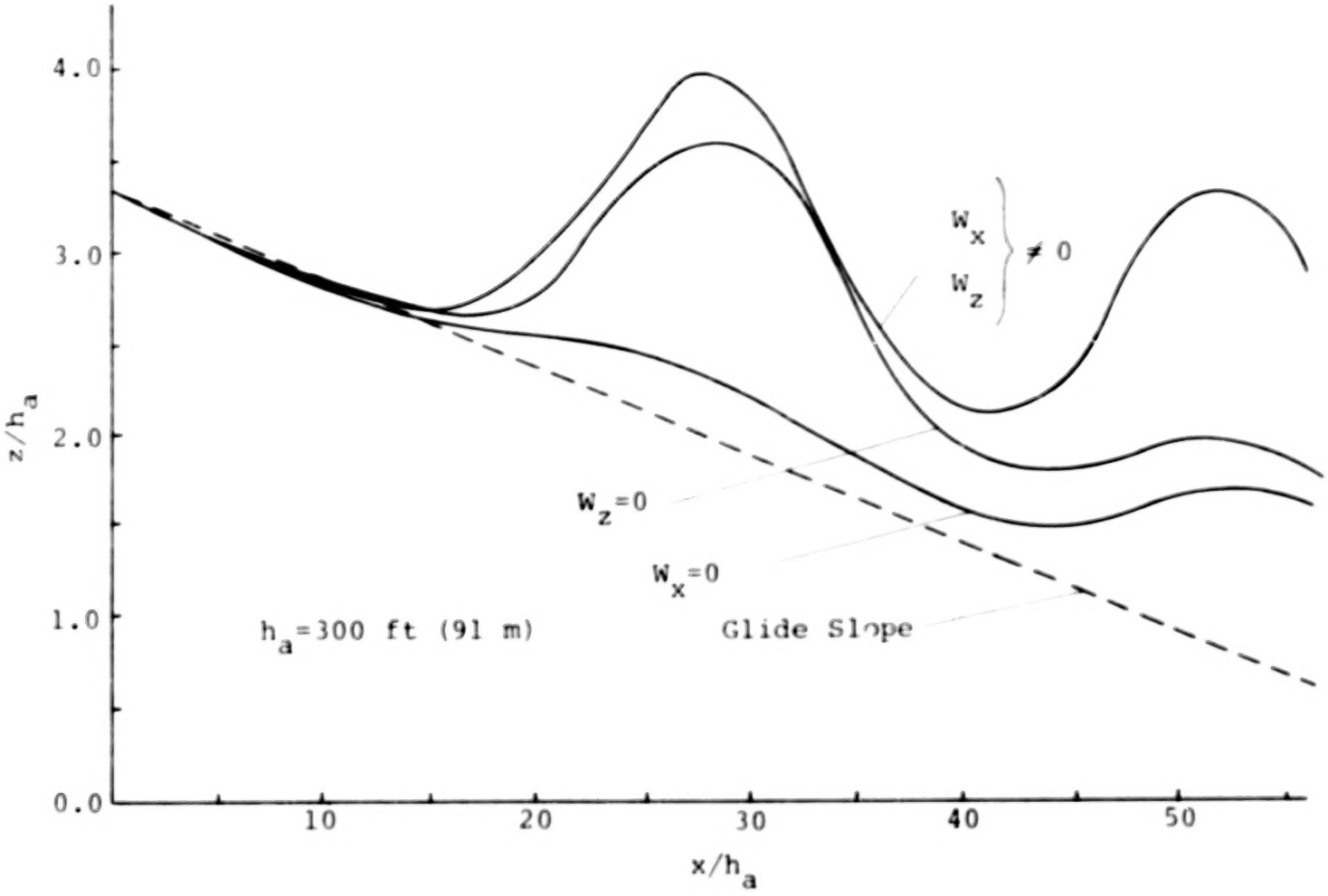

Figure 18. Comparison of DC-8 landing with fixed controls in thunderstorm case 9 considering individual wind components and both wind components.

(Beechcraft Baron) made a successful landing, although it did experience a heavy sink rate and an airspeed drop of 20 knots (10.3 m s^{-1}). Their premise is that medium-size jet transport aircraft tend to experience larger excursions in velocity and altitude when flying through horizontal gusts having large spectral components near the phugoid frequency than do lighter aircraft. This observation is in complete agreement with the results shown in Figure 17.

On the other hand, Fujita [15] analyzed the same Eastern 66 accident and attributes the accident to the strong downburst resulting from flying through the center of the down draft zone of the thunderstorm's cell. Figure 19 shows the flight path of a DC-8 type aircraft landing through the wind field associated with the Kennedy accident as tabulated for computer application by Keenan [16]. Results for the case of the total wind field (flight path A) and for the case where each wind component is individually set equal to zero are shown (flight path B, $W_x = 0$; flight path C, $W_z = 0$). On top of the figure are shown the wind speeds encountered along flight path A.

The interesting observation is that the downburst of approximately $W_z = 12$ m s^{-1} at $x/h_a = 18.5$ applied separately would cause the aircraft with fixed controls to crash at approximately $x/h_a = 30$. However, when coupled with the increasing headwind, the aircraft manages to negotiate the severe down drafts and land although experiencing large amplitude oscillations. The horizontal wind shear component alone causes less severe flight conditions.

It appears that the combined effect of both wind shear components is important. Had the longitudinal wind speed been shearing out, i.e., a decreasing headwind, the aircraft would have landed even shorter.

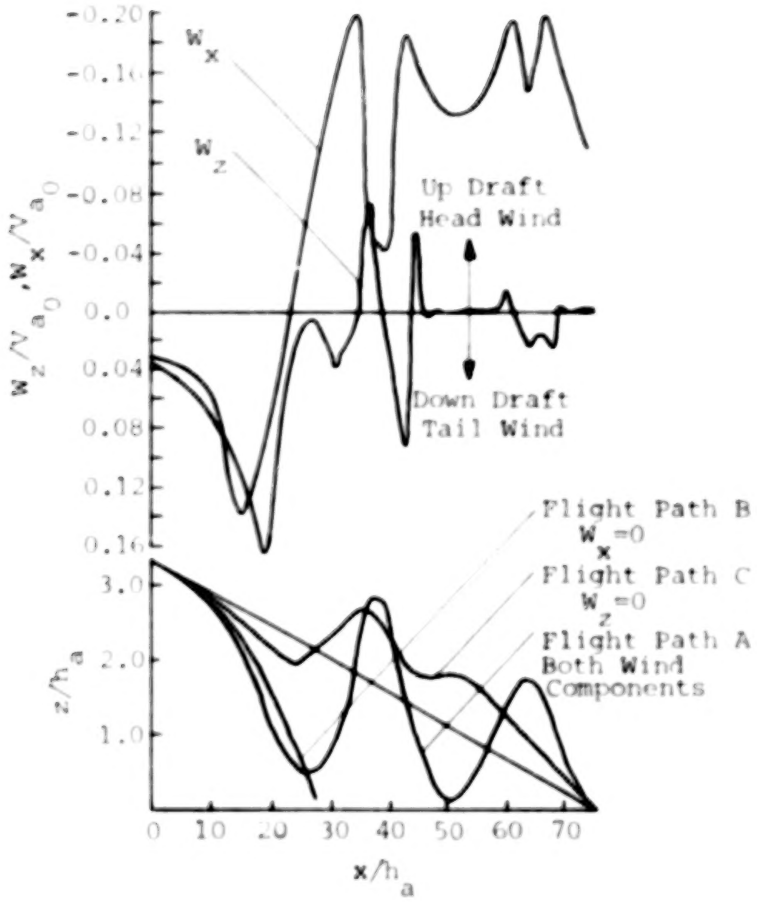

Figure 19 DC-8 type aircraft landing with fixed controls in windfield associated with JFK Eastern 66 accident and winds encountered along flight path A.

Therefore, the conclusion of Blick, et al. [17] are not confirmed in this study. Further study is required to determine how longitudinal and lateral wind shears combine to create hazardous effects.

Comparing the DC-8 and B-747 flight path angle γ and indicated airspeed V_a landing through the two representative wind fields (Figures 20, 21, and 22) contributes a broadening picture of aircraft behavior with fixed controls in thunderstorms. The initial trimmed condition of flight path angle (Figure 20) is -0.04712 radian (or -2.7°) and is represented by the broken line. Deviation from this line is the perturbed flight from the specified glide slope. For Figures 21 and 22, the indicated airspeed is non-dimensionalized with the initial aircraft velocity relative to the air V_{a_o}, and is plotted against the non-dimensionalized horizontal distance $\hat{x}$, resulting in a unique speed profile for each of the two aircraft considered. Figure 21 indicates that the airspeed reaches a low of 118 kts (61 m s^{-1}) twice for the DC-8 model, and two independent lows of 105 kts (54 m s^{-1}) and 100 kts (52 m s^{-1}) for the B-747. All four low points are attained at a pitch angle of 0.0 radian. The level stall speed for a DC-8 and a B-747 is 113 kts (57 m s^{-1}) and 108 kts (55 m s^{-1}), respectively, which indicates the DC-8 aircraft is operating at an unsafe margin above stall and the B-747 would stall. Stall, at the altitudes indicated by Figures 7 and 12, pages 20 and 25, respectively, could prove to be catastrophic since recovery may not be possible. The flight path angle and IAS curves for flight through Case 11 for the two aircraft appears more "tame" than for the previous example, Case 9. In fact, the two lowest points of Figure 22, representing $V_{a_{DC-8}}$ = 127 kts (66 m s^{-1}) and $V_{a_{B-747}}$ = 120 kts (62 m s^{-1}), are reasonably above the stall speeds

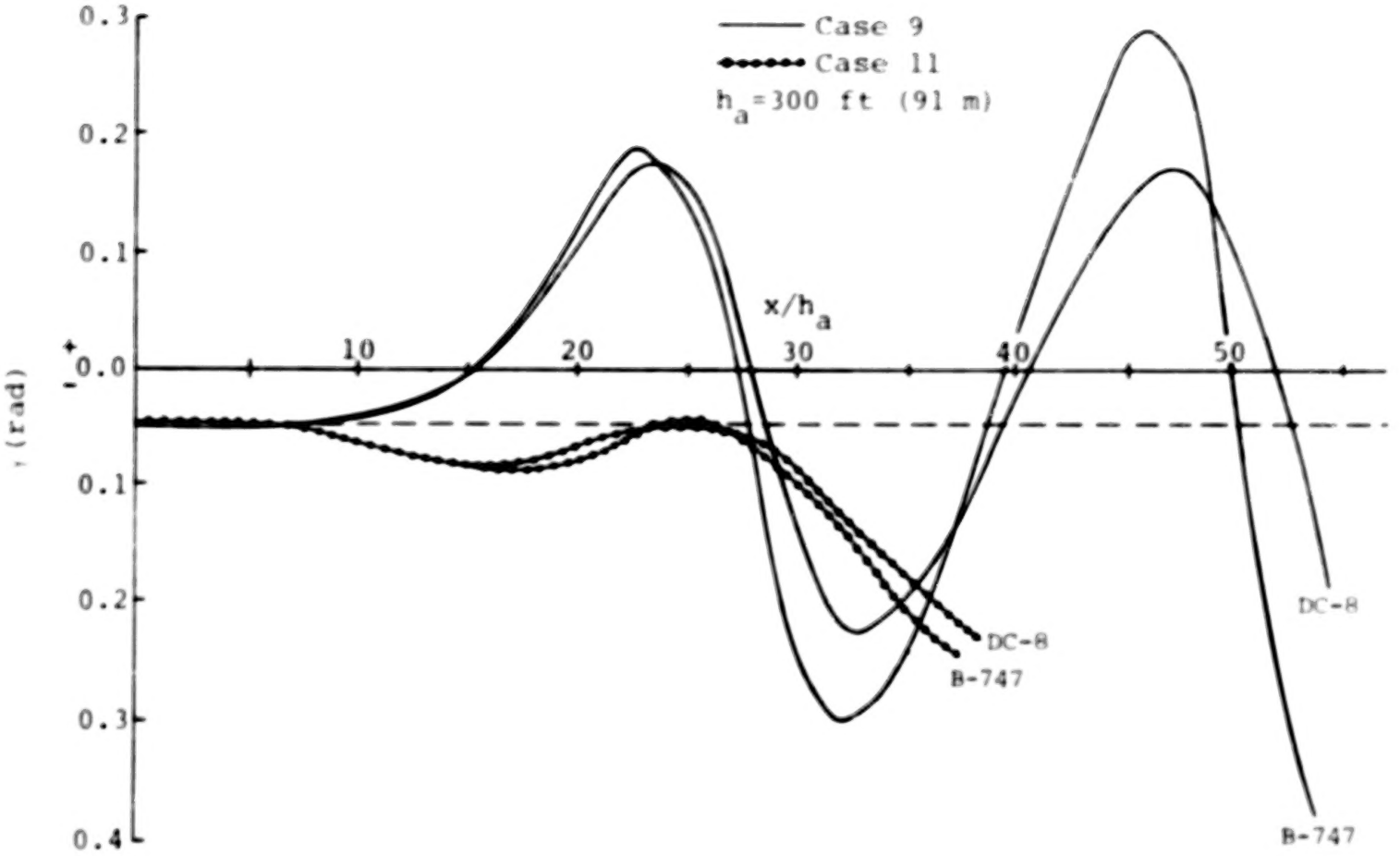

Figure 20. Comparison of flight path angle of DC-8 and B-747 landing with fixed controls in thunderstorm cases 9 and 11.

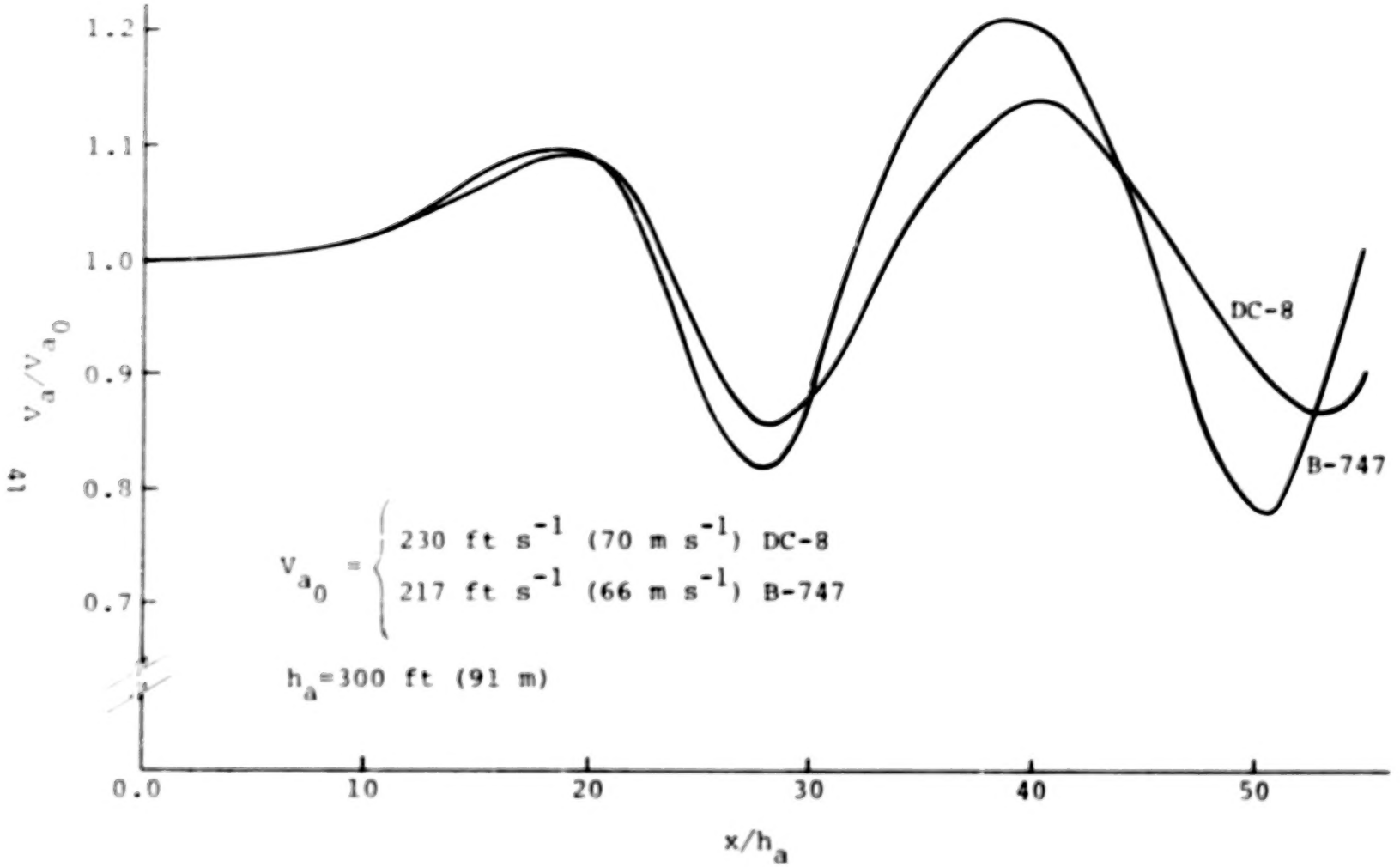

Figure 21. Comparison of indicated airspeed of DC-8 and B-747 landing with fixed controls in thunderstorm case 9.

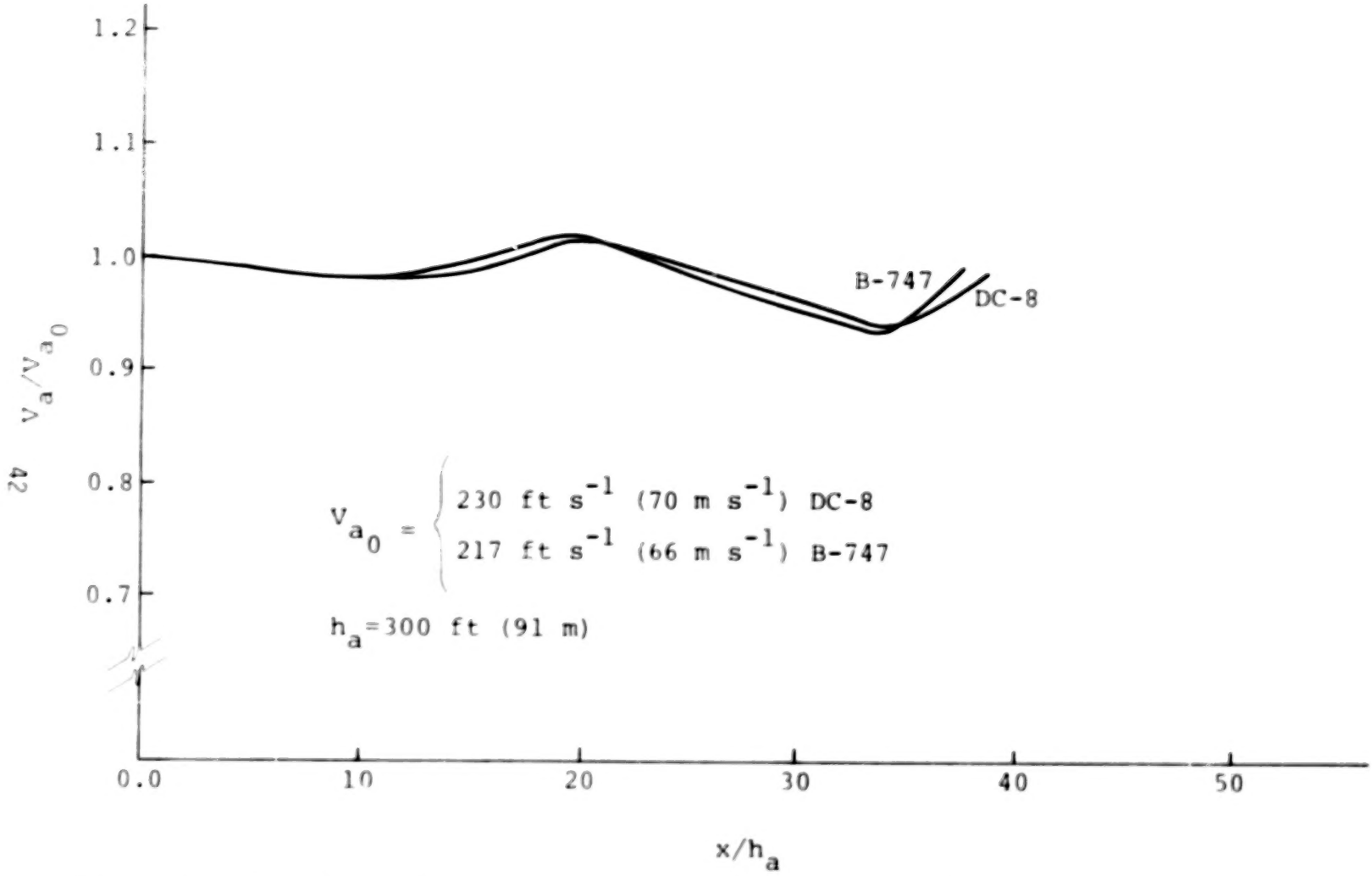

Figure 22. Comparison of indicated airspeed of DC-8 and B-747 landing with fixed controls in thunderstorm case 11.

for the respective aircraft. Since these minimum velocities occur at an angle other than $\gamma = 0$, the stall speeds are found by the following equations:

$$V_{S_{DC-8}} = 147 \text{ kts}/1.3 \cos \gamma \text{ or } 74 \text{ m s}^{-1}/1.3 \cos \gamma$$

and

$$V_{S_{B-747}} = 140 \text{ kts}/1.3 \cos \gamma \text{ or } 71 \text{ m s}^{-1}/1.3 \cos \gamma \quad [18] .$$

Before proceeding to the next figure, a discussion of ground effect calculations used in this study is necessary. For the DC-8 and B-747 the ground effect terms included in the equations of the aerodynamic coefficients are dissimilar in nature, but the effects are approximately the same. It was found from flight path studies in which 15 comparison flights were conducted (4 for DC-8 and 11 for B-747), that inclusion of ground effect had negligible effect on the flight path (see Figure 23). However, the ground effect terms for the augmentor-wing STOL are an important consideration because they come into play at a much higher altitude--close to 200 ft (61 m) AGL. The specific ground effect terms used in these computations are given below for a DC-8, B-747, and augmentor-wing STOL [19]:

For DC-8:

$$\Delta C_{L_{GE}} = 0.063(C_{L_\infty})_{GE} ,$$

$$\Delta C_{D_{GE}} = (-0.02 + 0.332 \alpha')_{GE} ,$$

$$\Delta C_{m_{GE}} = 0.066(C_{L_\infty})_{GE} ,$$

where

$$\phi_{GE} = 0.972\, e^{-h/17} ,$$

$$h = \text{wheel height} ,$$

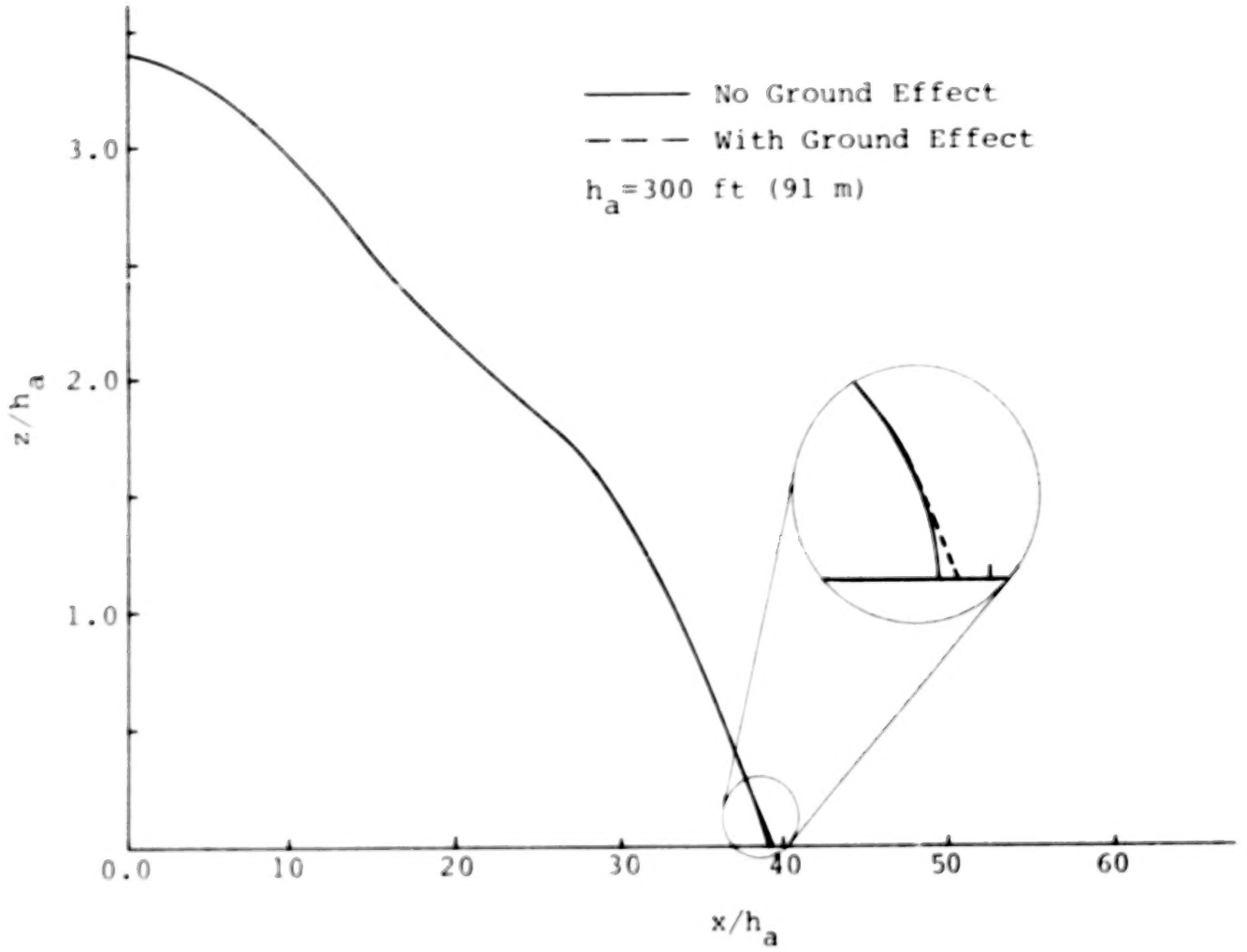

Figure 23. Example of the role of ground effect terms.

C_{L_∞} = free stream value of C_L .

For B-747:

$$\Delta C_{L_{GE}} = K^B_{GE}(0.240)\cos[8.036(\alpha' - 0.00526)] ,$$

$$\Delta C_{D_{GE}} = K^A_{GE}(2.308\ \alpha'^3 - 0.9796\ \alpha'^2 - 0.1769\ \alpha' - 0.00384) ,$$

$$\Delta C_{m_{GE}} = K^B_{GE}(2.736\ \alpha'^2 - 0.621\ \alpha' - 0.115) ,$$

where

$$K^A_{GE} = 1.7034\text{x}10^{-6}\ h^3 - 1.0736\text{x}10^{-4}\ h^2 - 1.4813\text{x}10^{-2}\ h + 1.0 ,$$

$$K^B_{GE} = 3.7906\text{x}10^{-6}\ h^3 - 4.937\text{x}10^{-4}\ h^2 + 2.807\text{x}10^{-3}\ h + 1.0 ,$$

noting the ground effect terms are included only during the last 82.5 ft (25.0 m) of flight.

The ground effect terms for the STOL aircraft are more important than for conventional aircraft. The complexity of these terms is also increased and given by:

$$C_{L_{WB_{GE}}} = [\ C_{L_{C_j}}\ C_j(1 - q/q_\infty) + C_{L_{WB_\alpha}}\ q/q_\infty\ ][\ 1/(\ 1 - \frac{\Delta\alpha}{C_L})\ C_{L_{WB_\alpha}}\ ] ,$$

$$\Delta C_{D_{GE}} = (\ C_{D_o} + C_{D_\alpha}\ \alpha'\ )(q/q_\infty - 1) - [\ C^2_{L_{WB_\infty}}\ (\frac{\Delta\alpha}{C_L})\ ](q/q_\infty)$$

$$+ (1 - q/q_\infty)C_{D_{C_j}}\ C_j ,$$

$$\Delta C_{m_{GE}} = (\ C_{m_o} + C_{m_\alpha}\ \alpha'\ )(q/q_\infty - 1) + C'_{m_\alpha}\ (\frac{\Delta\alpha}{C_L})\ C_{L_{WB_{GE}}}$$

$$+ C_{m_{C_j}} C_j(1 - q/q_\infty) ,$$

where

$$q/q_\infty = \left\{1 + \frac{C_{L_{\alpha_B}}}{8\pi\, h/\bar{c}}\left[1 + 16\left(\frac{h}{\bar{c}\cdot AR}\right)^2\right]^{-1/2}\right\}^{-2} ,$$

$$\frac{C_{L_\alpha}}{C_L} = \left\{2\pi\, AR\left[1 + 16\left(\frac{h}{\bar{c}\cdot AR}\right)^2\right]\right\}^{-1} ,$$

and

C_j = thrust coefficient = 0.75 (for this study).

For the DHC-6 ground effect terms were unknown, and consequently, their influence was not assessed.

The influence of glide slope angle on the flight paths through the storm is considered next. In Figure 24 the spatial position of the aircraft during landing is shown for the augmentor-wing STOL, DHC-6, and B-747 in thunderstorm Cases 9 and 11. Notice that two glide slopes, 6° and 7°, are indicated in the illustration. The glide slope of 7° is the initial trim condition for the STOL and DHC-6 Twin Otter and is representative of the usual approach angle for this type of aircraft. The 6° glide slope is the initial trim condition for the B-747 and is included to investigate the effect of approach angle on alleviation of the wind shear hazard. This 6° glide slope is not unusual for a two-step ILS approach [20]; however, the aircraft usually establishes the standard 2.7° approach angle, at a given altitude, for the duration of the flight. In this study, however, the B-747 was not allowed to make the transition to a reduced approach angle, and thus is

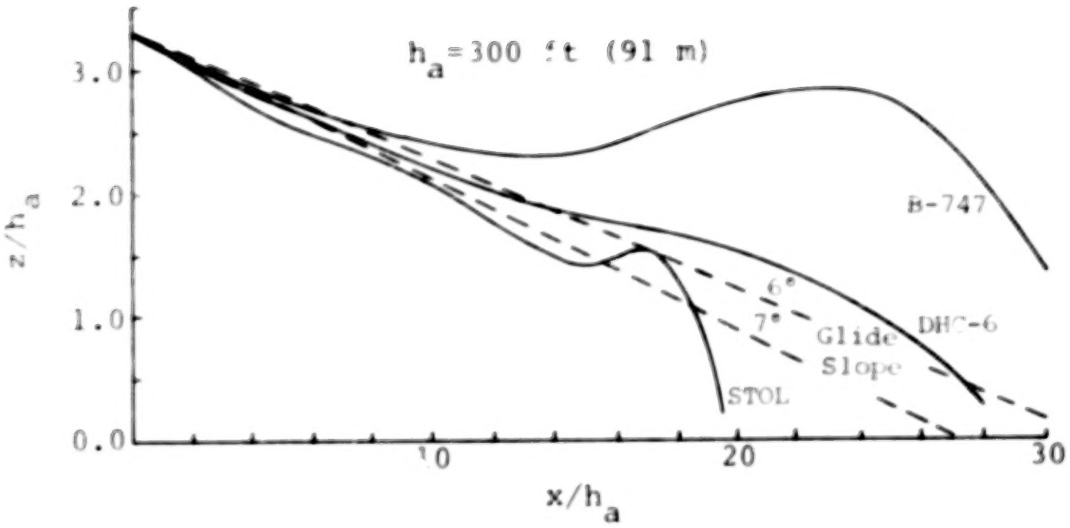

(a) Case 9 comparison

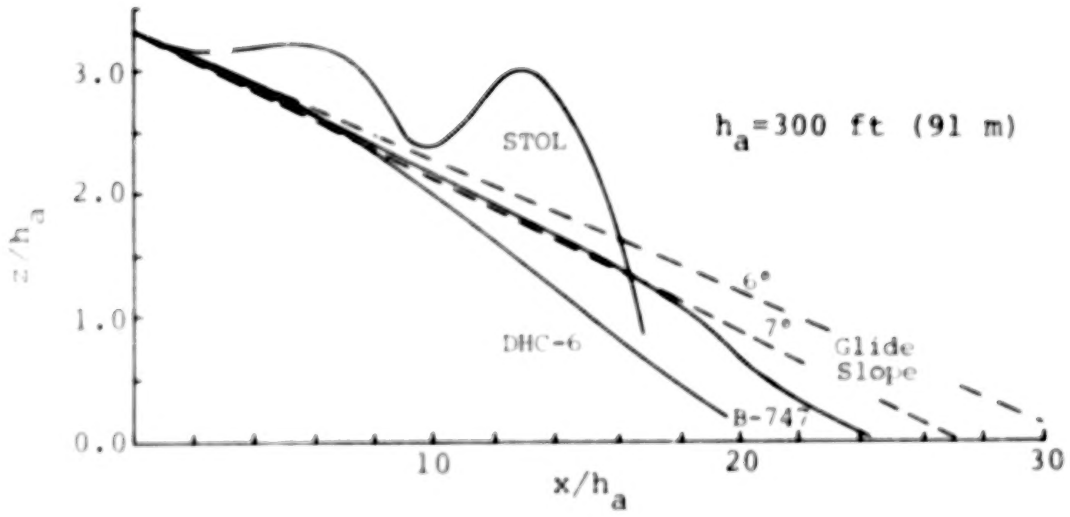

(b) Case 11 comparison

Figure 24. Flight path comparison of aircraft landing with fixed controls from 1,000-ft (305 m) level with increased approach angle in thunderstorm cases 9 and 11.

forced to land steep. Landing the aircraft steeply provided information on the effect of increased glide slope angle on conventional aircraft.

The influence of glide slope angle is investigated only for Cases 9 and 11 which are indicative of all flights in this phase of the study, except for augmentor-wing STOL Cases 7 and 8, which loop at a low altitude. As noted previously, this loop characteristic is most probably related to the inability of the STOL aircraft to maintain a stable condition with fixed controls through these particular thunderstorm cases and is not considered a realistic simulation. B-747, Case 9, has the most extreme departure from the glide slope, but a majority of the B-747 flights follow similar trajectories. The DeHavilland Twin Otter's flight path is an appreciably damped version of the phugoidal motion experienced for cases where previously the glide slope was -2.7°. This is also true, to a reasonable extent, for the B-747 (refer to Figure 12, page 25, and Figure 24). This observation tends to suggest an inverse relationship between wind shear effects and approach angle, as evident from inspection of Table 4.

Figure 25 illustrates the flight paths for the STOL and DHC-6 aircraft entering at the 300-ft (91 m) level. Note that the B-747 was not run from the 300-ft (91 m) level with a 6.0° glide slope; therefore, it is excluded from the figure. Examination of this figure shows that the violent phugoid oscillations present for entry at the 1,000-ft (305 m) level (see Figure 24) have yielded to a more stable flight. Only the augmentor-wing STOL has a remanent oscillatory motion. Because of a strong damping effect, brought about by increased glide slope angle (-7°) and decreased initial shear encounter altitude

Table 4. Comparison in Touchdown Point Deviations from the 1,000-Ft (305 m) Level Using Different Glide Slope Angles

Aircraft	Thunderstorm Case Number 1	2	3	4	5	6	7	8	9	10	**	Remarks
Augmentor-wing STOL	-3,105 (-946)	OD	-2,955 (-901)	OD	-2,385 (-727)	OD	LP	LP	OD	-2,265 (-690)	-3,405 (-938)	Condition 2
DHC-6 Twin Otter	-270 (-82)	+405 (+123)	+180 (+55)	+480 (+146)	-945 (-288)	+330 (+101)	-1,570 (-479)	-1,020 (-311)	+330 (+101)	+630 (+192)	-1,958 (-597)	Condition 2
	8,280 (2,525)	UNK	2,670 (814)	1,395 (425)	4,305 (1,312)	8,370 (2,550)	7,170 (2,045)	6,705	UNK	UNK	8,352 (2,560)	Improvement over Condition 1; n:distance closer to T.D. point
B-747	-690 (-210)	+1,290 (+393)	+840 (+256)	+1,770 (+540)	-810 (-247)	+450 (+137)	-1,650 (-503)	-660 (-202)	+690 (+210)	+1,470 (+448)	-2,190 (-668)	Condition 3
	UNK	UNK	1,260 (384)	UNK	2,415 (736)	1,800 (550)	6,075 (1,852)	7,815 (2,382)	UNK	330 (100)	7,260 (2,213)	Improvement over Condition 1; n:distance closer to T.D. point

*n: Deviation from touchdown point in feet (meters). LP: Looped.

OD: Out of data range. UNK: Difference not calculable, previous value unknown.

Condition 1: Aircraft trimmed at 1,000-ft (305 m) level for -2.7° glide slope.

Condition 2: Aircraft trimmed at 1,000-ft (305 m) level for -7.0° glide slope.

Condition 3: Aircraft trimmed at 1,000-ft (305 m) level for -6.0° glide slope.

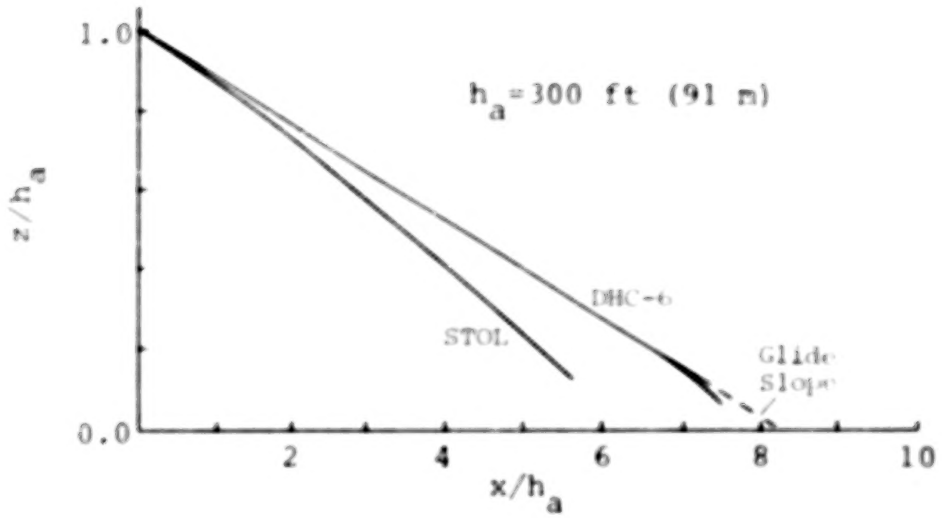

(a) Case 9 comparison

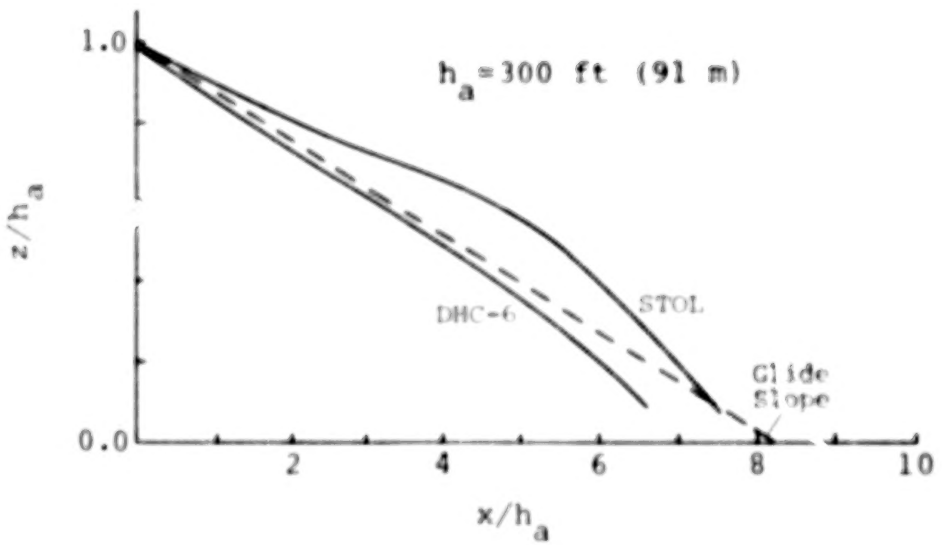

(b) Case 11 comparison

Figure 25. Flight path comparison of STOL and DHC-6 landing with fixed controls from 300-ft (91 m) level, glide slope -7.0°, in thunderstorm cases 9 and 11.

(z = 300 ft = 91 m), many of the flights land within close proximity to the desired touchdown point, as shown in Table 5.

Table 5 shows the influence of height at which the aircraft enters the wind field on the departure from expected touchdown. It is shown that less deviation in touchdown occurs for entry at a lower altitude than for entry at a higher altitude. Of course, this effect is strongly dependent on the characteristics of the storm and the particular point of entry. These deviations are felt to be representative since eleven arbitrary thunderstorms are considered. However, considerably more simulations starting at different positions in the flow field are necessary before any positive conclusions can be drawn.

Automatic Controls

Figure 36 illustrates several of the test simulations using fixed controls, automatic controls, and flight with turbulence with airplane characteristics of a DC-8. Since the fixed control flight paths have already been reviewed in previous text and illustrations, this discussion is devoted to the automatic control landing cases. From the figure it is seen that Cases 1, 2, and 9 remain on the desired ILS glide slope until flare initiation altitude, at which time the DC-8 prepares to land. On the other hand, Case 11 assumes an altitude slightly below the glide slope--a condition arising from the combination of sustained head wind and severe vertical downdraft sufficiently strong that the automatic landing system could not overcome it. However, the DC-8 does flare to land "on target." For the simulation having turbulence effects included (Case 1), the resulting

Table 5. Comparison in Horizontal Deviation from Touchdown Points from Different Altitudes with Different Glide Slope Angles

Aircraft	Thunderstorm Case Number											Remarks
	1	2	3	4	5	6	7	8	9	10	11	
Augmentor-wing STOL	-417 (-127)	-132 (-40)	-837 (-255)	-12 (-4)	-942 (-287)	+258 (+79)	-282 (-86)	-132 (-40)	-567 (-173)	-792 (-241)	-102 (-31)	Condition 4
	2,688 (819)	UNK	2,118 (645)	UNK	1,443 (440)	UNK	UNK	UNK	UNK	1,473 (450)	2,943 (897)	Improvement over Condition 2; n.distance closer to T.D. point
DHC-6 Twin Otter	-402 (-123)	+1,533 (+467)	+78 (+24)	-72 (-22)	+33 (+10)	-72 (-22)	-162 (-49)	-162 (-49)	-36 (-11)	-72 (-22)	-345 (-104)	Condition 4
	-132 (-40)	-1,128 (-344)	102 (31)	408 (124)	912 (278)	258 (79)	1,368 (417)	858 (262)	294 (90)	558 (170)	1,616 (493)	Improvement over Condition 2; n:distance closer to T.D. point; minus values indicate increased landing distances
	8,148 (2,485)	UNK	2,772 (845)	1,803 (550)	5,217 (1,590)	2,478 (755)	8,538 (2,600)	7,563 (2,305)	UNK	UNK	10,008 (3,050)	Improvement over Condition 1

ft: Deviation from touchdown point in feet (meters).

UNK: Difference not calculable, previous value unknown.

Condition 1: Aircraft trimmed at 1,000-ft (305 m) level for -2.7° glide slope.

Condition 2: Aircraft trimmed at 1,000-ft (305 m) level for -7.0° glide slope.

Condition 4: Aircraft trimmed at 300-ft (91 m) level for 7.0° glide slope.

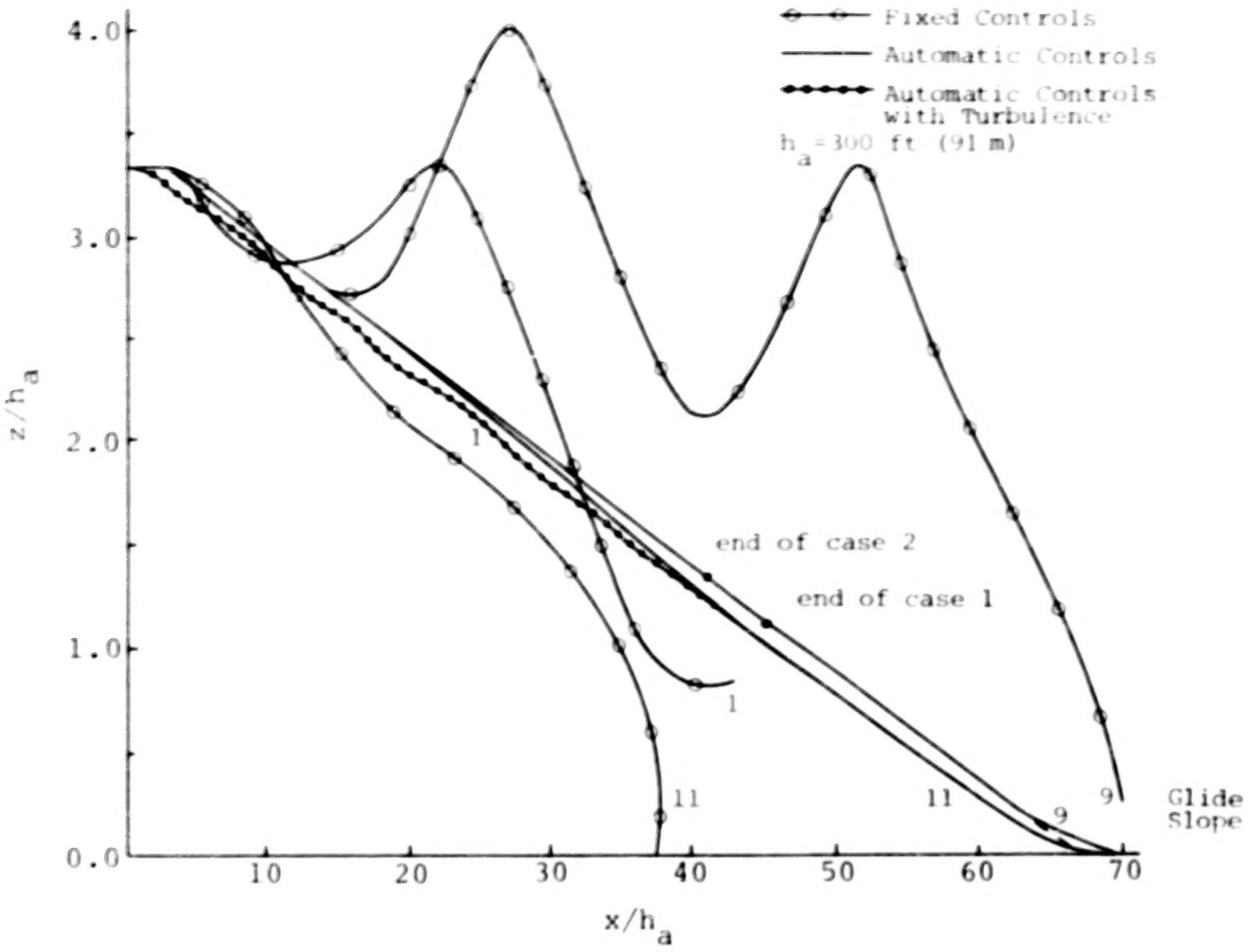

Figure 26. Flight path comparison of DC-8 landing with (1) fixed controls, (2) automatic controls, and (3) automatic controls with turbulence included, in several different thunderstorm cases.

aircraft motion exhibits a mild oscillation, due to the variability of the wind field, and also immediately departs from the desired trajectory. It should be noted, however, that each flight path will be different when turbulence is superimposed because of the random nature of the flow field. At approximately $\hat{x} = 41.5$ the DC-8 flight simulation terminates due to flight outside the wind data provided for thunderstorm Case 1.

Figure 27 and 28 illustrate typical wind profiles along a -2.7° glide slope for thunderstorm Cases 9 and 11, respectively. These wind profiles, associated with the DC-8 having automatic controls, appear considerably different from the same thunderstorm cases profiled for the DC-8 in Figure 16, page 30, since the path traced by the aircraft is different. Notice that both Cases 9 and 11 show similar longitudinal head wind components $\hat{W}_x$, but the vertical wind components W_z for the two cases differ (particularly below $\hat{z} < 2.0$). Again, the wind speeds have been non-dimensionalized with the initial airspeed V_a.

Next, consider Figure 29 which shows the thrust command signal FT as a function of time T for the DC-8 with automatic controls. FT has been non-dimensionalized by the equivalent thrust FTD for which Case 9, FTD = 2.65×10^4 lbs (1.29×10^4 kg), and for Case 11, FTD = 1.87×10^4 lbs (8.43×10^3 kg). From the literature it is quite plain that frequent and abrupt changes in thrust are necessary to maintain the specified glide slope. In fact, the time required to increase the thrust needed to maintain the desired position is often greater than the actual rate at which thrust can be increased for the DC-8 engines when encountering shear conditions. The rate at which

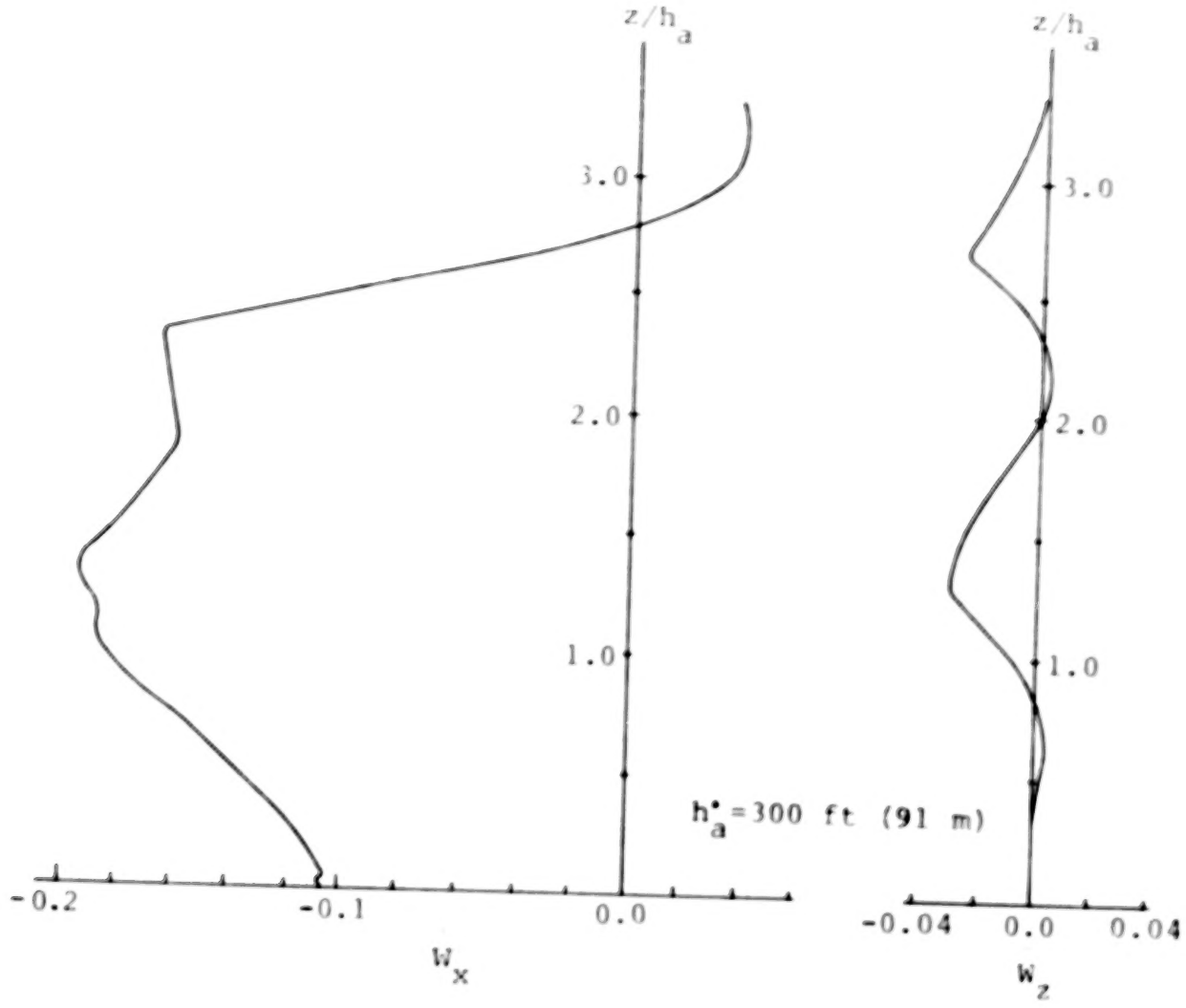

Figure 27. Typical wind profiles along a -2.7° glide slope as "seen" by DC-8 landing with automatic controls in thunderstorm case 9.

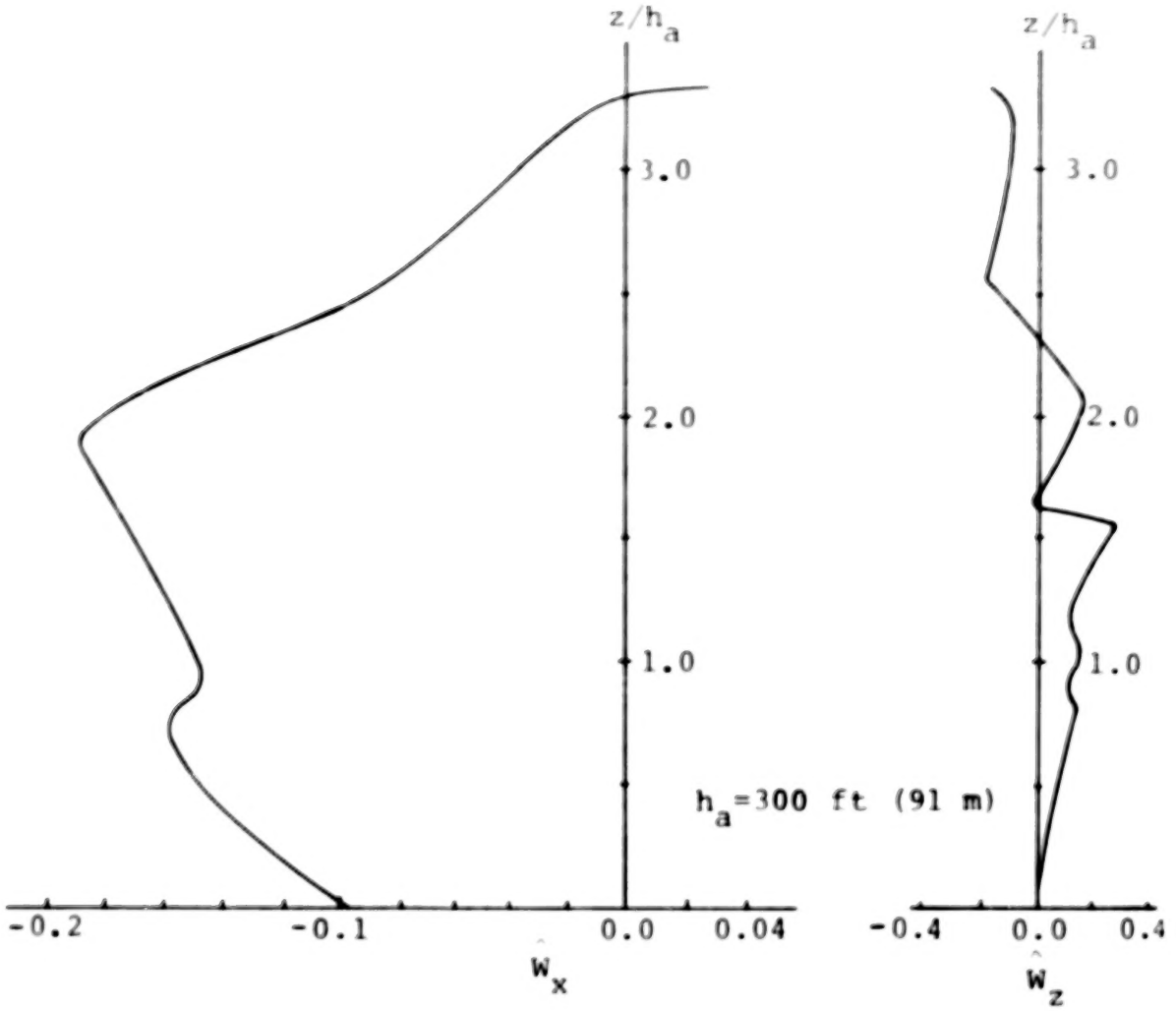

Figure 28. Typical wind profiles along a -2.7° glide slope as "seen" by DC-8 landing with automatic controls in thunderstorm case 11.

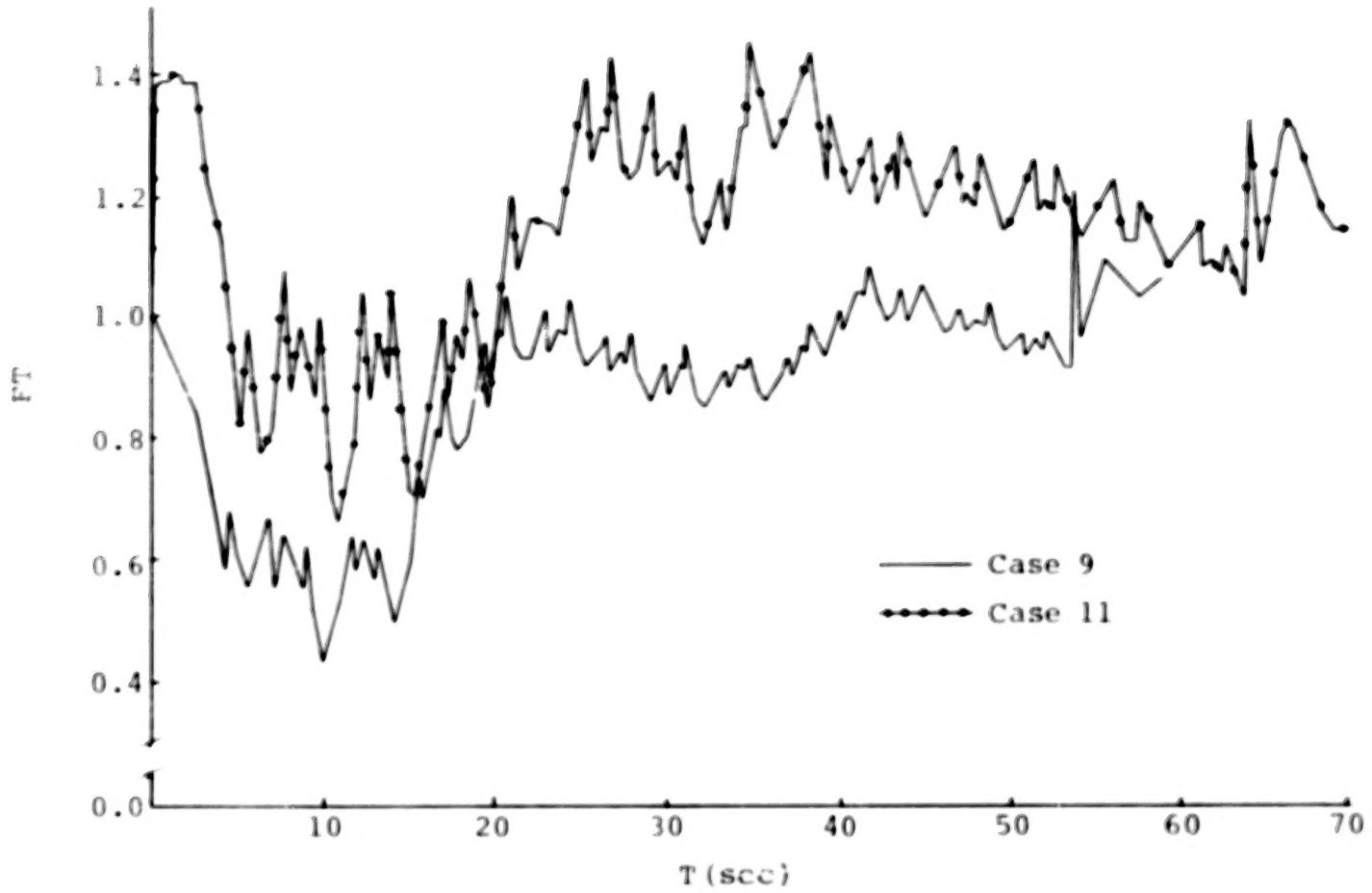

Figure 29. Rate of change of thrust required of DC-8 landing with automatic control system in thunderstorm cases 9 and 11.

thrust can be increased for the Pratt-Whitney JT-3D engines on a DC-8 is given approximately by 7.92×10^3 lbs s^{-1} (3.6×10^3 kg s^{-1}) [21]. Changes in thrust beyond the capability of the engine are not possible, thus precluding the possibility of the aircraft's remaining on the ILS glide slope. Because this maximum thrust exceedance occurs on certain excursions, a thrust rate limiter was added to the automatic control system. The approach paths followed with thrust rate limiters being utilized are compared with those having no thrust rate limitation in Figure 30. The flight path of the DC-8 type aircraft without any limit on the maximum thrust, departure from the desired trajectory is approximately 29.5 ft (9 m), whereas with the limiter, the maximum departure is 65.6 ft (20 m). The thrust rate limited aircraft does not follow ILS beam as closely in the earlier part of the approach, but both simulations do intercept the beam at approximately x = 10,500 ft (3200 m), and track precisely along the beam flaring on target.

The other important command signal, elevator angle δ_E, is represented graphically in Figures 31 and 32 as a function of time. Here, reasonable aircraft response to rate change of the elevator angle to maintain the glide slope is demonstrated by the DC-8 within thunderstorm Cases 9 (Figure 31) and 11 (Figure 32). Observation shows the maximum $d\delta_E/dt$ occurring in either of the two illustrations is

$$\left|\frac{d\delta_E}{dt}\right|_{max} = 3.3° s^{-1},$$

in Figure 31. This is well within the range of response for a DC-8, since aerodynamic response times are quite small--on the order of 10^{-3} sec [22].

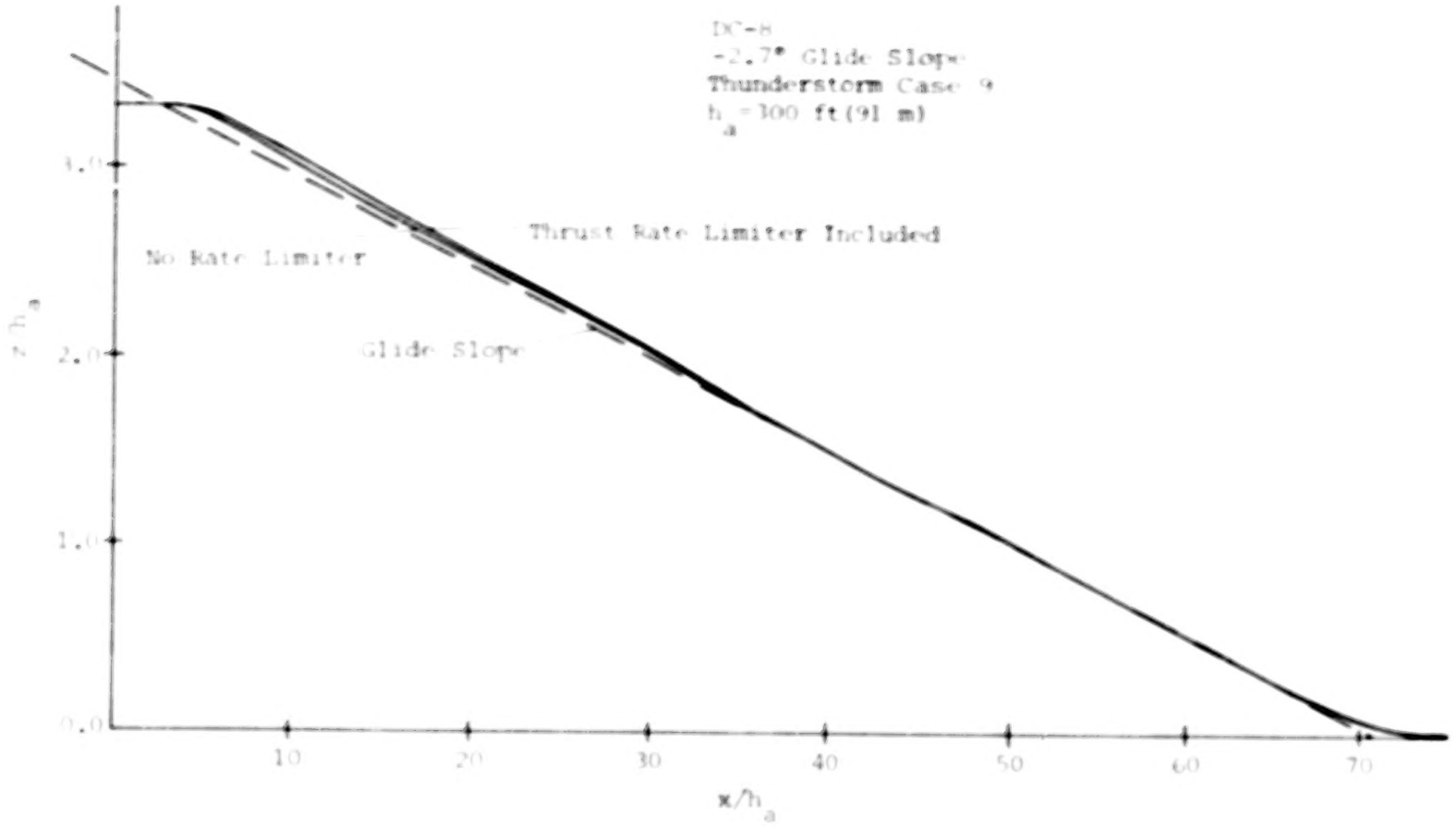

Figure 30 Comparison of flight paths for DC-8 type aircraft with and without thrust rate limiter.

TABLE OF CONTENTS

CHAPTER		PAGE	
I.	INTRODUCTION.	1	1/A13
II.	FLIGHT PATH STUDIES--BASIC CONCEPTS	5	1/B3
III.	GENERATION OF THUNDERSTORM AND TURBULENCE MODELS.	9	1/B7
IV.	RESULTS AND DISCUSSION.	17	1/C1
V.	CONCLUSION.	64	2/A9
REFERENCE LIST		66	2/A11
APPENDICES		70	2/B1
A.	EQUATIONS OF MOTION.	71	2/B2
B.	COMPUTER PROGRAM DOCUMENTATION	80	2/B11

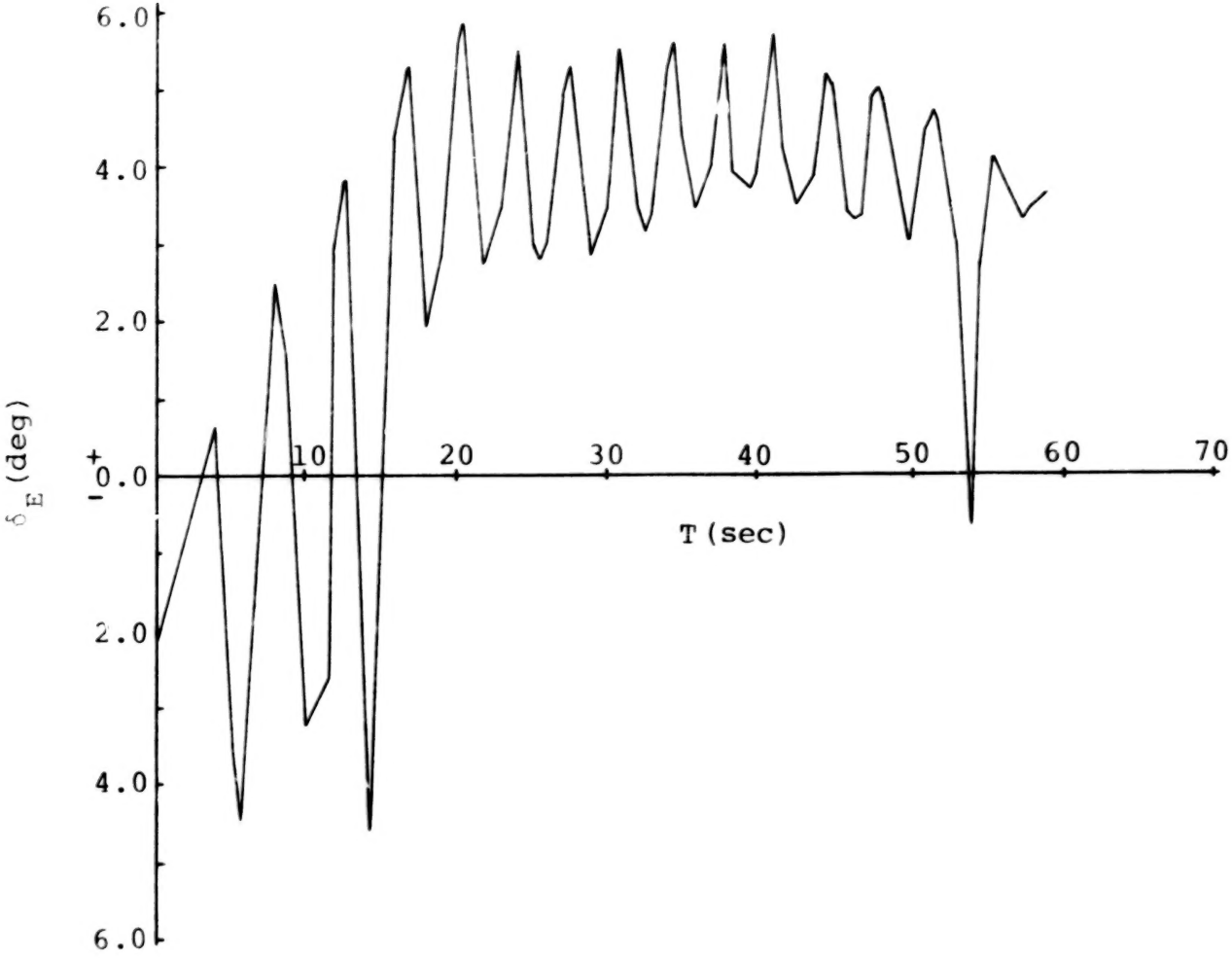

Figure 31. Rate of change of elevator angle required of DC-8 landing with automatic control system in thunderstorm case 9.

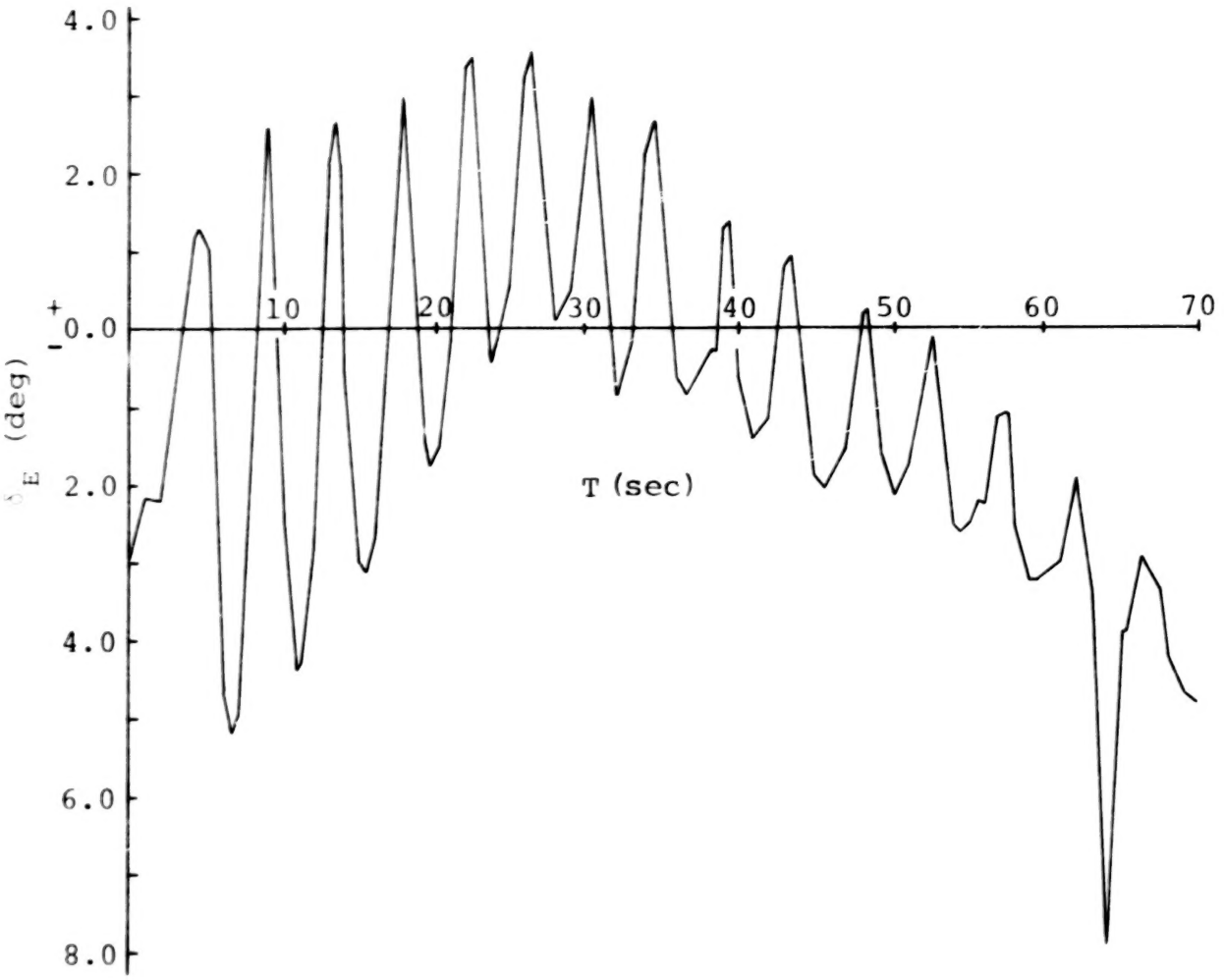

Figure 32. Rate of change of elevator angle required of DC-8 landing with automatic control system in thunderstorm case 11.

The previous discussion concerning automatic control systems is actually an "idealized" system. In this system, the control loop assumes that the variables α', $\dot{\alpha}'$, δ, and q can be monitored during the approach and fed back into the landing system to calculate the variable gains continuously along the glide slope. The idealized control loop also assumed that the ground speed components $\dot{z}/v$ and $\dot{x}/v$ are available as feedback inputs to the sevro-mechanisms for the thrust and elevator control.

An alternate or simplified automatic control loop assumes that only the relative airspeed, V_a, is monitored during the approach and is available for computing the variable gains. Additionally, this control loop does not allow for $\dot{z}$ and $\dot{x}$ as feedback input, but rather expresses $\dot{z}/V$ as $-\sin\gamma$ and $\dot{x}/V$ as $\cos\gamma$. The value of γ was set equal to zero during the hold and flare modes and then equal to the glide path angle during the capture and tracking modes.

The results of this more "conventional" landing system as opposed to the "idealized" control system may be found in Figure 33. The figure shows a DHC-6 type aircraft landing through thunderstorm Case 9 wind field. Neither simulation establishes the designated trajectory along the ILS beam. This is probably due to inadequate specification of capture control parameters for the DHC-6 type aircraft. However, the tracking control does establish a well defined trajectory which includes a successful landing. The results shown in Figure 33 are indicative of the control which can be achieved through rather severe thunderstorm wind shear with appropriate control systems.

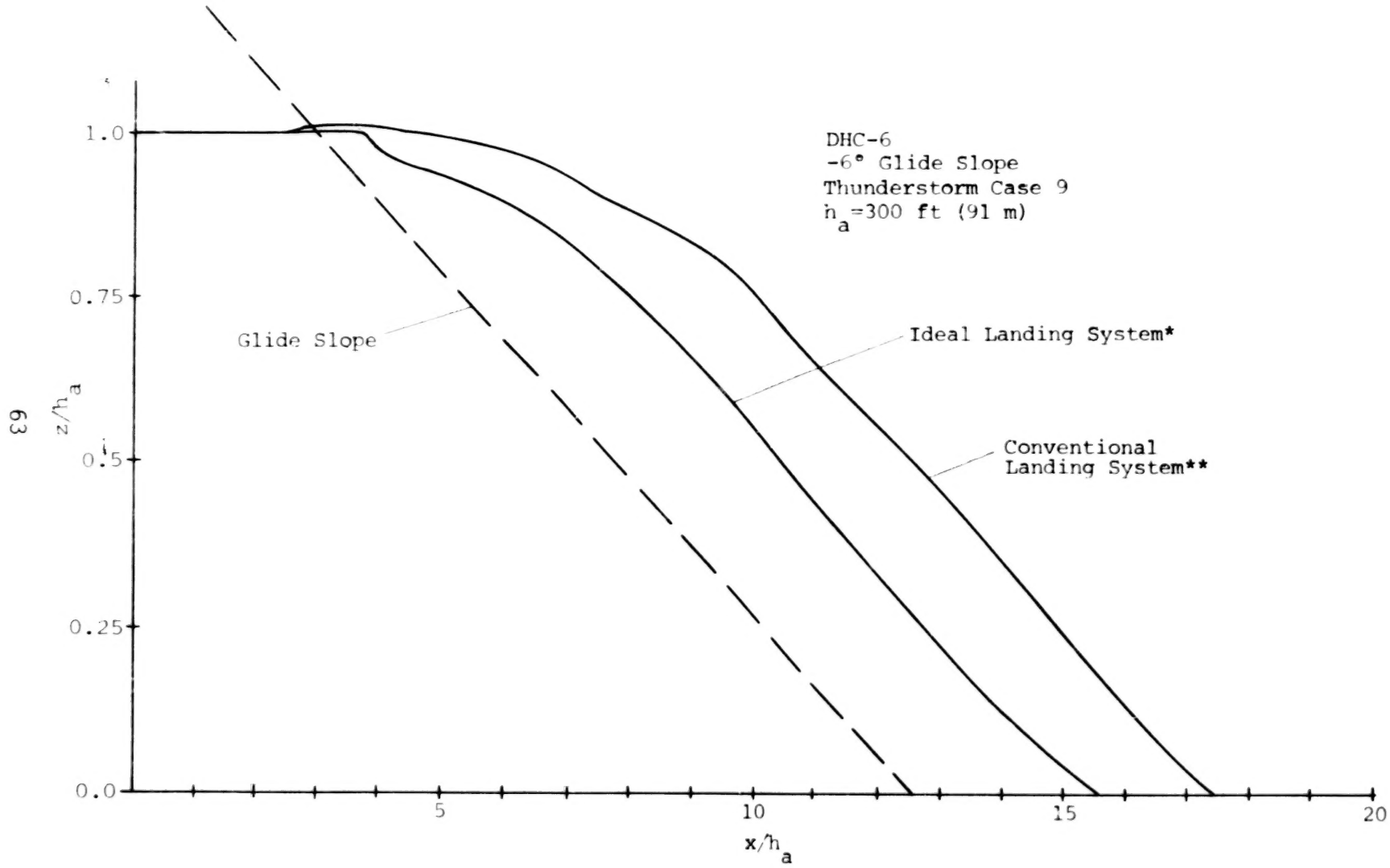

Figure 33 Comparison of flight paths with idealized and more conventional control systems for DHC-6 type aircraft.

63

CHAPTER V

CONCLUSION

From the results presented in this investigation it is evident that thunderstorm outflows are a hazard to aircraft operations in and around the airport terminal area. The danger primarily exists here, rather than during cruise flight, because of the aircraft's particular configuration (namely, little speed margin above stall, high drag, and for some airplanes, limited excess power) and because of its close proximity to the ground.

It has been shown that serious departures from the glide slope occur during landing simulations of aircraft having fixed controls (i.e., no pilot input) through thunderstorm gust fronts. Correspondingly, control inputs are large and response times are small for aircraft using an automatic control system in the same thunderstorm cases.

The results of this study show that the phugoid oscillations of aircraft with fixed controls landing through typical thunderstorm gust fronts are highly amplified. This is particularly true for the larger transport type aircraft. The amplitude of the oscillations tend to be reduced for lighter type aircraft typical of a DHC-6 Twin Otter. This is partly due to the characteristics of the aircraft and partly due to the steeper landing paths followed. The larger transport type aircraft approaching at steeper glide paths than those conventionally used in aviation operations have somewhat damped phugoid oscillations, but still experience large excursions from the desired landing path. The

strong influence of horizontal gradients in thunderstorm associated wind fields on the phugoidal oscillation support the Blick, et al. [15] hypothesis that accidents associated with commercial aircraft landing through thunderstorm gust fronts may result from the horizontal wind shear, but do not rule out that severe downburst can be equally responsible for accidents. Investigation of flight through the thunderstorm wind fields established by Fujita [16] indicate that the downburst can cause accidents. On the other hand, the downburst combined with the longitudinal wind shear, for the one case studied results in the aircraft negotiating the wind field. However, it does experience severe oscillations.

Automatic control systems using variable gains can almost completely eliminate the severe perturbations from the flight path for the 11 thunderstorm models considered in this study. This does not imply that automatic control systems can be utilized to land aircraft through thunderstorms in all situations. The thunderstorm models utilized in this study are obviously not all inconclusive and represent only the gust front portion. The automatic control systems have not been applied to the extreme downburst winds that have been reported to occur in the center of the thunderstorm cell [16]. Moreover, the computer simulation treats only two-dimensional effects and therefore excludes additional control inputs required to stabilize roll and yaw motions.

The fact that the automatic control systems do however appreciably eliminate flight path excursions tend to support the arguments that accidents in thunderstorms are not a result of aircraft limitations but often are precipitated during transition from automatic to manual control [4].

REFERENCE LIST

REFERENCE LIST

1. Goff, R. Craig. "Thunderstorm Outflow Kinematics and Dynamics," NOAA Technical Memorandum ERL NSSL-75, National Severe Storms Laboratory, Norman, Oklahoma, December, 1975.

2. National Transportation Safety Board. "Eastern Airlines, Inc., Boeing 727-225, John F. Kennedy International Airport, Jamaica, New York, June 24, 1975," Aircraft Accident Report No. NTSB-AAR-76-8, National Transportation Safety Board, Washington, D. C., March 12, 1976.

3. National Transportation Safety Board. "Continental Airlines, Inc., Boeing 727-224, N88777, Stapleton International Airport, Denver, Colorado, August 7, 1975," Aircraft Accident Report No. NTSB-AAR-76-14, National Transportation Safety Board, Washington, D. C., May 5, 1976.

4. National Transportation Safety Board. "Iberia Lineas Aereas de Espana (Iberian Airlines), McDonnell Douglas DC-10-30, EC CBN, Logan International Airport, Boston, Massachusetts, December 17, 1973," Aircraft Accident Report No. NTSB-AAR-74-14, National Transportation Safety Board, Washington, D. C., November 8, 1974.

5. National Transportation Safety Board. "Delta Airlines, Inc., Douglas DC-9-32, N3323L, Chattanooga Municipal Airport, Chattanooga, Tennessee, November 27, 1973," Aircraft Accident Report No. NTSB-AAR-74-13, National Transportation Safety Board, Washington, D. C., November 8, 1974.

6. Reddy, K. R. "Investigation of Aircraft Landing in Variable Wind Fields." Unpublished Master's thesis, The University of Tennessee, Knoxville, 1977.

7. Frost, W., D. W. Camp, and S. T. Wang. "Wind Shear Modeling for Aircraft Hazard Definition." Report prepared under Inter-agency Agreement No. DOT-FA76-WAI-620, supported by Federal Aviation Administration, Wind Shear Office, by FWG Associates, Inc., Tullahoma, Tennessee, December, 1977.

8. Low Level Wind Shear. Advisory Circular Account No. 00-50. Washington, D. C.: Department of Transportation, Federal Aviation Administration, 1976.

9. Frost, W., and D. W. Camp. "Wind Shear Modeling for Aircraft Hazard Definition." Interim report No. FAA-RD-77-36 prepared for U. S. Department of Transportation, Federal Aviation Administration, Systems Research and Development Service, by FWG Associates, Inc., Tullahoma, Tennessee, March, 1977.

10. McRuer, D., I. Ashkenas, and D. Graham. Aircraft Dynamics and Automatic Control. Princeton, New Jersey: Princeton University Press, 1973.

11. McCarthy, J., and E. F. Blick. "Effects of Wind Turbulence and Shear on Landing Performance of Jet Transports." Paper presented at the AIAA 16th Aerospace Sciences Meeting, Huntsville, Alabama, January, 1978.

12. Reeves, P. M., R. G. Joppa, and V. M. Ganzer. "A Non-Gaussian Model of Continuous Atmospheric Turbulence for Use in Aircraft Design," National Aeronautics and Space Administration CR-2639, Ames Research Center, Sunnyvale, California, January, 1976.

13. Etkin, B. Dynamics of Atmospheric Flight. New York: John Wiley and Sons, Inc., 1972.

14. McCarthy, J., and E. F. Blick. "Aircraft Response to Boundary Layer Turbulence and Wind Shear Associated with Cold-Air-Outflow from a Severe Thunderstorm." Paper presented at the 7th Conference on Aerospace and Aeronautical Meteorology and Symposium on Remote Sensing from Satellites, American Meteorological Society, Melbourne, Florida, November 16-19, 1976.

15. Blick, E. F., et al. "Effect of Wind Turbulence and Shear on Landing Performance of Jet Transports." Paper presented at the AIAA Conference, Huntsville, Alabama, 1978.

16. Fujita, T., and F. Caracena. "An Analysis of Three Weather Related Aircraft Accidents." Research conducted at the Department of the Geophysical Sciences, The University of Chicago, Illinois, 1977.

17. Keenan, M. G. Personal communications, October 1977.

18. Bliss, Jack. Private communication. Flying Tiger Airlines, Los Angeles, California, November, 1977.

19. Luers, J. K., and J. B. Reeves. "Effect of Shear on Aircraft Landing," National Aeronautics and Space Administration CR-2287, George C. Marshall Space Flight Center, Huntsville, Alabama, July, 1973.

20. Horonjeff, R. Planning and Design of Airports. Second edition. St. Louis: McGraw-Hill, Inc., 1975.

21. Smith, V. K. Private communication. The University of Tennessee Space Institute, Tullahoma, Tennessee, October, 1977.

22. Norman, W. S. Unpublished classroom notes. The University of Tennessee Space Institute, Tullahoma, Tennessee, November, 1977.

23. Frost, Walter. "Flight in Variable Mean Winds." Report in preparation under NASA Contract No. NASQ-29584 by The University of Tennessee Space Institute, Tullahoma, Tennessee, 1977.

24. Ralston, A., and H. S. Wilf. Mathematical Methods for Digital Computers. New York: John Wiley and Sons, Inc., 1960.

APPENDICES

APPENDIX A

EQUATIONS OF MOTION

Equations of Motion

The two-dimensional model for aircraft motion presented in this appendix follows the general form developed by Frost [23]. It accounts for both vertical and horizontal mean wind components having both time and spatial variations.

The aircraft trajectory model employed in this study was derived based on the following assumptions:

1. The earth is flat and non-rotating.
2. The acceleration of gravity, g, is constant, 32.2 ft sec^{-2} (9.8 m s^{-2}).
3. Air density is constant, 0.002378 slug ft^{-3} (12 kg m^{-3}).
4. The airframe is a rigid body.
5. The aircraft is constrained to motion in the vertical plane.
6. The aircraft has a symmetry plane (the x-z plane).
7. The mass of the aircraft is constant.
8. Initial flight conditions are for steady-state flight.

Figure 34 illustrates the forces acting on the aircraft. These include:

$\vec{F}_T$ = thrust of the engines,

$\vec{L}$ = lift,

$\vec{D}$ = drag,

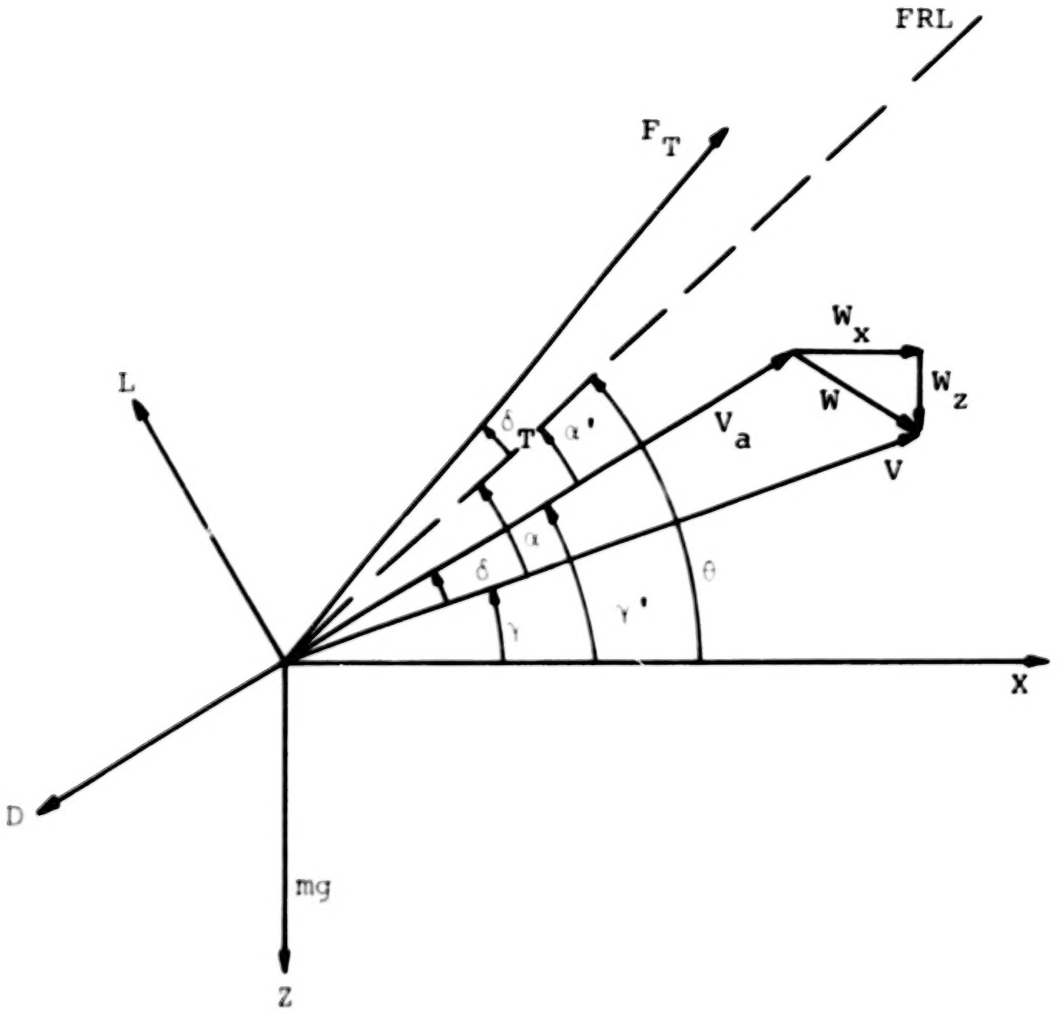

Figure 34. Relationship between the various forces acting on an aircraft [23].

$\vec{W}$ = wind vector,

$m\vec{g}$ = gravitational force.

The figure shows the orientation of the forces with respect to the velocity relative to the earth ($\vec{V}$), the velocity relative to the air mass ($\vec{V}_a$), and the fuselage reference line (FRL) of the aircraft. The x-axis is parallel to the surface of the earth and the z-axis is perpendicular to the surface of the earth (positive downward).

From a direct force balance along the direction $\vec{V}$ and along the direction perpendicular to $\vec{V}$, respectively, it follows from Figure 34 that

$$m\dot{V} = - L \sin \delta - D \cos \delta - mg \sin \gamma + F_T \cos (\delta_T + \alpha) \qquad (1)$$

and

$$mV\dot{\gamma} = L \cos \delta - D \sin \delta - mg \cos \gamma + F_T \sin (\delta_T + \alpha) . \qquad (2)$$

The aerodynamic forces and the thrust from the engines exert a pitching moment on the aircraft. The equation describing the momentum balance about y is

$$\dot{q} = \frac{d^2\theta}{dt^2} = \frac{F_T L_T}{I_{YY}} + \frac{M}{I_{YY}} , \qquad (3)$$

where the dot refers to the derivative with respect to time, and

g = magnitude of the acceleration of gravity,

V = magnitude of the velocity relative to the earth,

γ = angle between $\vec{V}$ and x-axis (the flight path angle),

F_T = magnitude of the thrust vector,

m = aircraft mass,

δ_T = angle between the thrust vector and the fuselage reference line (FRL),

α = angle between $\vec{V}$ and the FRL,

δ = angle between $\vec{V}_a$ and $\vec{V}$,

$\dot{q}$ = time derivative of the pitching rate (q),

L_T = effective moment arm of the thrust vector,

M = pitching moment,

I_{YY} = moment of inertia about the symmetry plane of the aircraft.

By considering a different coordinate system in which the x-axis is along the vector $\vec{V}_a$, called "wind" frame of reference by Etkin [13], similar force equations can be developed by summing up the forces parallel and perpendicular to $\vec{V}_a$. These are

$$m(\dot{V}_a + \dot{W}_{x_w}) + m\, q_w\, W_{z_w} = F_{T_{x_w}} - D - mg \sin \gamma' \qquad (4)$$

and

$$m\, \dot{W}_{z_w} - m\, q_w (V_a + W_{x_w}) = F_{T_{z_w}} - L + mg \cos \gamma' \,. \qquad (5)$$

It is convenient to express these in terms of the wind components relative to an earth-fixed coordinate system, since most wind correlations from the meteorological literature are expressed in such coordinates.

$$W_{x_w} = W_x \cos \gamma' - W_z \sin \gamma' \ , \tag{6}$$

$$W_{z_w} = W_x \sin \gamma' + W_z \cos \gamma' \ . \tag{7}$$

Taking the time derivative of W_{x_w},

$$\dot{W}_{x_w} = \dot{W}_x \cos \gamma' - \dot{W}_z \sin \gamma' - W_x \sin \gamma' \frac{d\gamma'}{dt} - W_z \cos \gamma' \frac{d\gamma'}{dt} \ . \tag{8}$$

Then, since

$$q_w = \frac{d\gamma'}{dt} \ ,$$

$$\dot{W}_{x_w} = \dot{W}_x \cos \gamma' - \dot{W}_z \sin \gamma' - W_{z_w} q_w \ . \tag{9}$$

Also, since

$$F_{T_{x_w}} = F_T \cos(\delta_T + \alpha')$$

and

$$F_{T_{z_w}} = F_T \sin(\delta_T + \alpha') \ ,$$

Eq. (4) becomes

$$m \dot{V}_a = F_T \cos(\delta_T + \alpha') - D - mg \sin \gamma'$$

$$- m(\dot{W}_x \cos \gamma' - \dot{W}_z \sin \gamma') \ . \tag{10}$$

From Eq. (7), taking the time derivative of W_{z_w},

$$\dot{W}_{z_w} = \dot{W}_x \sin \gamma' + \dot{W}_z \cos \gamma' + W_x \cos \gamma' \frac{d\gamma'}{dt} - W_z \sin \gamma' \frac{d\gamma'}{dt} \ , \tag{11}$$

and Eq. (5) becomes

$$- m V_a q_w = - F_T \sin(\delta_T + \alpha') - L + mg \cos \gamma' - m(\dot{W}_x \sin \gamma' + \dot{W}_z \cos \gamma') \ . \quad (12)$$

The moment equation remains the same as Eq. (3). The governing force equations in "wind" frame of reference are thus

$$m \dot{V}_a = F_T \cos (\delta_T + \alpha') - D - mg \sin \gamma' - m(\dot{W}_x \cos \gamma' - \dot{W}_z \sin \gamma') \ , \quad (13)$$

$$m V_a \dot{\gamma}' = F_T \sin(\delta_T + \alpha') + L - mg \cos \gamma' + m(\dot{W}_x \sin \gamma' + \dot{W}_z \cos \gamma') \ , \quad (14)$$

and

$$\dot{q} = \frac{F_T L_T}{I_{YY}} + \frac{M}{I_{YY}} \ , \quad (15)$$

where

W_x = horizontal wind speed,

W_z = vertical wind speed,

α' = (angle of attack) angle between V_a and the FRL.

Incorporation of Wind Shear

The wind is seen to enter the equations in the form of a gradient or wind shear $\dot{W}_x$ and $\dot{W}_z$. The expanded form of these equations is:

$$\dot{W}_x = \frac{\partial W_x}{\partial t} + \frac{\partial W_x}{\partial x}\frac{dx}{dt} + \frac{\partial W_x}{\partial z}\frac{dz}{dt}$$

or

$$\dot{W}_x = \frac{\partial W_x}{\partial t} + V\left[\cos\gamma\,\frac{\partial W_x}{\partial x} - \sin\gamma\,\frac{\partial W_x}{\partial z}\right], \tag{16}$$

and, similarly,

$$\dot{W}_z = \frac{\partial W_z}{\partial t} + V\left[\cos\gamma\,\frac{\partial W_z}{\partial x} - \sin\gamma\,\frac{\partial W_z}{\partial z}\right]. \tag{17}$$

Thus, both spatial variations and temporal variations in atmospheric motion influence the equations in the wind coordinate system.

Generally, care is needed in evaluating $\partial W_x/\partial z$ and $\partial W_z/\partial z$, since the wind speed is normally expressed in terms of altitude measured upward from the surface of the earth, whereas in aerodynamic coordinates, z is measured downward.

Additional kinematic relationships necessary to solve for the aircraft motion are as follows:

The relative velocity as a function of inertial and wind velocity is

$$V_a = \left[(\dot{x} - W_x)^2 + (\dot{z} - W_z)^2\right]^{1/2}, \tag{18}$$

and, in turn,

$$V = W_x\cos\gamma - W_z\sin\gamma + \left[(W_z\sin\gamma - W_x\cos\gamma)^2 + V_a^2 - (W_x^2 + W_z^2)\right]^{1/2}. \tag{19}$$

The angle between $\vec{V}$ and $\vec{V}_a$ is given by

$$\sin \delta = \frac{W_x \sin \gamma + W_z \cos \gamma}{V_a} . \tag{20}$$

Other angular relationships are:

$$\alpha' = \theta - \gamma - \delta = \theta - \gamma' \tag{21}$$

and

$$\alpha = \theta - \gamma . \tag{22}$$

The derivative of α' is

$$\dot{\alpha}' = \dot{\theta} - \dot{\gamma}' = q - \dot{\gamma}' ,$$

where $\dot{\gamma}'$ is given by Eq. (14), hence,

$$\dot{\alpha}' = q - \frac{F_T \sin(\delta_T + \alpha')}{m V_a} - \frac{L}{m V_a}$$

$$+ \frac{g \cos \gamma'}{V_a} + \frac{1}{V_a}[\dot{W}_x \sin \gamma' + \dot{W}_z \cos \gamma'] . \tag{23}$$

Also required for solution of the preceding equations are the aerodynamic coefficients:

$$C_L = C_L(\alpha', \delta_E, V, q, \dot{\alpha}') ,$$

$$C_D = C_D(\alpha', \delta_E, V, q, \dot{\alpha}', C_L) ,$$

$$C_m = C_m(\alpha', \delta_E, V, q, \dot{\alpha}') , \tag{24}$$

where

δ_E = elevator deflection angle.

As is indicated above, the aerodynamic coefficients are functions of a number of variables. The expressions for C_L, C_D, and C_m, along with the stability derivative data and aircraft physical data are given in the following sections.

The equations of motion discussed in this appendix can be solved for the flight of an aircraft flying through spatially and temporally varying two-dimensional wind fields.

APPENDIX B

COMPUTER PROGRAM DOCUMENTATION

Program Description

This part of the appendix describes a computer program, written in FORTRAN IV, designed to solve the equations of motion for aircraft flight through spatially and temporally varying two-dimensional wind fields developed in Appendix A. The aircraft may assume a fixed control mode (i.e., neglects pilot input) or use the automatic control subroutines which provide adjustments to the control surfaces (see Figures 35 and 36). In addition, an option to include a non-Gaussian turbulent field with the modeled thunderstorms for the automatic control mode is described schematically in Figure 37 and detailed in [7].

Main Program

The main calling program first reads the aircraft physical data and stability derivatives from the user-supplied data deck. Next, the dimensionless groups are calculated. The main program then calls subroutine INIT which supplies the initial conditions for the equations of motion. Subroutine EQUIL, which computes initial values for thrust, elevator angle, and angle of attack from the equilibrium conditions, is called secondly. Now with initial conditions, error weights, and so forth, for the Runge-Kutta scheme defined, subroutine RKGS is called and does not return to the main program until the aircraft has landed.

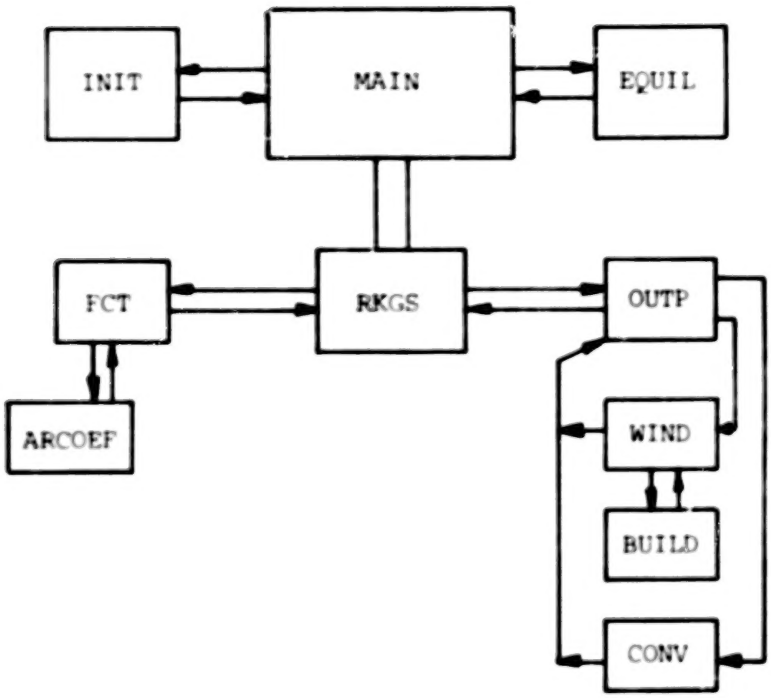

Figure 35. Main calling program flow diagram for aircraft with fixed controls.

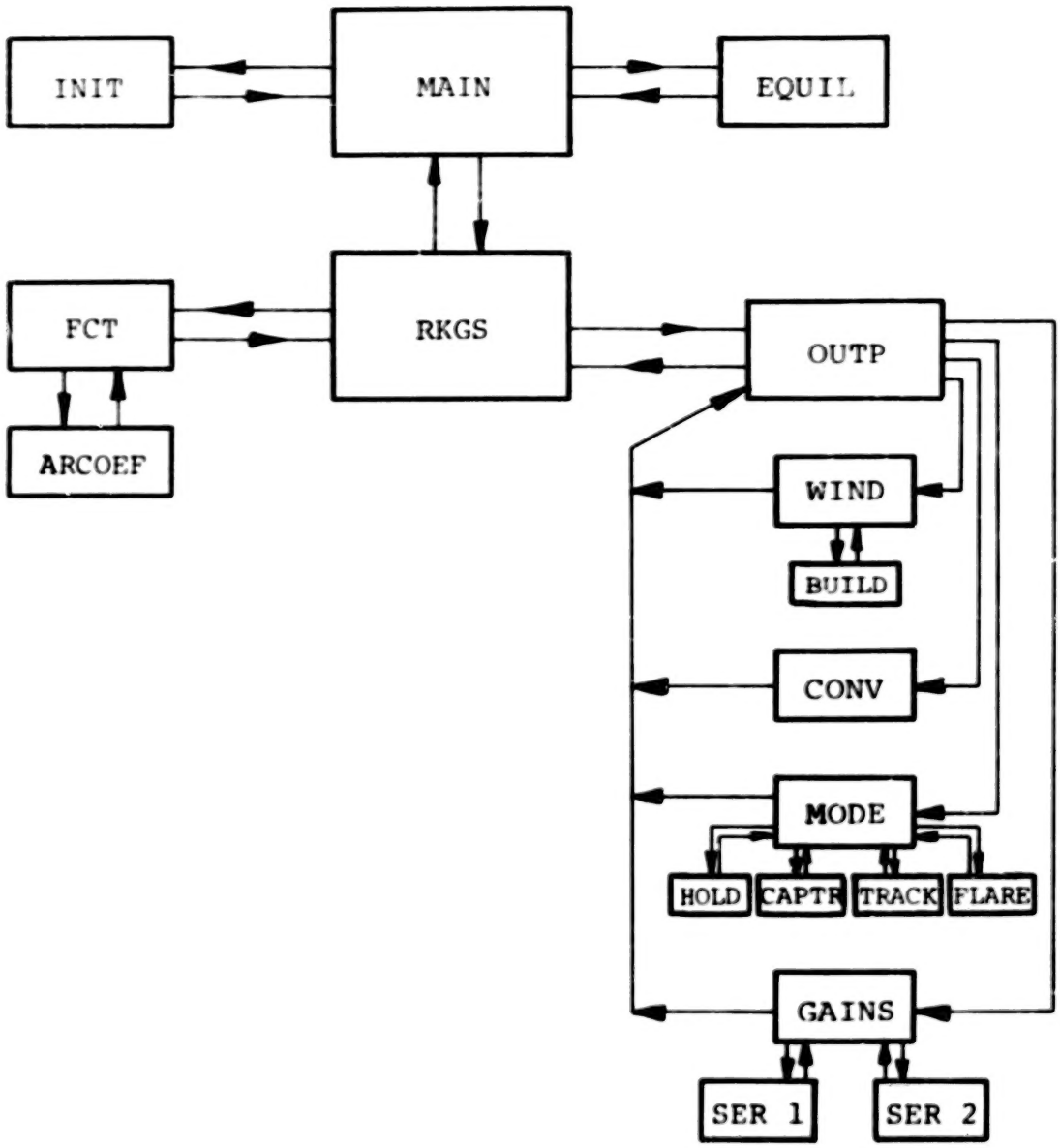

Figure 36. Main calling program flow diagram for aircraft with automatic controls.

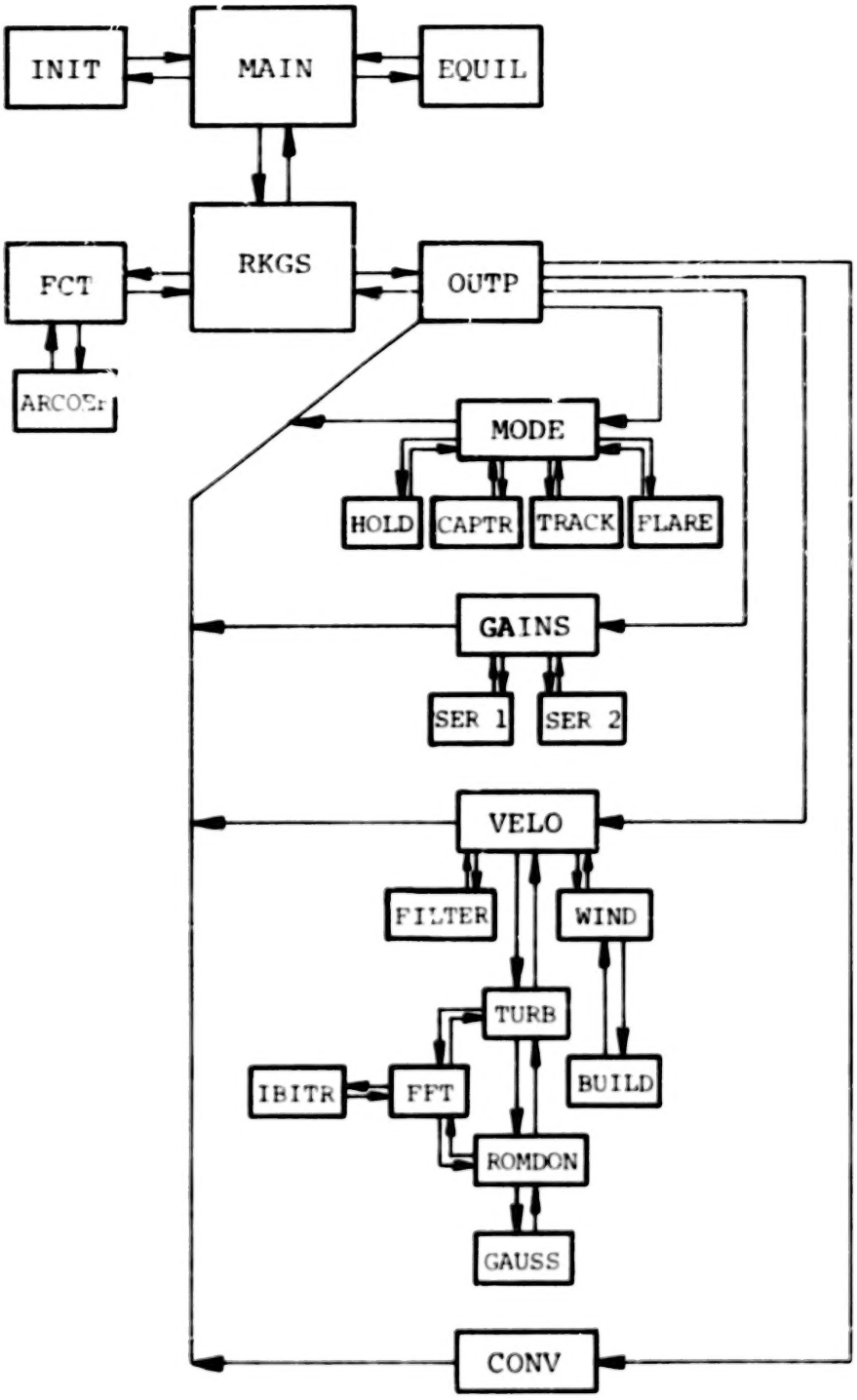

Figure 37. Main calling program flow diagram for aircraft with automatic controls, including turbulence generation subroutines.

Nomenclature

Main program input data:

NCR		Read unit number
NWR		Write unit number
PI	π	PI = 3.1415927
RHO	ρ	RHO = 0.075
G	g	Acceleration due to gravity
TEST		TEST = 0
NP		NP = 0
NCO		NCO = 20
QV	qV	QV = $\rho/2$
PLANE		Airplane name
AMASS	m	Aircraft weight (lb)
SA	s	Aircraft wing area (ft^2)
CORD	$\bar{c}$	Wing mean aerodynamic chord (ft)
VAIR	V_a	Airspeed ($ft\ s^{-1}$)
ALT	L_T	Effective moment arm of thrust vector
HA	h_a	Reference altitude, HA = 300 ft (91 m)
YYI	I_{YY}	Moment of inertia about the symmetry plane of the aircraft
DELT	δ_T	Angle between the thrust vector and the fuselage reference line
CLO	C_{L_o}	Lift parameter
CLA	C_{L_α}	Lift parameter
CLDEL	$C_{L_{\delta_E}}$	Lift parameter

CLQ	C_{L_q}	Lift parameter
CLADOT	$C_{L_{\dot{\alpha}}}$	Lift parameter
CDO	C_{D_o}	Drag parameter
CDA	C_{D_α}	Drag parameter
CDA2	$C_{D_{\alpha^2}}$	Drag parameter
CMO	C_{m_o}	Pitching moment parameter
CMA	C_{m_α}	Pitching moment parameter
CMDEL	$C_{m_{\delta_E}}$	Pitching moment parameter
CMQ	C_{m_q}	Pitching moment parameter
CMADOT	$C_{m_{\dot{\alpha}}}$	Pitching moment parameter

Main program dimensionless groups:

DN1	$\frac{QV*SA*HA}{AMASS}$	
DN2	$\frac{G*HA}{(VAIR)^2}$	
DN4	$\frac{CORD}{2HA}$	
DN5	$\frac{QV*SA*CORD*HA^2}{G*YYI}$	
DN6P	$\frac{HA*G}{AMASS*VAIR^2}$	
DN7P	$\frac{ALT*HA^2}{(VAIR)^2*YYI}$	
PRMT		Input-output vector for subroutine RKGS
PRMT(1)		Lower bound of the interval PRMT(1)=0.0

PRMT(2) Upper bound of the interval PRMT(2)=100

PRMT(3) Initial increment of the independent variable

PRMT(3)=0.01

PRMT(4) Upper error bound PRMT(4)=1.0

DERY Input vector of error weights for subroutine RKGS

NDIM Number of equations to be integrated NDIM=6

Listing of Main Program

```
      DIMENSION PLANE(20)
      DIMENSION A(3,3),B(3)
      DIMENSION Y(6),DERY(6),AUX(6,6),PRMT(5)
      DIMENSION              DXX(2,2),DXZ(2,2),DZX(2,2),DZZ(2,2)
      COMMON CL,CLO,CLA,CLDEL,CLQ,CLADOT,CLGE
      COMMON CD,CDO,CDA,CDA2,CDGE
      COMMON CM,CMO,CMA,CMDEL,CMQ,CMADOT,CMGE
      COMMON QV,AMASS,G,PI,SA,CBRD,ALI,mA,YYI,WAIR
      COMMON DN1,DN2,DN3,DN4,DN5,DN6,DN7,DN6P,DN7P
      COMMON FI,DELI,DEL,DELE,V4,GAMP
      COMMON TEST,NS,NP,NCO
      COMMON/DMKOMN/Y
      COMMON/VARIBL/DERY
      COMMON/INI/VO
      COMMON/mINDS/mX,mZ,mXT,mZI,mXX,mXZ,mZX,mZZ,mXDOT,mZDOT,ZO,USTAR
      COMMON/II/AXA(41,11,2),DX,DZ
      EXTERNAL FCT,OUTP
C
      NCR=5
      NP=0
      NMK=6
      NCO=20
      PI=3.14159265
      RHO=0.075
      G=32.2
      QV=0.5*RHO
C     RUNGE-KUTTA PARAMETER SET UP
      NDIM=6
      DO 1 I=1,NDIM
1     DERY(I)=0.001
      PRMT(1)=0.
      PRMT(2)=100.
      PRMT(3)=0.01
      PRMT(4)=1.0
      TEST=PRMT(1)
      READ (NCR,33) PLANE
   33 FORMAT(20A4)
```

```
      WRITE(NWK,41)PLANE
      READ (NCH,34) AMASS,SA,CORD,VAIR,ALI,HA,YYI,DELT
   41 FORMAT(6A,20A4)
   34 FORMAT (8F10.5)
      READ(NCH,35)    CLO,CLA,CLDEL,CLQ,CLADOT
   35 FORMAT(5F10.5)
      READ(NCH,36)    CDO,CDA,CDA2
   36 FORMAT(3F10.5)
      READ(NCH,37) CMO,CMA,CMDEL,CMQ,CMADOT
   37 FORMAT(5F10.5)
      WRITE(NWK,43)
   43 FORMAT(80('S'))
      WRITE(NWK,44)AMASS,SA,CORD,VAIR,ALI,HA,YYI,DELT
   44 FORMAT (6X,'AMASS = ',F10.2,/,6X,'WING AREA = ',F10.4,/,6X,
     1'CORD = ',F10.4,/,6X,'VAIR = ',F10.4,/,6X,'ALI(MOMENT ARM) = ',
     2F 8.4,/,6X,'HA = ',F10.4,/,6X,'YYI=',E13.5,/,6X,'DELT =',F10.5)
      DELT=DELT*PI/180.
      WRITE(NWK,42  )
   42 FORMAT(1X,'LIFT COEFFICIENT ')
      WRITE(NWK,45)    CLO,CLA,CLDEL,CLQ,CLADOT
   45 FORMAT(2X,             'CLO=',F10.5,'CLA=',F10.5,'CLDEL=',F10.5,
     1'CLQ=',F10.5,'CLADOT=',F10.5)
      WRITE(NWK,46)
   46 FORMAT(1X,'DRAG COEFICIENTS')
      WRITE(NWK,47)   CDO,CDA,CDA2
   47 FORMAT(2X,             'CDO=',F10.5,'CDA=',F10.5,'CDA2=',F10.5)
      WRITE(NWK,48)
   48 FORMAT(1X,'MOMENT COEFICIENTS')
      WRITE(NWK,49) CMO,CMA,CMDEL,CMQ,CMADOT
   49 FORMAT(2X,'CMO=',F10.5,'CMA=',F10.5,'CMDEL=',F10.5,'CMQ=',F10.5,
     1'CMADOT=',F10.5,/)
C       CALCULATE DIMENSIONLESS GROUPS
      DN1=QV*SA*HA/(AMASS)
      DN2=G*HA/(VAIR**2)
      DN3=0.
      DN4=CORD/(2.*HA)
      DN5=QV*SA*CORD*HA**2/(YYI*32.2)
      DN6P=HA*G/(AMASS*VAIR**2)
      DN7P=ALI*(HA**2)/((VAIR**2)*YYI)
      CALL INIT(1)
      CALL EQUIL
      PRMT(1)=T
      CALL RKGS(PRMT,NDIM,IHLF,FCT,OUTP,AUX)
  222 CONTINUE
      RETURN
      END
```

Common Blocks

This program has five common blocks. COMMON/UNKNOWN/ contains the solutions of the state variables at time step T. COMMON/VARIBL/ contains derivatives of the state variables at time step T. COMMON/WINDS/ contains wind data at time step T. COMMON/TT/ contains wind

data. Unlabeled commons contain the aircraft data. The common blocks are used to transfer data from one subroutine to another.

Common Block from Main Program

```
      COMMON CL,CLO,CLA,CLDEL,CLQ,CLADOT,CLGE
      COMMON CD,CDO,CDA,CDA2,CDGE
      COMMON CM,CMO,CMA,CMDEL,CMQ,CMADOT,CMGE
      COMMON QV,AMASS,G,PI,SA,CONV,ALT,HA,YYI,VAIR
      COMMON DN1,DN2,DN3,DN4,DN5,DN6,DN7,DN6P,DN7P
      COMMON FT,DELT,DEL,DELE,VA,GAMP
      COMMON TEST,NS,NP,NCO
      COMMON/UNKOWN/Y
      COMMON/VARIBL/DERY
      COMMON/INI/VO
      COMMON/WINDS/WX,WZ,WXT,WZT,WXX,WXZ,WZX,WZZ,WXDOT,WZDOT,ZO,USTAR
      COMMON/II/AXA(41,11,2),DX,DZ
```

Common Block from Subroutine INIT

```
      COMMON CL,CLO,CLA,CLDEL,CLQ,CLADOT,CLGE
      COMMON CD,CDO,CDA,CDA2,CDGE
      COMMON CM,CMO,CMA,CMDEL,CMQ,CMADOT,CMGE
      COMMON QV,AMASS,G,PI,SA,CONV,ALT,HA,YYI,VAIR
      COMMON DN1,DN2,DN3,DN4,DN5,DN6,DN7,DN6P,DN7P
      COMMON FT,DELT,DEL,DELE,VA,GAMP
      COMMON TEST,NS,NP,NCO
      COMMON/UNKOWN/V,GAM,Q,AP,X,Z
      COMMON /VARIBL/VDOT,GMDOT,QDOT,APDOT,XDOT,ZDOT
      COMMON/INI/VO
      COMMON/WINDS/WX,WZ,WXT,WZT,WXX,WXZ,WZX,WZZ,WXDOT,WZDOT,ZO,USTAR
      COMMON/II/AXA(41,11,2),DX,DZ
```

Subroutine INIT

Subroutine INIT is called by the main program. This subroutine defines and also initializes the various aircraft parameters.

Nomenclature

Subroutine INIT:

APDOT $\dot{\alpha}$ Time derivative of angle of attack

GAMD γ Flight path angle in degrees

GAM	γ	Flight path angle in radians
T	t	Time
Q	q	Pitching rate
FT	F_T	Thrust
HAD		Reference altitude in meters
Z	z	Vertical component of aircraft position, positive downward
X	x	Horizontal component of aircraft position
VA	V_a	Aircraft velocity relative to air
V	V	Aircraft velocity relative to ground
VADOT	$\dot{V}_a$	Time derivative of air velocity
DEL	δ	Angle between $\vec{V}_a$ and $\vec{V}$
GAMP	γ'	Flight path angle in wind coordinate system
VO	V_{a_o}	Initial velocity

Listing of Subroutine INIT

```
      SUBROUTINE INIT(T)
      COMMON CL,CLO,CLA,CLDEL,CLQ,CLADOT,CLGE
      COMMON CD,CDO,CDA,CDA2,CDGE
      COMMON CM,CMO,CMA,CMDEL,CMQ,CMADOT,CMGE
      COMMON GV,AMASS,G,PI,SA,CONV,ALT,HA,YYI,VAIR
      COMMON DN1,DN2,DN3,DN4,DN5,DN6,DN7,DN6P,DN7P
      COMMON FT,DELT,DEL,DELE,VA,GAMP
      COMMON TEST,MS,NP,NCO
      COMMON/UNKOWN/V,GAM,Q,AP,X,Z
      COMMON /VARIBL/VDOT,GMDOT,QDOT,APDOT,XDOT,ZDOT
      COMMON/IN1/VO
      COMMON/WINDS/WX,WZ,WXT,WZT,WXX,WXZ,WZX,WZZ,WXDOT,WZDOT,ZO,USTAR
      COMMON/II/AXA(41,11,2),DX,DZ
C
```

```
      NWR=6
      APDOT=0.
      GAMD=0.0
      GAM=GAMD*PI/180.
      I=0.0
      Q=0.
      FI=1.
      HAD=HA*0.3048
      KCK=1
      HAM=HAD
      Z=-1000.0/HA
      X=0.0
      XGM=X
      ZM=-Z
      CALL        WIND (XGM,ZM,HAM,KCK,WX,WZ,WXX,WXZ,WZX,WZZ)
      CALL      CONV(VAIR,HAD,X,Z,XGM,ZM)
10    FORMAT(2X,8E12.5)
      WRITE(6,10) WX,WZ,WXI,WZI,WXX,WXZ,WZX,WZZ
      VADOT=0.0
      VA=1.0
      V=WX* COS(GAM)-WZ* SIN(GAM)+((WZ* SIN(GAM)-WX* COS(GAM))**2
     1+VA**2-(WX**2+WZ**2))**0.5
      DEL= ARSIN((WX* SIN(GAM)+WZ* COS(GAM))/VA)
      GAMP=GAM+DEL
      VO=V
      WRITE(NWR,1) GAMD
    1 FORMAT(2X,'INITIAL FLIGHT PATH ANGLE=',E12.5,'DEG.',/)
      RETURN
      END
```

Subroutine EQUIL

Called from main program, this subroutine calculates initial values of the angle of attack, elevator angle, and thrust from the equations of motion by assuming equilibrium conditions:

$$A(i,j) = B(i) \ ,$$

$$A_{11}\ \alpha' + A_{12}\ \delta_E + A_{13}\ F_T = B_1 \ ,$$

$$A_{21}\ \alpha' + A_{22}\ \delta_E + A_{23}\ F_T = B_2 \ ,$$

$$A_{31}\ \alpha' + A_{32}\ \delta_E + A_{33}\ F_T = B_3 \ ,$$

from the following equations,

$$-D_1 V_a^2 C_D - D_2 \sin\gamma' + D_6 \cos(\delta_T + \alpha')F_T - \bar{W} = 0 ,$$

$$D_1 V_a^2 C_L - D_2 \cos\gamma' + D_6 \sin(\delta_T + \alpha')F_T + \bar{\bar{W}} = 0 ,$$

$$D_5 V_a^2 C_m + D_7 F_T = 0 ,$$

where

$$\bar{W} = -\dot{W}_x \cos\gamma' + \dot{W}_z \sin\gamma' ,$$

$$\bar{\bar{W}} = \dot{W}_x \sin\gamma' + \dot{W}_z \cos\gamma' ,$$

and the initial conditions,

$$\gamma' = \dot{V}_a = \dot{q} = \dot{\alpha}' = q = 0 .$$

Listing of Subroutine EQUIL

```
      SUBROUTINE EQUIL
      COMMON CL,CLO,CLA,CLDEL,CLQ,CLADOT,CLGE
      COMMON CD,CDO,CDA,CDA2,CDGE
      COMMON CM,CMO,CMA,CMDEL,CMQ,CMADOT,CMGE
      COMMON QV,AMASS,G,PI,SA,CBMD,ALT,HA,VVI,VAIR
      COMMON DN1,DN2,DN3,DN4,DN5,DN6,DN7,DN6P,DN7P
      COMMON FI,DELT,DEL,DELE,VA,GAMP
      COMMON TEST,NS,NP,NCO
      COMMON/UNKOWN/V ,GAM ,Q,AP,X,Z
      COMMON/WINDS/WX,WZ,WXI,WZI,WXX,WXZ,WZX,WZZ,WXDOT,WZDOT,ZO,USTAR
      DIMENSION A(3,3),B(3)
C
      NWR=6
      AP=0.
    1 AP1=AP
      VA2=VA**2
      A(1,1)=-DN1*VA2*(CDA+CDA2*AP)
      A(1,2)=0.
      A(1,3)=DN6P* COS(DELT+AP)
      A(2,1)= DN1*VA2*CLA
      A(2,2)= DN1*VA2*CLDEL
      A(2,3)=DN6P* SIN(DELT+AP)
      A(3,1)=DN5*VA2*CMA
      A(3,2)=DN5*VA2*CMDEL
      A(3,3)=DN7P
```

```
      WZDOT=WZT-V *(WZX*COS(GAM )-WZZ*SIN(GAM ))
      WXDOT=WXT+V *(WXX*COS(GAM )-WXZ*SIN(GAM ))
      W1=WXDOT* COS(GAMP)-WZDOT* SIN(GAMP)
      B(1)=W1+DN1*VA2*CDD+DN2* SIN(GAMP)
      W2=WXDOT* SIN(GAMP)+WZDOT* COS(GAMP)
      B(2)=-W2-DN1*VA2*CLD+DN2* COS(GAMP)
      B(3)=-DN5*VA2*CMD
      D1=B(3)/A(3,1)-B(2)/A(2,1)
      C1=A(2,2)/A(2,1)-A(3,2)/A(3,1)
      C2=A(2,3)/A(2,1)-A(3,3)/A(3,1)
      D2=B(3)/A(3,1)+A(3,2)*D1/(A(3,1)*C1)
      C3=A(3,2)*C2/(A(3,1)*C1)-A(3,3)/A(3,1)
      FID=(A(1,1)*D2-A(1,2)*D1/C1-B(1))/(A(1,2)*C2/C1-A(1,1)*C3-A(1,3))
      AP=D2+C3*FID
      DELE=-D1/C1-C2/C1*FID
      IF( ABS(AP1-AP).GT.0.000001)GO TO 1
B1    AP1=180.*AP/PI
      WRITE(NWH,2)AP1,DELE,FID
    2 FORMAT(2X,'EQUIL. ANGLE OF ATTACK=',E12.5,'EQUIL. ELEVATOR ANGLE='
     1,E12.5,'EQUIL. THRUST=',E12.5,/)
      DN6=DN6P*FID
      DN7=DN7P*FID
      WRITE(NWH,3) DN1,DN2,DN3,DN4,DN5,DN6,DN7
    3 FORMAT(6X,'DN1=',F12.5,/,6X,'DN2=',F12.5,/,6X,'DN3=',F12.5,/,5X,'
     1DN4=',F12.5,/,6X,'DN5=',F12.5,/,6X,'DN6=',F12.5,/,6X,'DN7=',F12.5,
     2/)
      RETURN
      END
```

Subroutine RKGS

Subroutine RKGS evaluates a system of first order ordinary differential equations with given initial values by means of fourth order Runge-Kutta formulae in the modification due to Gill [24]. Accuracy is tested comparing the results of the procedure with single and double increment. This subroutine automatically adjusts the increment during the whole computation by halving and doubling. If more than ten bisections of the increment are necessary to get satisfactory accuracy, the subroutine returns with error message IHLF=11 into main program [21]. (See pages 85 and 86 of this study for description of input/output parameters for this subroutine.)

Subroutine FCT

Subroutine FCT is called by the subroutine RKGS. Subroutine FCT calculates the derivatives of the state equations at each time step.

Listing of Subroutine FCT

```
      SUBROUTINE FCT(T)
      DIMENSION Y(6),DERY(6)
      COMMON CL,CLO,CLA,CLDEL,CLQ,CLADOT,CLGE
      COMMON CD,CDO,CDA,CDA2,CDGE
      COMMON CM,CMO,CMA,CMDEL,CMQ,CMADOT,CMGE
      COMMON GG,AMASS,G,PI,S4,CONV,ALT,RA,VEI,VAIR
      COMMON DN1,DN2,DN3,DN4,DN5,DN6,DN7,DN6P,DN7P
      COMMON FI,DELT,DEL,DELE,VA,GAMP
      COMMON TEST,NS,NP,NCO
      COMMON/UNKOWN/Y
      COMMON/VARIBL/DERY
      COMMON/WIND5/WX,WZ,WXI,WZI,WXX,WXZ,WZX,WZZ,WADOT,WZDOT,ZO,USTAR
      EQUIVALENCE(DERY(1),VDOT),(DERY(2),GMDOT),(DERY(3),QDOT),
     1(DERY(4),APDOT),(DERY(5),XDOT),(DERY(6),ZDOT)
      EQUIVALENCE(Y(1),V),(Y(2),GAM),(Y(3),Q),(Y(4),AP),(Y(5),X),
     1(Y(6),Z)
      CALL AMCOEF
C
C     DERY(1)= VDOT,DERY(2)= GMDOT,DERY(3)=QDOT,DERY(4)=APDOT,DERY(5)=
C     XDOT,DERY(6)=ZDOT
C     Y(1)=V ,Y(2)=GAM ,Y(3)=Q,Y(4)=AP,Y(5)=X,Y(6)=Z
  101 DEL= ARSIN((WX* SIN(GAM)+WZ* COS(GAM))/VA)
      GAMP=Y(2)+DEL
      DERY(5)=V* COS(GAM)
      DERY(6)=-V* SIN(GAM)
      VA=((DERY(5)-WX)**2+(DERY(6)-WZ)**2)**0.5
      WZDOT=WZI-V *(WZX*COS(GAM )-WZZ*SIN(GAM ))
      WADOT=WXI+V *(WXX*COS(GAM )-WXZ*SIN(GAM ))
      DERY(1)=-DN1*(CD*COS(DEL)+CL*SIN(DEL))*VA**2-DN2*SIN(Y(2))+DN6
     1*COS(DELT+Y(4)+DEL)
      DERY(2)=DN1*VA**2*(CL*COS(DEL)-CD*SIN(DEL))/Y(1)-DN2*COS(Y(2))/
     1Y(1)+DN6*SIN(DELT+Y(4)+DEL)/Y(1)
      DERY(3)=DN7*FI+DN5*VA**2*CM
      GMPDOT =DN1*CL*(VA)-DN2* COS(GAMP)/VA  +DN6*FI* SIN(DELT+Y(4))/
     1VA  +(WXDOT* SIN(GAMP)+WZDOT* COS(GAMP))/VA
      DERY(4)=Y(3)-GMPDOT
10    RETURN
      END
```

Subroutine ARCOEF

Subroutine ARCOEF is called by subroutine FCT. Subroutine ARCOEF calculates the aerodynamic coefficients CL, CD, and C_m at each time step:

$$C_L = C_{L_o} + C_{L_\alpha}\,\alpha' + C_{L_{\delta_E}}\,\delta_E + \frac{\bar{c}q}{2V_a}\,C_{L_q} + \frac{\bar{c}\dot{\alpha}'}{2V_a}\,C_{L_{\dot{\alpha}}} + \Delta C_{L_{GE}} ,$$

$$C_D = C_{D_o} + C_{D_\alpha}\,\alpha' + C_{D_{\alpha^2}}\,\alpha'^2 + \Delta C_{D_{GE}} ,$$

$$C_m = C_{m_o} + C_{m_\alpha}\,\alpha' + C_{m_{\delta_E}}\,\delta_E + \frac{\bar{c}q}{2V_a}\,C_{m_q} + \frac{\bar{c}\dot{\alpha}'}{2V_a}\,C_{m_{\dot{\alpha}}} + \Delta C_{m_{GE}} \qquad [19] .$$

For the augmentor-wing STOL aircraft, the equations of the aerodynamic coefficients vary significantly from those presented above, and are expressed as:

$$C_L = C_{L_{WB_\infty}} + C_{L_{H_o}} + C_{L_{H_\alpha}}\,\alpha' + \frac{\bar{c}q}{2V_a}\,C_{L_q} + \frac{\bar{c}\dot{\alpha}'}{2V_a}\,C_{L_{\dot{\alpha}}} ,$$

$$C_D = C_{D_o} + C_{D_\alpha}\,\alpha' + \Delta C_{D_{GE}} ,$$

$$C_m = C_{m_o} + C_{m_\alpha}\,\alpha' + C_{L_{WB}}\left(\frac{\ell_W}{\bar{c}}\cos\alpha' + \frac{z_W}{\bar{c}}\sin\alpha'\right)$$

$$+ C_D\left(\frac{\ell_W}{\bar{c}}\sin\alpha' - \frac{z_W}{\bar{c}}\cos\alpha'\right) + \left(C_{L_{H_o}} + C_{L_{H_\alpha}}\,\alpha' + C_{L_{\delta_E}}\,\delta_E\right)$$

$$\left(\frac{z_H}{\bar{c}}\sin\alpha' - \frac{\ell_H}{\bar{c}}\cos\alpha'\right) + \frac{\bar{c}q}{2V_a}\,C_{m_q} + \frac{\bar{c}\dot{\alpha}'}{2V_a}\,C_{m_{\dot{\alpha}}} + \Delta C_{m_{GE}} ,$$

where

$$C_{L_{WB_\infty}} = C_{L_{WB_0}} + C_{L_{WB_\alpha}} \alpha' ,$$

prior to inclusion of ground effect terms [19].

Since the ground effect terms are negligible for conventional aircraft (see Figure 23, page 44), they are set equal to zero for convenience. Their inclusion is a trivial task when given the particular equations for each of the terms, as presented in Chapter IV.

Listing of Subroutine ARCOEF

```
      SUBROUTINE ARCOEF
      COMMON CL,CLO,CLA,CLDEL,CLQ,CLADOT,CLGE
      COMMON CD,CDO,CDA,CDA2,CDGE
      COMMON CM,CMO,CMA,CMDEL,CMQ,CMADOT,CMGE
      COMMON GV,AMASS,G,PI,SA,CORD,ALT,HA,YY1,VAIR
      COMMON DN1,DN2,DN3,DN4,DN5,DN6,DN7,DN6P,DN7P
      COMMON PI,DELT,DEL,DELE,VA,GAMP
      COMMON TEST,NS,NP,NCD
      COMMON/UNKOWN/V,GAM,Q,AP,X,Z
      COMMON /VARIBL/VDOT,GMDOT,QDOT,APDOT,XDOT,ZDOT
C
      CLGE=0.
      CDGE=0.
      CMGE=0.
      CL=CLO+CLA*AP+CLDEL*DELE+DN4*(CLQ*Q+CLADOT*APDOT)/VA+CLGE
      CD=CDO+CDA*AP+CDA2*AP**2+CDGE
      CM=CMO+CMA*AP+CMDEL*DELE+DN4*(CMQ*Q+CMADOT*APDOT)/VA+CMGE
      RETURN
      END
```

Subroutine OUTP

Subroutine OUTP is called by the subroutine RKGS at every time step. Subroutine OUTP is an external output subroutine used to print the results. Subroutine OUTP in turn calls subroutine WIND and updates the WIND speed parameters. Also, if the automatic control system is desired, subroutine OUTP calls subroutines MODE and GAINS which

computes the control parameters F_T and δ_E. Subroutine OUTP terminates the integrating subroutine RKGS when the aircraft reaches ground, z = 0, by changing the value of PRMT(5) to a non-zero value.

Listing of Subroutine OUTP

```
      SUBROUTINE OUTP(T,INLF,NDIM,PRMT)
      DIMENSION Y(6),PRMT(5),DERY(6)
      COMMON CL,CLO,CLA,CLDEL,CLQ,CLADOT,CLGE
      COMMON CD,CDO,CDA,CDA2,CDGE
      COMMON CM,CMO,CMA,CMDEL,CMQ,CMADOT,CMGE
      COMMON QV,AMASS,G,PI,SA,CORD,AI,RA,XXI,VAIR
      COMMON DN1,DN2,DN3,DN4,DN5,DN6,DN7,DN6P,DN7P
      COMMON FT,DELT,DEL,DELE,VA,GAMP
      COMMON TEST,NS,N2,NCO
      COMMON/UNKOWN/Y
      COMMON/VARIBL/DERY
      COMMON/IN1/VO
      COMMON/WINDS/WX,WZ,WXT,WZT,WXX,WXZ,WZX,WZZ,WXDOT,WZDOT,ZO,USTAR
      COMMON/IT/AXA(41,11,2),DX,DZ
      EQUIVALENCE(DERY(1),VDOT),(DERY(2),GMDOT),(DERY(3),QDOT),
     1(DERY(4),APDOT),(DERY(5),XDOT),(DERY(6),ZDOT)
      EQUIVALENCE(Y(1),V),(Y(2),GAM),(Y(3),Q),(Y(4),AP),(Y(5),X),
     1(Y(6),Z)
C
35    NWR=6
      HAD=HA*0.3048
      XGM=X*HAD
      ZM=-Z*HAD
      IF(N2.GT.1) GO TO 4
      IIC=0
      M1=N2
      M2=N2
      M3=N2
      M4=N2
      M5=N2
      M6=N2
      ICHK=0
      M1=20
      M7=0
      IR=0.
    4 N2=2
      DI=I-IR
      IR=I
      IF(NCO.LT.10) GO TO 100
      NCO=0
      WRITE(NWR,12)T
12    FORMAT(5X,'TIME = ',F12.6)
      WRITE(NWR,10)(Y(I),I=1,NDIM)
10    FORMAT(2X,'V    = ',F9.5,2X,'GAMMA       = ',F9.5,2X,'PITCH RATE =
     1',F9.5 ,/,2X,'ALPHA PRIME = ',F9.5,2X,'HORIZONTAL POSITION = ',
     2F9.5,2X,'VERTICAL POSITION = ',F9.5)
```

```
      WRITE(NWR,13) (DERY(I),I=1,NDIM)
13    FORMAT(2X,' VDOT = ',E15.5,2X,' GMDOT = ',E15.5,2X,'QDOT = ',E15.5
     1,/,2X,'APDOT = ',E15.5 ,2X,'XDOT = ',E15.5,2X,'ZDOT = ',E15.5)
      WRITE(NWR,30) WX,WZ,WXDOT,WZDOT,GAMP,VA,DEL
30    FORMAT(2X,'WX =',E12.5,1X,'WZ =',E12.5,1X,'WXDOT =',E12.5,1X,
     2'WZDOT =',E12.5,1X,'GAMP=',E11.4,1X,'VA=',E11.4,1X,'DEL =',E11.4)
      WRITE(6,81) CL,CD,CM
   81 FORMAT(6X,'CL=',E12.5,'CD=',E12.5,'CM=',E12.5)
      WRITE(6,1001) XGM,ZM
 1001 FORMAT(2X,'XGM=',E12.5,'ZM=',E12.5)
      WRITE (6,8888) FT,DELE,THET
 8888 FORMAT (4X,'FT=',E12.5,2X,'DELE=',E12.5,2X,'THET=',E12.5)
  100 NCO=NCO+1
    5 CONTINUE
      XGM=X
      ZM=-Z
      KCK=2
      HAM=HAD
      CALL MODE (M1,M2,M3,M4,Z,ZDOT,X,VO,V,GAM,DT,THET)
      CALL GAINS (THET,M5,M6)
      CALL       WIND (XGM,ZM,HAM,KCK,WX,WZ,WXX,WXZ,WZX,WZZ)
      CALL     CONV(VAIR,HAD,X,Z,XGM,ZM)
      CHK1=X*HAD
      CHK2=-Z*HAD
      ENDZ=10.*DZ
      ENDX=40.*DX
      IF(CHK1.GT.ENDX) GO TO 300
      IF(CHK2.GT.ENDZ) GO TO 300
      IF(Z) 200,300,300
  300 PRMT(5)=1.0
  200 CONTINUE
      IF(IHLF-10)1,1,2
2     WRITE(NWR,11)IHLF
11    FORMAT(2X,'ERROR IHLF = ',I4)
1     CONTINUE
      RETURN
      END
```

Subroutine MODE

Subroutine MODE is called by the subroutine OUTP. The input parameters M_1, M_2, M_3, and M_4 are initially zero. Other input parameters are Z, ZDOT, X, VO, V, GAM, and DT. The output parameter is THET. Subroutine MODE in turn calls one of the subroutines HOLD, CAPTR, TRACK, or FLARE, depending upon the position of the aircraft mode control logic.

Listing of Subroutine MODE

```
      SUBROUTINE    MODE(M1,M2,M3,M4,Z,ZDOT,X,VO,V,GAM,DT,THET)
      IF(ABS(Z).LE.0.2) GO TO 23
      IF(X.LT.3.0) GO TO 20
      IF(ABS(GAM).GE.0.047) GO TO 22
      IF(X.GE.3.4) GO TO 22
      IF(X.GE.3.0) GO TO 21
   20 CALL    HOLD(M1,Z,DT,THET)
      GO TO 24
   21 CALL CAPTR(M2,Z,ZDOT,DT,X,GAM,VO,THET)
   22 CALL    TRACK(M3,Z,ZDOT,DT,X,GAM,VO,THET)
      GO TO 24
   23 CALL           FLARE(M4,Z,ZDOT,V,DT,THET,IC)
      IF(IC.EQ.1) GO TO 22
   24 CONTINUE
      RETURN
      END
```

Subroutine HOLD

Subroutine HOLD is called by the subroutine MODE. The input parameters are I, Z, and DT. Input parameter I is initially zero and then set to I = 2 in this subroutine. The output parameter is THET.

The following difference equations are solved in this subroutine:

$$\Delta Z = Z - HR ,$$

$$C_1 = e^{a_1 DT} ,$$

$$C_2 = \left\{ \frac{K_1}{a_1} (1 - C_1) \right\} ,$$

$$C_3 = K_2(a_2 DT - 1) ,$$

$$TH_j = C_1 TH_{j-1} + C_2 \Delta Z_{j-1} ,$$

$$THET_j = THET_{j-1} + K_2 TH_j + C_3 TH_{j-1} .$$

Listing of Subroutine HOLD

```
      SUBROUTINE    HOLD(I,Z,DT,THET)
C     HOLD MODE
      HR=Z
      T1A=1.
      T1K=0.1
      T2A=0.1
      T2K=0.05
      IF(I.GT.1)GO TO 5
      T1R=0.
      T2R=0.
      T3R=0.
      I=1+2
    5 CONTINUE
      T1=Z-HR
      T1C=EXP(-T1A*DT)
      T1D=T1K*(1.-T1C)/T1A
      T2=(T1C*T2R+T1D*T1R)
      T2C=T2K*(T2A*DT-1.)
      T3=T3R+T2K*T2+T2C*T2R
      THET=T3
      T3R=T3
      T2R=T2
      T1R=T1
      RETURN
      END
```

Subroutine CAPTR

Subroutine CAPTR is called by subroutine MODE. Input parameters for this subroutine are I, Z, ZDOT, DT, and VO. Input parameter I is initially zero and then set to I = 2. In this subroutine the output parameter is THET.

The following difference equations are solved in this subroutine:

$$TH_j = C_1\ TH_{j-1} - C_2\ TH_{j-2} + C_3\ \Delta ZD_{j-1} + C_4\ ZD_{j-2} + \Delta THETP\ ,$$

$$\Delta ZD_j = HCD - ZDOT\ ,$$

and where

$$C_1 = 1 + e^{-DT/\tau} ,$$

$$C_2 = e^{-DT/\tau} ,$$

$$C_3 = K_3 K_4 [DT + \tau (C_2 - 1)] ,$$

$$C_4 = K_3 K_4 [DT - C_2(T + 1)] .$$

Listing of Subroutine CAPTR

```
      SUBROUTINE CAPTR(I,Z,ZDOT,DT,X,GAM,VO,THET)
      TAU=0.01
      CT1K=0.1
      THETP=-0.05
      IF(I.GT.1)GO TO 5
      CT1R=0.
      CT1RR=0.
      CT2R=0.
      CT2RR=0.
      I=I+2
    5 CONTINUE
      RCD=VO*SIN(4.71239E-2)
      CT1=RCD-ZDOT
      CT1C1=1.+EXP(-DT/TAU)
      CT1C2=EXP(-DT/TAU)
      CT1D1=CT1R*(DT+TAU*(CT1C2-1.))
      CT1D2=CT1R*(TAU-CT1C2*(DT+TAU))
      CT2=CT1C1*CT2R-CT1C2*CT2RR+CT1D1*CT1R+CT1D2*CT1RR
      CT2=CT2*0.01
      THET=CT2
      CT1R=CT1
      CT1RR=CT1R
      CT2R=CT2
      CT2RR=CT2R
      THET=THET+THETP
      RETURN
      END
```

Subroutine TRACK

Subroutine TRACK is called by subroutine MODE. Input parameters for this subroutine are I, Z, R, DOT, X, GAM, and VO. Input parameter I is initially zero and then set to I = 2 in this subroutine. The output parameter is THET. The following difference equations are solved in the subroutine:

$$\gamma_j = GAM_j - GAMR ,$$

$$TH_j = K_4(Z_j - ZR) + K_5(ZDOT_j - ZD) ,$$

$$TT1_j = C_1\ TT1_{j-1} + C_2\ \gamma_{j-1} ,$$

$$TT2_j = TT2_{j-1} + K_6\ TT1 + C_3\ TT1_{j-1} ,$$

$$THET_j = TH_j + TT2_j ,$$

where

$$C_1 = e^{-a_2 DT/\tau_2} ,$$

$$C_2 = \frac{K_3}{a_2}(1 - C_1) ,$$

$$C_3 = K_6(a_3\ DT - 1) .$$

Listing of Subroutine TRACK

```
      SUBROUTINE    TRACK(I,Z,ZDOT,DT,X,GAM,VD,THET)
C     TRACKING MODE
      TT3K=0.01
      TT3K=0.005
      TT3K=0.05
      TT4K=0.05
      TT4K=1.
      TT4K=0.00325
      TAU=0.1
      TAU=0.01
      TT1A=1./TAU
      TT1K=1./TAU
      TT2K=1.
      TT2K=0.125
      TT2K=0.00125
      TT2A=0.01
      GAMR=-0.0471239
      HR=-(63-X)*TAN(-GAMR)
      DFH=Z-HR
```

```
      IF(I.GT.1)GO TO 5
      TT2R=0.
      TT1R=0.
      EPSR=0.
      I=I+2
    5 CONTINUE
      DRH=ZDOT-VO*SIN(-GAMR)
      EPS=GAMR-GAM
      TT1C=EXP(-TT1A*DT)
      TT1D=TT1R*(1.-TT1C)/TT1A
      TT1=TT1C*TT1R+TT1D*EPSR
      TT2C=TT2R*(TT2A*DT-1.)
      TT2=TT2R+TT2R*TT1+TT2C*TT1R
      THETT=TT2+TT3R*DRH+TT4R*DRH
      THET=THETT
      TT1R=TT1
      EPSR=EPS
      TT2R=TT2
C     RATE  LIMITER
      IF(GAMR-GAM)1,4,2
    1 IF(THET)4,4,3
    2 IF(THET)3,4,4
    3 THET=-0.5*THET
    4 RETURN
      END
```

Subroutine FLARE

Subroutine FLARE is called by subroutine MODE. Input parameters for this subroutine are M, Z, ZDOT, V, DT, and IC. Input parameters IC and M are initially zero and then set to IC = 1 and M = 2 in this subroutine. The output parameter is THET. In this subroutine initially when M = 0, three different reference heights (HSTP, HF, and HRMP) for FLARE are calculated. Depending upon the altitude of the aircraft Z, the output parameter THET is calculated. The following difference equations are solved in this subroutine:

$$P5_j = (P5_{j-1} - THR_{j-1})\ DT\ ,$$

$$P1_j = (ZDOT_j - ZD)\ AA2 + Z_j\ ,$$

$$P2_j = P1_j\ K_1\ AA\ ,$$

$$P3_j = P3_{j-1} + P2_j ,$$

$$P6_j = C_1 P6_{j-1} + K(THP_j - THP_{j-1}) ,$$

$$THET_j = P2_j - P3_j + P5_j + P6_j ,$$

where

$$C_1 = e^{-A6*DT} .$$

Listing of Subroutine FLARE

```
      SUBROUTINE     FLARE(M,Z,ZDOT,V,DT,THET,IC)
C     FLARE  MODE
      IF(M.GT.1) GO TO 2
      ICL=0.
      P4=0.0
      P5=0.0
      P6=0.0
      P3R=0.
      P5R=0.
      P6R=0.
      THRR=0.
      THPR=0.
      HSTP=3.5*ZDOT/V
      HRMP=0.6*HSTP
      HF=0.8*HSTP
      THP=0.9*ZDOT/V
      THR=((0.255*ZDOT/V)-0.0001315)*DT
      WRITE(6,12)Z,HSTP,THP,THR
   12 FORMAT(/,5X,4E20.6,/)
    2 M=2
      ZDOTC=0.01
      AK1= 0.00024
      AA1=0.00333
      AA2=5.0
      AKP=2.
      AAP=5.
      IF(ABS(Z).GT.HSTP) GO TO 6
      IF(ABS(Z).GT.HF)   GO TO 5
      IF(ABS(Z).GT.HRMP) GO TO 4
      P5=(P5R+THRR)*0.01
      P5R=P5
      THRR=THR
      ICL=ICL+DT
    4 CONTINUE
```

```
      P1=(ZDOT-ZDOTC)*AA2+Z
      IF(TCL.GT.4.0) P5=0.
      P11=P1*AK1
      IF(P11.GE.0.)AA=AA1
      IF(P11.LT.0.)AA=AA1/2.
      P2=P11*AA
      XNR=P2
      P3=P3R+XNR
      P3R=P3
      P4=P2-P3
    5 CONTINUE
      C1P=EXP(-AAP*DT)
      P6=C1P*P6R+AKP*(THP-THPR)
      P6R=P6
      THPR=THP
      THET=P4+P5+P6
C     RATE  LIMITER
      IF(THET.GT.0.1)THET=0.1
      IF(THET.LT.0.2E-04)THET=0.2E-04
      GO TO 7
    6 IC=1
      GO TO 8
    7 IC=0
    8 CONTINUE
      RETURN
      END
```

Subroutine GAINS

Subroutine GAINS is called by subroutine OUTP. Input parameters for this subroutine are THET, M1, and M2. Aerodynamic coefficients, AP, APDOT, DEL, Q, and VA are brought in by common statements. This subroutine in turn calls subroutines SER1 and SER2 calculates elevator and thrust signals. The following equations are solved in this subroutine:

$$F_{TC} = KT1\ VA - KT2\ \dot{Z}/V + KT3\ \dot{X}/V + K4\ THET\ ,$$

$$\delta_{EC} = KD1\ VA - KD2\ \dot{Z}/V - KD3\ \dot{X}/V - KD4\ THET\ ,$$

where

$$\begin{pmatrix} KT1 \\ KT2 \\ KT3 \\ KT4 \end{pmatrix} = \begin{pmatrix} G_{10} & G_{11} & -G_{12} \\ D2 & 0 & 0 \\ 0 & -D2 & 0 \\ 0 & -1 & 0 \end{pmatrix} \begin{pmatrix} H_9 \\ H_{10} \\ H_{11} \\ \end{pmatrix}$$

and

$$\begin{pmatrix} KD1 \\ KD2 \\ KD3 \\ KD4 \end{pmatrix} = \begin{pmatrix} -G_{10} & G_{11} & G_{12} \\ -D2 & 0 & 0 \\ 0 & -D2 & 0 \\ 0 & -1 & 0 \end{pmatrix} \begin{pmatrix} H_6 \\ H_7 \\ H_8 \\ \end{pmatrix}$$

Listing of Subroutine GAINS

```
      SUBROUTINE     GAINS(IHET,M1,M2)
      COMMON CL,CLO,CLA,CLDEL,CLQ,CLADOT,CLGE
      COMMON CD,CDO,CDA,CDA2,CDGE
      COMMON CM,CMO,CMA,CMDEL,CMQ,CMADOT,CMGE
      COMMON QV,AMASS,G,PI,SA,CORD,ALT,HA,YII,VAIR
      COMMON DN1,DN2,DN3,DN4,DN5,DN6,DN7,DN6P,DN7P
      COMMON FI,DELT,DEL,DELE,VA,GAMP
      COMMON TEST,NS,NP,NCO
      COMMON/UNKOWN/V ,GAM ,Q,AP,X,Z
      COMMON /VARIBL/V DOT,GM DOT,QDOT,APDOT,XDOT,ZDOT
      COMMON/GNS/AFK1,AFK2,AFK3,AFK4,ADK1,ADK2,ADK3,ADK4
      F1=AP
      F2=APDOT
      F3=DEL
      F4=VA
      F5=Q
      FA=COS(F3)
      FB=SIN(F3)
      FC=COS(DELT+AP+DEL)
      FD=SIN(DELT+AP+DEL)
      C1=DN1*CDA
      C2=DN1*CDA2
      C3=DN1*CLA
      C4=DN1*CLDEL
      C5=DN5*CMA
      C6=DN5*CMDEL
      C7=DN1*CDO
      C8=DN1*CLO
      C9=DN1*DN4*CLQ
      C10=DN1*DN4*CLADOT
      C11=DN5*CMQ
      C12=DN5*DN4*CMQ
      C13=DN5*DN4*CMADOT
```

```
G1=DN7
G2=-C1*FA-C2*FA*F1-C3*F3
G3=-C4*FB
G4=DN6*FC
G5=C3*FA-C1*FB-C2*FB*F1
G6=C4*FA
G7=DN6*FD
G8=C5
G9=C6
G10=C7*F4*FA+C8*F4*FB+C9*F5*FB+C10*F2*FB
G11=C8*F4*FA+C9*F5*FA+C10*F2*FA-C7*F4*FB
G12=C11*F4+C12*F5+C13*F2
H1=G6*G1-G7*G9
H2=G5*G1-G7*G8
H3=G5*G9-G6*G8
H4=G2*H1-G3*H2+G4*H3
H5=F4*H4
H6=H2/(F4*H5)
H7=(G2*G1-G4*G8)/(F4*H5)
H8=(G2*G7-G4*G5)/(F4*H5)
H9=H3/H4
H10=(G2*G9-G3*G8)/H4
H11=(G2*G6-G3*G5)/H4
ADK1=G12*H8-G11*H7-G10*H6
ADK2=-DN2*H6
ADK3=-DN2*H7
ADK4=-H7
AFK1=G10*H9+G11*H10-G12*H11
AFK2=DN2*H9
AFK3=-DN2*H10
AFK4=-H10
GA1=ADK1*VA-ADK2*ZDOT/V-ADK3*XDOT/V-ADK4*THET
GA2=AFK1*VA-AFK2*ZDOT/V+AFK3*XDOT/V+AFK4*THET
CALL      SER1(M1,GA1,DELE,DT)
CALL      SER2(M2,GA2,FI,DT)
RETURN
END
```

Subroutine SER1

Subroutine SER1 is called by subroutine GAINS. Input parameters for this subroutine are M, XN, and DT. Input parameter M is initially zero and then set to M = 2 in this subroutine. Output parameter is control variable DELE. This subroutine calculates the control variable DELE from the control signal XN (calculated in subroutine GAINS) using an elevator control servo. The difference equations solved in this subroutine are as follows:

$$T1_j = C_1\, T1_{j-1} + K/\tau\ (XN_j - XN_{j-1}) ,$$

$$DELE_j = C_2\, DELE_{j-1} - C_3\, DELE_{j-2} + C_4\, T1_j + C_5\, T1_{j-1} + C_6\, T1_{j-1} ,$$

where

$$C_1 = e^{-a_1/\tau\ DT}$$

$$C_2 = 2e^{-a_2 DT} \cos b ,$$

$$C_3 = e^{-2a_2 DT} ,$$

$$C_4 = K_2/RT\ (1/RT - \sin \omega/b) ,$$

$$C_5 = K_2/RT\ (RD1 + \sin(\omega\ DT) + RD2) ,$$

$$C_6 = K_2/RT\ e^{a_2 DT}\ (RD3 - RD4) .$$

Listing of Subroutine SER1

```
      SUBROUTINE     SER1(M,XN,DELE,DT)
C     SERVO SYSTEM
      IF(M.GT.0) GO TO 2
      T1M=0.
      T1MM=0.
      T2M=0.
      T2MM=0.
      XNM=0.
    2 M=2
      AK1=1.
      AA1=0.00036
      TA1=0.995
      DT=0.01
      AAT=AA1/TA1
      AKT1=AK1/TA1
      C1=EXP(-AAT*DT)
      AK2=390000.
      AA2=883.17469
```

```
      BB=1.5707963
      RT=SQRT((AA2*AA2)+(BB*BB))
      AKT2=AK2/RT
      PSI=ATAN(-BB/AA2)
      XXP=EXP(-AA2*DT)*COS(BB)
      CT2=EXP(-2.*AA2*DT)
      DT1=AKT2*((1./RT)-(SIN(PSI)/BB))
      CT1=2.*XXP
      RD1=-2.*XXP/RT
      RD2=EXP(-AA2*DT)*SIN(BB*DT+PSI)
      DT2=AKT2*(RD1*SIN(PSI*DT)+RD2)
      RD3=EXP(-AA2*DT)/RT
      RD4=-SIN(BB*DT+PSI)/BB
      DT3=AKT2*EXP(-AA2*DT)*(RD3-RD4)
      I1=C1*I1H+AKT1*(XN-XNR)
      I2=CT1*I2H-CT2*I2HR+DT1*I1+DT2*T1H+DT3*I1RH
      I1RH=I1H
      I1R=T1
      I2RH=I2H
      I2H=T2
      XNR=XN
      DELE=T2
      RETURN
      END
```

Subroutine SER2

Subroutine SER2 is called by subroutine GAINS. Input parameters for this subroutine are M, XN, and DT. Input parameter M is initially zero and then set to M = 2 in this subroutine. Output parameter is control variable F_T. This subroutine calculates the control variable from the control signal XN (input from subroutine GAINS) using a thrust control servo. The difference equations solved in this subroutine are as follows:

$$T1_j = C_1\, T1_{j-1} + K/\tau\ (XN_j - XN_{j-1}) ,$$

$$FT_j = C_2\, FT_{j-1} - C_3\, FT_{j-2} + C_4\, T1_j + C_5\, T1_{j-1} + C_6\, T1_{j-2} ,$$

where

$$C_1 = e^{-a_1/\tau\ DT} ,$$

$$C_2 = 2e^{-a_2 DT} \cos b ,$$

$$C_3 = e^{2a_2 DT} .$$

$$C_4 = K_2/RT \ (1/RT - \sin \ ./b) .$$

$$C_5 = K_2/RT \ (RD1 + \sin (\ DT) + RD2) .$$

$$C_6 = K_2/RT \ e^{-a_2 DT} \ (RD3 - RD4) .$$

Listing of Subroutine SER2

```
      SUBROUTINE     SER2(M,XN,FI,DT)
C     SERVO SYSTEM
      IF(M.GT.0) GO TO 2
      T1M=0.
      T1MM=0.
      T2M=0.
      T2MM=0.
      XNM=0.
    2 M=2
      DT=0.01
      AK1=1.
      AA1=0.00036
      TA1=0.995
      AA1=AA1/TA1
      AKT1=AK1/TA1
      C1=EXP(-AA1*DT)
      AK2=390000.
      AA2=883.17469
      BB=1.5707963
      RT=SQRT((AA2*AA2)+(BB*BB))
      AKT2=AK2/RT
      PSI=ATAN(-BB/AA2)
      XXP=EXP(-AA2*DT)*COS(BB)
      CT2=EXP(-2.*AA2*DT)
      DT1=AKT2*((1./RT)-(SIN(PSI)/BB))
      CT1=2.*XXP
      RD1=-2.*XXP/RT
      RD2=EXP(-AA2*DT)*SIN(BB*DT+PSI)
      DT2=AKT2*(RD1+SIN(PSI+DT)+RD2)
      RD3=EXP(-AA2*DT)/RT
      RD4=-SIN(BB*DT+PSI)/BB
      DT3=AKT2*EXP(-AA2*DT)*(RD3-RD4)
      T1=C1*T1M+AKT1*(XN-XNM)
      T2=CT1*T2M-CT2*T2M     *T1+DT2*T1M+DT3*T1MM
      T1MM=T1M
      T1M=T1
      T2MM=T2M
      T2M=T2
      XNM=XN
      FI=T2
      RETURN
      END
```

$$C_3 = e^{2a_2 DT} ,$$

$$C_4 = K_2/RT \ (1/RT - \sin \psi/b) ,$$

$$C_5 = K_2/RT \ (RD1 + \sin (\psi \ DT) + RD2) ,$$

$$C_6 = K_2/RT \ e^{-a_2 DT} \ (RD3 - RD4) .$$

Listing of Subroutine SER2

```
      SUBROUTINE      SER2(M,XN,FT,DT)
C     SERVO SYSTEM
      IF(M.GT.0) GO TO 2
      T1M=0.
      T1RM=0.
      T2M=0.
      T2RM=0.
      XNM=0.
    2 M=2
      DT=0.01
      AK1=1.
      AA1=0.00036
      TA1=0.995
      AAT=AA1/TA1
      AKT1=AK1/TA1
      C1=EXP(-AAT*DT)
      AK2=340000.
      AA2=883.17469
      BB=1.5707963
      RT=SQRT((AA2*AA2)+(BB*BB))
      AKT2=AK2/RT
      PSI=ATAN(-BB/AA2)
      XXP=EXP(-AA2*DT)*COS(BB)
      CT2=EXP(-2.*AA2*DT)
      DT1=AKT2*((1./RT)-(SIN(PSI)/BB))
      CT1=2.*XXP
      RD1=-2.*XXP/RT
      RD2=EXP(-AA2*DT)*SIN(BB*DT+PSI)
      DT2=AKT2*(RD1*SIN(PSI*DT)+RD2)
      RD3=EXP(-AA2*DT)/RT
      RD4=-SIN(BB*DT+PSI)/BB
      DT3=AKT2*EXP(-AA2*DT)*(RD3-RD4)
      T1=C1*T1M+AKT1*(XN-XNR)
      T2=CT1*T2M-CT2*T2RM+DT1*T1+DT2*T1M+DT3*T1RM
      T1RM=T1M
      T1M=T1
      T2RM=T2M
      T2M=T2
      XNM=XN
      FT=T2
      RETURN
      END
```

1. REPORT NO.	2. GOVERNMENT ACCESSION NO.	3. RECIPIENT'S CATALOG NO.
NASA CR-3052		

4. TITLE AND SUBTITLE	5. REPORT DATE
Investigations of Simulated Aircraft Flight through Thunderstorm Outflows	September 1978
	6. PERFORMING ORGANIZATION CODE

7. AUTHOR(S)	8. PERFORMING ORGANIZATION REPORT #
Walter Frost and Bill Crosby	

9. PERFORMING ORGANIZATION NAME AND ADDRESS	10. WORK UNIT NO.
FWG Associates, Inc. R. R. 3, Box 331 Tullahoma, Tennessee 37388	M-263
	11. CONTRACT OR GRANT NO. NAS8-32217
	13. TYPE OF REPOR. & PERIOD COVERED Contractor

12. SPONSORING AGENCY NAME AND ADDRESS	14. SPONSORING AGENCY CODE
National Aeronautics and Space Administration Washington, D. C. 20546	

15. SUPPLEMENTARY NOTES

Prepared under the technical monitorship of the Atmospheric Sciences Division, Space Sciences Laboratory, NASA/Marshall Space Flight Center

16. ABSTRACT

The purpose of this study is to investigate the effects of wind shear on aircraft flying through thunderstorm gust fronts. This is carried out through the development of a computer program solving the two-dimensional, nonlinear equations of aircraft motion, including wind shear. The procedure described and documented thus accounts for spatial and temporal variations of the aircraft within the flow regime.

Analysis of flight paths and control inputs necessary to maintain specified trajectories for aircraft having characteristics of DC-8, B-747, augmentor-wing STOL, and DHC-6 aircraft is recorded in this study. From this analysis an attempt is made to find criteria for reduction of the hazards associated with landing through thunderstorm gust fronts.

17. KEY WORDS	18. DISTRIBUTION STATEMENT
Aviation Safety Low-Level Flight Turbulence Winds	Category 01

19. SECURITY CLASSIF. (of this report)	20. SECURITY CLASSIF. (of this page)	21. NO. OF PAGES	22. PRICE
Unclassified	Unclassified	121	$6.50

NASA - Form 1292 (May 1969)

For sale by the National Technical Information Service, Springfield, Virginia 22161

NASA-Langley, 1978

END

DEC 11 1978